

Cl-rich amphiboles as record for  
hydrothermal processes at very high  
temperatures in the deep oceanic crust:  
brine/rock interaction experiments and  
investigation on natural rocks

Von der Naturwissenschaftlichen Fakultät der  
Gottfried Wilhelm Leibniz Universität Hannover

zur Erlangung des Grades  
Doktorin der Naturwissenschaften (Dr. rer. nat.)

genehmigte Dissertation

von

Adriana Miriam Currin Sala, M. Sc  
(Niederlande)

2018

Referent: Prof. Dr. rer. nat. Jürgen Koepke

Korreferenten: Prof. Dr. rer. nat. Wolfgang Bach  
Prof. Dr. sci. nat. Ulrich Heimhofer

Tag der Promotion: 15.11.2018

## Abstract

Interactions between rock and high temperature seawater-derived fluids are recorded in hydrothermal veins and dykelets that cross-cut layered olivine gabbros deep in the plutonic section of the Samail Ophiolite, Wadi Wariyah, Sultanate of Oman. Here we present a study – using petrographic, microanalytical, isotopic, and structural methods – of amphiboles found in the aforementioned veins and dykelets, which show a conspicuous compositional variation from high-Ti magnesiohastingsite and pargasite via magnesiohornblende and edenite, to Cl-rich ferropargasite and hastingsite (with up to 5.4 wt% Cl) and actinolite. These minerals record a wide range of formation conditions from magmatic to hydrothermal at varying water/rock ratios and salinities, while the formation of super Cl-rich amphibole suggests the occurrence of phase separation, and  $^{87}\text{Sr}/^{86}\text{Sr}$  and stable  $\delta^{18}\text{O}$  isotope analyses confirm the influence of a hydrothermal fluid in a rock-dominated environment.

A parallel experimental study was conducted at hydrothermal (500 – 750 °C) and magmatic (900 °C) conditions at pressures of 2 kbar, and  $f\text{O}_2$  close to NNO, with an amphibole-containing natural olivine gabbro and saline fluid (6, 20 and 50 wt% NaCl). Results in subsolidus experiments demonstrate the growth of newly-formed amphibole with a wide range of compositions comparable to those seen in the lithologies sampled in Wadi Wariyah, and Cl-bearing amphiboles with Cl up to 0.47 wt. %. Our findings highlight the heterogeneities in fluid infiltration and Cl activity that account for the complexity of hydrothermal fluid/rock interactions in deep oceanic geological systems, providing insight into the subsolidus evolution of gabbro-hosted amphibole-rich veins in the presence of a seawater-derived fluid.

**Keywords:** *Cl-bearing amphibole; high-temperature hydrothermal activity; lower oceanic crust; Samail Ophiolite; phase separation; fluid-rock interaction; magmatic-hydrothermal transition; experimental petrology.*

## Zusammenfassung

Lagige Olivin-Gabbros aus den tiefen plutonischen Abschnitten des Samail Ophiolite (Wadi Wariyah, Sultanat Oman) werden von zahlreichen hydrothermalen Gängen durchzogen. Diese Gänge sind natürliche Archive für Wechselwirkungen zwischen Gestein und Hochtemperatur-Fluiden der ozeanischen Kruste. Diese Studie präsentiert petrographische-, mikroanalytische-, Isotopen- und strukturelle Daten von Amphibolen, die in den oben genannten Gängen vorkommen und eine auffällige kompositionelle Bandbreite von hoch-Ti Magnesiohastingsit und Pargasit, über Magnesiohornblende und Edenit, zu Cl-reichen Ferropargasit, Hastingsit (mit bis zu 5,4 Gew.-% Cl) und Actinolit zeigen. Die Minerale zeichnen sich durch einen breiten Bereich von magmatischen bis hydrothermalen Bildungsbedingungen, bei unterschiedlichsten Wasser / Gesteinsverhältnissen und Salinitäten aus. Die Bildung von extrem Cl-reichen Amphibolen lässt sich vermutlich durch eine Phasentrennung erklären, wohingegen  $^{87}\text{Sr}/^{86}\text{Sr}$  und  $\delta^{18}\text{O}$  Isotopenanalysen einen starken Einfluss von hydrothermalen Fluiden nahelegen.

Parallel wurde eine experimentelle Studie bei hydrothermalen (500 - 750°C) und magmatischen (900°C) Bedingungen bei einem Druck von 2 kbar durchgeführt.  $f\text{O}_2$  Bedingungen lagen nahe am NNO-Puffer. Startmaterialien waren ein amphibolhaltiger, natürlicher Olivin-Gabbro und verschiedene Salzlösungen (6, 20 und 50 Gew.-% NaCl). Ergebnisse der Subsolidus-Experimente zeigen eine zusätzliche Neubildung von Amphibolkristallen mit einem breiten Zusammensetzungsspektrum, welches vergleichbar ist mit der Lithologie des Wadi Wariyah. Zusätzlich treten auch Cl-reiche Amphibole mit Cl-Konzentrationen bis zu 0,47 Gew. % auf. Die Ergebnisse unterstreichen die Heterogenitäten der Fluidinfiltration und Cl-Aktivität, die für die Komplexität hydrothermalen Fluid-Gesteins-Wechselwirkungen in der tiefen ozeanischen Kruste verantwortlich sind. Zusätzlich liefert die Studie Einblicke in die Subsolidus-Entwicklung von Amphibol-reichen Gängen in Gabbros in Anwesenheit von Fluiden die ihren Ursprung im Meerwasser haben.

**Schlagerwörter:** Cl-haltige Amphibole; Hochtemperatur Hydrothermale Aktivität; Untere Ozeanische Kruste; Samail Ophiolit; Phasentrennung; Fluid-Gesteins-Wechselwirkungen; Magmatischen-hydrothermalen Übergangsbereich; Experimentelle Petrologie.



## Acknowledgements

The research leading to these results has received funding from the People Programme (Marie Curie Actions) of the European Union's Seventh Framework Programme FP7/2007-2013/ under REA grant agreement n°608001. This research used samples provided by the International Ocean Discovery Program (IODP).

My heartfelt thanks go to my supervisor, Prof. Dr. Jürgen Koepke, for accepting me on board this project, taking time to always review my work, and for his great patience. I also want to thank my co-supervisor Dr. Renat Almeev, for his guidance, his patience, and assistance at the microprobe. Many thanks to my mentor, Dr. Eric Wolff, for shedding light on the path, and Dr. Chao Zhang, for his help, discussions, and assistance at the microprobe. I wish to acknowledge Dr. Oliver Beermann (Uni Kiel), for his kind cooperation and thorough editing. My appreciation goes to Julian Feige for thin section preparation, Ulrich Kroll for technical assistance, and Prof. Dr. Harald Behrens and Dr. Marize Muniz da Silva for guidance in the operation of the CSPV. Also, many thanks to Dr. Sören Wilke for help performing IHPV experiments, and to André Stechern, for his assistance in the lab and being of invaluable help and encouragement. Thanks to Prof. Dr. François Holtz, for letting me teach in the microscopy course, to Dongmei Qi, Asiye Shabestari, Stefan Linsler, Kristina Schimetzek, Dr. Anna Maria Velc, Dr. David Neave, Dawid Murawski, Insa Cassens, Filippo Ridolfi, and all the other colleagues I have had in the last years for the help, discussions and great company. Thanks also to the students Malte and Torge Krummacker, for their contribution to the mineral separation work.

I am infinitely grateful to Dr. Margot Godard (Géosciences Montpellier), Dr. Benoit Ildefonse (Géosciences Montpellier), Prof. Dr. Damon Teagle (Southampton Uni), and all the other senior scientists in the ABYSS Marie Curie training network, for granting us this marvellous learning opportunity. Also to the people who helped me in Géosciences Montpellier (Dr. Benoit Ildefonse and Dr. Fabrice Barou at the EBSD) and Southampton (Barbara Zihlmann, Dr. Matt Cooper, Dr. J. Andy Milton, Dr. Aurelien Beaumais). I am especially grateful to the PhDs and PostDocs who participated in ABYSS for all that I learned from them, and from seeing the advancement of each of their projects, and the good times had.

There are many other people I would like to thank for having helped me grow in different ways, in parallel to PhD life, including my friends in Hannover, in Barcelona, and others spread around the world. Last, but not least, I want to show my appreciation to my parents and my fiancé for their invaluable emotional support.

<b>1</b>	<b>INTRODUCTION .....</b>	<b>8</b>
1.1	HYDROTHERMAL CIRCULATION IN THE LOWER OCEANIC CRUST .....	8
1.2	PETROLOGICAL BACKGROUND: THE LOWER GABBRO SECTION OF THE SAMAIL OPHIOLITE.....	10
1.3	HIGHLY SALINE FLUIDS & BRINES IN THE DEEP OCEANIC CRUST.....	11
1.4	THE ROLE OF AMPHIBOLE IN FLUID/ROCK INTERACTION.....	13
1.5	CL-BEARING AMPHIBOLE FORMATION AS A CONSEQUENCE OF HYDROTHERMAL CIRCULATION IN THE LOWER OCEANIC CRUST .....	15
1.6	OCCURRENCE OF CL-BEARING AMPHIBOLES .....	18
1.7	PREVIOUS EXPERIMENTAL STUDIES .....	19
1.8	AIMS OF THIS STUDY.....	19
1.9	OUTLINE OF THE STUDY.....	20
<b>2</b>	<b>CHLORINE-RICH AMPHIBOLE IN DEEP LAYERED GABBROS AS EVIDENCE FOR BRINE/ROCK INTERACTION IN THE LOWER OCEANIC CRUST: A CASE STUDY FROM THE WADI WARIYAH, SAMAIL OPHIOLITE, SULTANATE OF OMAN .....</b>	<b>21</b>
2.1	INTRODUCTION.....	21
2.2	ANALYTICAL TECHNIQUES .....	21
2.3	RESULTS.....	23
2.3.1	<i>Outcrop description and Petrography .....</i>	<i>23</i>
2.3.2	<i>Amphibole compositions (major and minor elements).....</i>	<i>29</i>
2.3.3	<i>EBSD analyses.....</i>	<i>32</i>
2.3.4	<i>Isotope analyses .....</i>	<i>33</i>
2.4	DISCUSSION .....	36
2.4.1	<i>Formation of different amphibole types and various episodes of fluid/rock interaction ...</i>	<i>36</i>
2.4.2	<i>Cl incorporation into amphibole .....</i>	<i>40</i>
2.4.3	<i>Relationship between Cl content in amphibole and microstructure.....</i>	<i>41</i>
2.4.4	<i>Fluid evolution: changing water/rock ratios and salinity .....</i>	<i>41</i>
2.5	CONCLUSIONS .....	42
<b>3</b>	<b>INTERACTION OF HIGHLY SALINE FLUID AND OLIVINE GABBRO: EXPERIMENTAL SIMULATION OF DEEP HYDROTHERMAL PROCESSES INVOLVING AMPHIBOLE AT THE BASE OF THE OCEANIC CRUST....</b>	<b>44</b>
3.1	INTRODUCTION.....	44
3.2	EXPERIMENTAL STRATEGY AND METHODS.....	45
3.2.1	<i>Starting material and sample preparation .....</i>	<i>46</i>
3.2.2	<i>Experimental apparatuses and procedure.....</i>	<i>49</i>
3.2.3	<i>Analytical methods.....</i>	<i>52</i>
3.3	RESULTS.....	53
3.3.1	<i>Preliminary experiments.....</i>	<i>53</i>
3.3.2	<i>Suprasolidus experiments.....</i>	<i>54</i>
3.4	DISCUSSION .....	63
3.4.1	<i>Compositional variations of newly-formed amphiboles .....</i>	<i>63</i>
3.4.2	<i>Suprasolidus conditions .....</i>	<i>65</i>

3.4.3	<i>Application to nature</i> .....	66
3.4.4	<i>Cl incorporation in amphiboles</i> .....	70
3.4.5	<i>Considerations on the experimental setup</i> .....	73
3.5	CONCLUSIONS .....	75
<b>4</b>	<b>CONCLUDING REMARKS</b> .....	<b>76</b>
<b>5</b>	<b>REFERENCES</b> .....	<b>78</b>
<b>6</b>	<b>APPENDIX (SUPPLEMENTARY DATA)</b> .....	<b>83</b>

# 1 Introduction

## 1.1 Hydrothermal circulation in the lower oceanic crust

Fluid/rock interactions play an important role in mineral genesis and hydrothermal alteration at mid-ocean ridges as well as in controlling the heat and mass transfer in the oceanic crust. Hydrothermal circulation in the oceanic crust originates through percolation of seawater into joints and fault zones in the seafloor (Manning & MacLeod, 1996; Manning et al., 2000). There is evidence that hydrothermal circulation is not restricted to the upper oceanic crust of fast-spreading mid-ocean ridges, but reaches beyond the sheeted dyke complex and down into the gabbro section (Fig. 1.1) (Gregory & Taylor, 1981; Zhang et al., 2014; 2017b; Harris et al., 2017), based on evidence from field studies in ophiolites (Gregory & Taylor, 1981; Bosch et al., 2004; Nicolas et al., 2003; Abily et al., 2011;), studies of drill cores obtained in the recent oceans (Alt & Bach, 2006; Coogan et al., 2006; 2007), and geophysical modelling (Hasenclever, 2014).

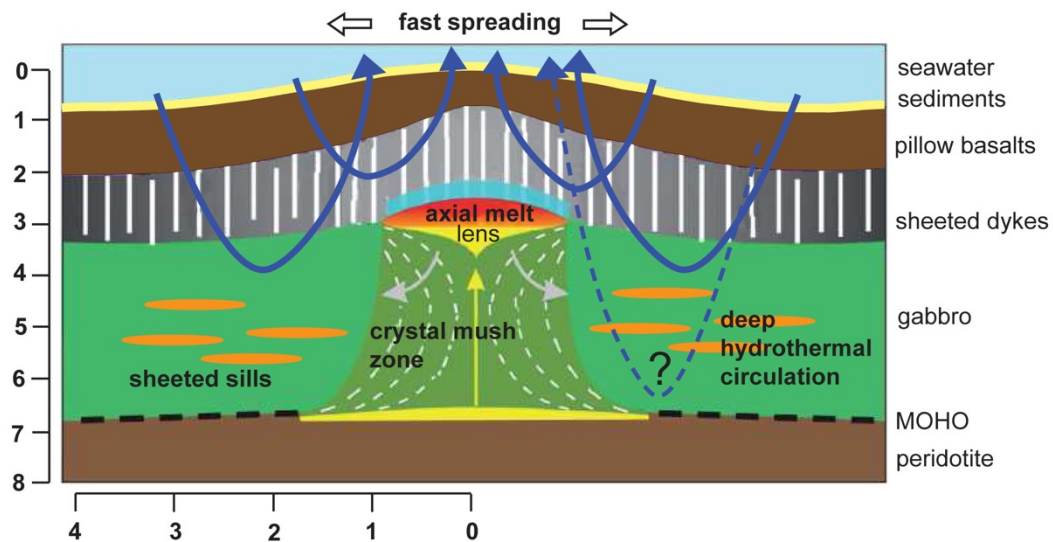


**Figure 1.1.** Sketch of the oceanic crust at fast-spreading ridges. Arrows denote hydrothermal circulation down to the bottom of the upper oceanic crust, but also down to the base of the lower oceanic crust. Modified after Zhang et al. (2017a).

Ridge spreading rate determines the structure of the oceanic crust (Sinton and Detrick, 1992). Prevailing accretion models of the oceanic crust differ on the depths reached by hydrothermal circulation. The gabbro glacier model (Fig. 1.2A, Henstock et al., 1993; Phipps et al., 1993) implies that hydrothermal circulation reaches the base of the sheeted dike complex, sustaining that lower crustal crystallization occurs mainly at the melt lens and that latent heat of crystallization is removed by fluid circulation above it. According to the sheeted sill model (Fig. 1.2B, Boudier et al., 1996; Kelemen et al., 1997), melt sills occur throughout the depth of the plutonic section, requiring hydrothermal cooling down to its base.

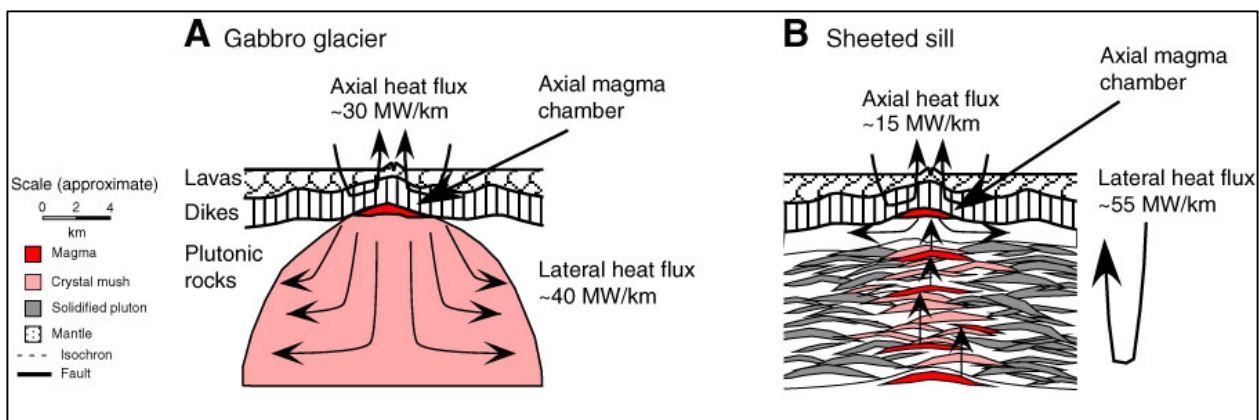


**Figure 1.2.** A: Gabbro glacier model; B: sheeted sill model; after Henstock et al. 1993; Phipps Morgan and Chen, 1993; Boudier et al., 1996; Kelemen et al., 1997; and references therein.

The accretion of the oceanic crust by solidification of magmatic bodies requires cooling of the crust. There is evidence that this cooling goes down to the lower oceanic crust, as shown by global flux calculations (Harris et al., 2017), and thermal models have shown that the hydrothermal system that accounts for the cooling of the oceanic crust reaches down to lower crustal depths of about 6 km (MacLennan et al., 2005). In addition, evidence of hydrothermal activity has been found in the field, in veins and dykelets containing hydrous minerals and alteration products in the deep areas of ophiolite sections (e.g. in the Samail Ophiolite, Sultanate of Oman; Bosch et al., 2004; Nicolas et al., 2003).

## **1.2 Petrological background: the lower gabbro section of the Samail Ophiolite**

Ophiolites are remnants of oceanic crust that have been obducted onto the continental crust. The study of ophiolites gives the chance to study fossil oceanic crust without drilling the seafloor. The Samail ophiolite in the Sultanate of Oman is believed to correlate to a fast-spreading mid-ocean ridge and is found amongst the most studied (Hopson et al., 1981), since the complete ophiolite sequence is exposed.

Previous studies on the Samail Ophiolite (Nicolas et al., 2003; Bosch et al., 2004; Wolff, 2014), partially including the Wadi Wariyah outcrop, describe an interconnected seawater-derived hydrothermal system in the Samail Ophiolite (Sultanate of Oman), made up of gabbroic dykelets (recharge) and hydrothermal veins (discharge). It is suggested that the deep penetration of seawater-derived fluids to within 100 m above the Moho transition zone and the consequent interactions with the host rock lead to hydrous partial melting under magmatic conditions and also trigger hydrothermal reactions (Bosch et al., 2004).

Hydrothermal veins and dykelets that cross-cut layered olivine gabbros deep in the plutonic section of the Samail Ophiolite, Sultanate of Oman, point towards the occurrence of hydrothermal circulation in the deep oceanic crust and record interactions between rock and high temperature seawater-derived fluids or brines. The occurrence of amphiboles in high temperature hydrothermal veins at such depths provides further evidence for the presence of seawater-derived aqueous fluids and brines flowing down to the base of the oceanic crust (Manning et al., 1996; Bosch et al., 2004; Coogan et al., 2001). The present work is focussed on the aforementioned hydrothermal veins and gabbroic dykes that contain Cl-rich amphibole, to further understand fluid/rock interactions in the lower oceanic crust.

Hydrothermal alteration occurs over a range of temperatures from very high temperatures (900-1020 °C) at granulite facies conditions down to lower temperature hydrothermal reactions at greenschist facies conditions (Bosch et al., 2004). In this study, we focus on the formation of amphiboles by hydrothermal

fluid/rock interactions at different temperatures in gabbros outcropping in the Wadi Wariyah, Wadi Tayin Massif, Samail Ophiolite.

As defined by Bosch et al. (2004, p. 1188) hydrothermal veins are “cracks filled with greenschist-facies minerals that induce metamorphic reactions in the adjacent country rocks, and gabbroic dykes as planar intrusive bodies produced by the crystallization of magma”. Such hydrothermal veins can be formed at various temperatures from high temperatures (containing amphibole) to low temperatures (containing prehnite, epidote, chlorite and low temperature amphibole, actinolite). The different assemblages formed at different temperatures through hydrothermal alteration were also described by Nehlig and Juteau (1988). A more detailed description of the lithologies outcropping in Wadi Wariyah is given in chapter 2.

### **1.3 Highly saline fluids & brines in the deep oceanic crust**

Hydrothermal fluids play a key role in mineral reactions and heat transport in the oceanic crust. Even though they find their origin in seawater (Nehlig, 1991), the composition of these fluids is complex and variable, depending on temperature, pressure, oxygen fugacity and ion exchanges during fluid/rock interaction, and are rather different from a simple solution of NaCl and water (Manning and Aranovich, 2014).

Chlorides, such as NaCl, KCl, and CaCl<sub>2</sub>, are the most abundant halides in fluids on Earth, (Harlov and Aranovich, 2017), and are important components of seawater and seawater-derived crustal fluids. Phase separation is an important mechanism of brine formation by concentration of such salts in the fluid (Driesner, 2007; Aranovich et al., 2010). Chloride-rich fluids can travel long distances along grain boundaries (Harlov and Aranovich, 2017) and in the ocean crust, seawater-derived fluids can be found as deep as the crust-mantle transition (Newton and Manning, 2010; Manning and Aranovich, 2014).

Driesner and Heinrich (2017) describe the physical behaviour of a saline fluid as defined by its NaCl content, temperature, and pressure. The H<sub>2</sub>O-NaCl system changes state depending on these variables. For instance, at a given NaCl concentration in fluid and a given temperature, there is a certain pressure at which the fluid will boil, and from then onwards (with increasing temperature and pressure) the resulting vapour will coexist with NaCl precipitate. As temperature and pressure increase, after a certain threshold the system will develop phase separation, forming a vapour and a brine, and, after the following threshold, there will no longer be any dissociated components, though the fluid will then have changing properties from fluid to vapour-like (Driesner and Heinrich, 2017). However, natural brines and highly saline fluids found in the crust are usually different from single-component systems, and are therefore even more complex, and their physical properties more difficult to predict. Manning and Aranovich (2014) stress the lack of coverage in the literature of components other than NaCl in hydrothermal brines. In addition, filtration and differential transport of fluid components may play a role in the formation of saline solutions to a lesser extent, occurring during the passage of the fluid through grain boundaries (Kullerud, 2000; Kullerud et al., 2001).

Seawater-derived Cl-rich fluids transport elements at very high temperature and react with host minerals during their passage through the oceanic crust while changing their compositional makeup (Coogan et al., 2001). A seawater-derived fluid may become saturated in Cl (brine) after being consumed by contributing to the formation of hydrous minerals (Coogan et al., 2001; Ito & Anderson, 1983). The increase of Cl concentration in fluid occurs with increasing depth, as amphibole vol. % decreases, since the fluid is no longer able to hydrate any more minerals to form new amphibole, and is saturated enough in Cl to incorporate it into wall rock minerals (Ito & Anderson, 1983).

Salinity measurements of hydrothermal vent fluids give values that greatly depart from seawater salinity (Nehlig, 1991; Coumou et al., 2009, and references therein). This evidence suggests that infiltrated seawater reacts with host rocks during percolation through the oceanic crust before exiting at discharge



zones at the seafloor. High salinity of circulating fluids is achieved through different mechanisms, such as desiccation during the passage of the fluid through the oceanic crust, i.e. from the volatilization of seawater-derived fluids, magmatic fluids, or from hydration of wall rock minerals during fluid flow – since OH partitions strongly into the solid phase – resulting in high salinities remaining in the fluid. The main mechanism by which seawater-derived fluids become highly saline - or brine - is phase separation, a mechanism by which a Cl-bearing fluid undergoes unmixing into different fluid phases when affected by changes in temperature and pressure (Manning and Aranovich, 2014; and references therein).

#### **1.4 The role of amphibole in fluid/rock interaction**

Volatile-bearing minerals such as amphiboles can provide essential information on the interaction between fluids and rocks. The study of amphiboles can therefore contribute to our understanding on the cycling of volatiles and volatile budgets on the Earth and other planets (e.g., Sautter et al., 2006, Filiberto & Treiman, 2009; Taylor et al., 2010).

In the oceanic crust – which covers two thirds of our planet – amphibole-bearing assemblages found in oceanic gabbros have the potential to provide information on the record of interaction between seawater-derived fluids and rock down to the base of the oceanic crust near mid-ocean ridges (Manning et al., 1996; Silantyev et al., 2008; Bosch et al., 2004; Nicolas et al., 2003; Coogan et al., 2001; among others). Due to their large range of temperature stability, amphiboles are able to record the whole evolution of hydrothermal systems from the magmatic regime, via the ductile-brittle transition at early stage formation of the oceanic crust (e.g., Bosch et al., 2004, Coogan et al., 2001) down to increasing hydrothermal activity upon progressive brittle deformation in the greenschist and sub-greenschist facies (at temperatures above ca. 300 °C, Alt, 2004), and can provide useful information on the temperature of fluid-rock interactions that formed them (e.g., Ernst and Liu, 1998).

Amphibole has been proven an important Cl reservoir in altered oceanic crust (e.g., Ito et al., 1983; Straub et al. 2003; Zhang et al., 2017a), since the same structural site that can host (OH) groups in amphibole can accommodate other anions such as F or Cl (Vanko et al., 1986; Chan et al., 2016; Oberti et al., 1993). Therefore, by investigating Cl-rich amphiboles found in nature and associated minerals, we can follow the evolution of interactions between lower crustal rocks and seawater-derived chlorine-rich hydrothermal fluids.

It is worth noting that amphibole's wide range of stability covers the transition from the suprasolidus to the subsolidus regime, and is therefore a key phase in the study of high temperature hydrothermal processes that bridge magmatic conditions and low-temperature hydrothermal conditions. Coogan et al. (2001) explain the geochemical differences between amphiboles formed above and below solidus in terms of trace elements, to understand the processes that take place in the progression from the suprasolidus regime to the subsolidus regime in oceanic gabbros. They measured different types of calcium amphiboles from a slow-spreading ridge setting of varying morphology and composition, with Cl contents of up to 0.25 wt. %. However, other occurrences of amphiboles in oceanic gabbro have been shown to contain considerably higher chlorine contents. Ito and Anderson (1983), who studied the alteration of gabbros in a slow-spreading ridge, suggest temperatures from 550 to 750 °C for calcium amphibole formation in the analysed gabbros. They found Cl-bearing amphibole with varying Cl contents, from 0.02 up to 6 wt% Cl, in addition to the occurrence of chlorite and actinolite. Along these lines, Silantyev et al. (2008) describe the alteration of gabbros due to percolation of seawater-derived fluids at slow-spreading mid-ocean ridges after the emplacement of magmatic bodies. They report the formation of calcium amphiboles due to pyroxene hydration, specifically actinolite, edenite and hastingsite, evidencing a large variability in Si-Al and Mg-Fe between the different amphiboles and Cl contents of up to 2 wt. %.

## **1.5 Cl-bearing amphibole formation as a consequence of hydrothermal circulation in the lower oceanic crust**

The Cl content of hydrous minerals has been found to correlate to the Cl content of the fluid with which it was equilibrated (Munoz and Swenson, 1981; Munoz, 1984; Harlov et al., 2002). The higher Cl contents found in amphiboles in the lower oceanic crust at deeper levels vs. the Cl content of amphiboles in the upper oceanic crust (or just shallower levels) reflects the variation of fluid salinity with depth, correlating also with a decrease in water/rock ratio with depth and higher temperature conditions (Bach et al., 2013; Kendrick, 2018).

Compositional changes occurring in amphibole suggest partial equilibration with seawater-derived fluids at different temperatures above and below the gabbro solidus, at different fluid/rock ratios and varying salinities and thus provide evidence for the passage and evolution of fluids through the oceanic crust (e.g., Bosch et al., 2004). This is often expressed by the incorporation of halogens (mainly Cl) in the amphibole structure, substituting the hydroxyl group. Studies on the occurrences of Cl-rich amphiboles in various types of low to high grade metamorphosed and hydrothermally altered rocks have led to the general conclusion that these amphiboles indeed interacted with highly saline fluids (e.g., Vanko, 1986; Kullerud, 1996; Morrison, 1991; Léger et al., 1996; Liu et al., 2009; Enami et al., 1999; McCormick & McDonald, 1999). Variations of the Cl contents in amphibole are considered to record changing gradients in fluid activity ratio ( $a_{\text{Cl}}/a_{\text{OH}}$ ) during mineral growth (Kullerud et al., 2000) and may record changes in the fluid/rock ratio along different stages of fluid interaction. Hydrous minerals preferentially take up OH from circulating hydrothermal fluids more readily than Cl, thus resulting in a progressive increase of Cl in fluid as the fluids react with the host rock and as fluid/rock ratio – and therefore hydrothermal activity – decreases (Kullerud, 1996; Kullerud et al., 2000). Such processes of Cl-enrichment can be considered specifically for the deeper oceanic crust, where the higher pressure largely impedes heat flux induced opening of fluid phase solvi (flushing) and, in case of Cl-bearing fluids, fluid unmixing into low-Cl

vapour and high-Cl liquid or brine (Aranovich et al., 2010). Hence, a seawater-derived fluid may become saturated in Cl (brine) after being consumed by contributing to the formation of hydrous minerals (Coogan et al., 2001; Ito & Anderson, 1983). The increase of Cl concentration in fluid occurs with increasing depth, as the abundance of amphibole decreases, since the fluid is no longer able to hydrate any more minerals to form new amphibole, and is saturated in Cl to an extent that it is able to incorporate it into wall rock minerals (Ito & Anderson, 1983).

Cl-bearing amphiboles form in the presence of highly saline fluids. Thus, varying Cl contents in amphibole record changing gradients in fluid activity ratio ( $a_{\text{Cl}}/a_{\text{H}_2\text{O}}$ ) during mineral growth (Kullerud et al., 2001). Cl in amphibole may evidence the desiccation of a fluid in different stages, since at high fluid/rock ratios Cl tends to be incorporated into the fluid, and at low fluid/rock ratios there is a higher probability of Cl incorporation into the rock in larger amounts (Kullerud, 1996). Cl-bearing amphiboles can also be found as reaction rims of other minerals such as clinopyroxene in altered rocks from the oceanic crust and from eclogites (Vanko, 1986; Liu et al., 2009).

The chlorine content of amphiboles formed in the deep oceanic crust may vary along a range from below several tenths of ppm ( $\mu\text{g/g}$ ) to  $> 5$  wt. % Cl, demonstrating variations in salinity of the reacting fluid (i.e. Wolff, 2014; Vanko, 1986; Coogan et al., 2001; Silantyev et al., 2008). The importance in the progression from the suprasolidus to the subsolidus hydrothermal regime for early Cl-enrichment of lower crustal amphiboles from the Mid-Atlantic Ridge was emphasized by Coogan et al. (2001), based on thermometry and the systematics between Cl, major element, trace element and rare-earth element compositions and F contents in amphiboles. These authors constrained the most Cl-rich amphiboles (containing  $\sim 0.25$  wt. % Cl) to have preferentially formed from gabbro at high-temperatures mainly in a narrow interval from  $\sim 725$  to  $825$  °C closely below the gabbro solidus ( $860 \pm 30$  °C). Other occurrences of amphiboles in oceanic gabbro have been shown to contain considerably higher chlorine contents. Vanko (1986) reported analyses of natural Cl-amphiboles in gabbroic rocks from the Mathematician ridge failed spreading centre

at the East Pacific Rise, with the most Cl-rich amphibole (hastingsite) sample containing 4 wt. % Cl, formed under greenschist facies conditions in association to actinolite within a quartz-epidote matrix that grew in the presence of a highly saline fluid (50 wt. % NaCl) at temperatures of 400-500 °C; whereas hornblendes formed at higher temperature (~ 600 °C) were moderately Cl-rich (0.1 to 0.5 wt. %). Silantyev et al. (2008) describe the alteration of gabbroic rocks due to percolation of seawater-derived fluids in a drill core obtained by the ODP (Ocean Drilling Program) at the Mid-Atlantic Ridge (15°45'N; Hole 1275B). They report the formation of amphiboles due to pyroxene hydration, specifically actinolite, edenite and hastingsite, evidencing a large variability in Si-iv/Al and Mg-Fe between the different amphiboles at fluid/rock ratios throughout 1-10 (determined from Nd and Sr isotope characteristics). Most strikingly, amphiboles formed at higher temperature (500-600 °C) were most Cl-rich with up to 2 wt. % found in hastingsite and ferro-pargasite in altered dolerite. Such Cl-rich amphiboles have also been reported in ophiolites, as is the case of hydrothermally induced dikelets and high-temperature veins hosted in layered gabbro near the crust/mantle transition in the Wadi Wariyah, Samail ophiolite (Oman). In these samples, large variations in Cl content and cation configurations are found even within single zoned amphibole crystals. These zones containing magmatic pargasite (<0.2 wt. % Cl) to metamorphic highly chlorine-rich ferro-pargasite (>5 wt. % Cl), and magnesio-hornblende (Cl= 0.2-2 wt%) suggest partial equilibration of the amphibole with a fluid of changing salinity and variations in fluid/rock ratio, and thus reveal a complex history of hydrothermal cooling in a wide temperature range from ~1000°C down to 450°C (Wolff, 2014; Currin et al., this issue). Based on estimates on the oxygen isotope composition, the formation temperatures of the most Cl-rich amphiboles were estimated to be ~550-650 °C (Wolff, 2014). Calculated water/rock ratios were 0.2-0.5 for layered gabbro, 0.4-6 for amphibole-rich veins formed at 900-1000, and 0.7-15.2 for epidote veins formed at lower temperature (300-500 °C).

## 1.6 Occurrence of Cl-bearing amphiboles

Amphiboles containing chlorine have been found in a wide range of lithologies and geological settings including metamorphosed gabbroic rocks (Vanko, 1986; Kullerud, 1996), granulite facies gneisses (Morrison, 1991; Léger et al., 1996), retrograde metamorphism of eclogites (Liu et al., 2009), metasandstone and metabasite associated to active geothermal systems (Enami et al., 1999), or related to Ni-Cu mineralization (McCormick & McDonald, 1999). The study of such occurrences using thermobarometry has led to the general agreement that the genesis of Cl-bearing amphibole occurs mainly during metamorphism in the presence of a highly saline fluid at amphibolite or greenschist facies conditions, in a high temperature hydrothermal setting.

The aforementioned studies have shed light on the range of formation temperatures for hydrothermal Cl-bearing amphiboles – using thermobarometry of natural occurrences and experiments – which may be found between 500 and 850 °C. Given such a wide range, other variables such as fluid composition, Cl activity, oxygen fugacity, cation composition and starting mineral assemblage probably exert a greater influence on the formation of Cl amphibole.

Volfinger et al. (1985) applied his observations on the incorporation of Cl in biotite to amphibole. He found that Cl accommodation is favoured by cation configurations that also allow for a large opening in the A site, not only in the W site. Thus, according to these authors, the cation arrangement in biotite that favours Cl incorporation also does so for K – which is larger than Na – thus fitting better to an enlarged A site.

## **1.7 Previous experimental studies**

Previous experimental studies have focussed on the action of hydrothermal fluids in the context of the lower oceanic crust and in the presence of Cl-rich brines or highly saline fluid, in some cases involving amphibole. Several investigations conducted experiments in the supra-solidus regime involving partial melting triggered by Cl-enriched fluid (Koepke et al., 2004; 2007; Khodorevskaya and Aranovich, 2016; Sato et al., 2005; Wolff et al., 2013). Other experimental studies investigated the incorporation of Cl into amphibole in the sub-solidus regime using synthetic starting oxides (Chan et al., 2016; Mueller et al., 2017). Mueller et al. (2017) formed experimental ferropargasite with Cl contents up to 1.7 wt. %, at temperatures of 650 to 850 °C.

## **1.8 Aims of this study**

The main aim of the present study is to characterize amphibole compositions from high-T veins and dikes found in layered gabbro and perform experiments focussed on Cl-rich amphibole formation to study the interaction between seawater-derived brines and lower oceanic crustal rocks at temperatures between 500 and 900 °C.

The first part of the study (chapter 2) features the analysis of amphibole phases formed at different conditions above and below solidus, occurring in veins and dykelets that crosscut layered olivine gabbro in the Wadi Wariyah, Samail Ophiolite, using petrographic, microanalytical (EPMA), isotopic (Sr and O), and structural methods (EBSD). The aim of this part of the study is to describe the compositional and structural differences between amphiboles formed at different conditions and discuss the origin of the hydrothermal fluids involved in their alteration.

The second part of this work (chapter 3) includes the experimental simulation of the interaction of seawater-derived fluids with gabbroic rocks in the deep oceanic crust, in order to investigate the role of fluids in the alteration of the lower oceanic crust, typically consisting of gabbro. Temperatures from 900 °C to 500 °C were applied, covering the interval from the partial molten state into the metamorphic regime down to greenschist facies conditions. The main focus of these experiments is the compositional variation of amphiboles, which were obtained in all runs, as a function of temperature and salinity of the fluid. Due to the direct approach of using only gabbro and fluid as starting material at a pressure of 200 MPa – corresponding to the base of the oceanic crust – these experiments are highly relevant to natural fluid/rock interactions in the deep oceanic crust, and our experimental results can thus be directly applied to nature. An additional aspect of this study is to investigate the possibility of incorporation of Cl into the amphibole structure, as a response to experimental parameters, and to highlight the crystalchemical constraints for Cl substitution.

## **1.9 Outline of the study**

This study is made up of two parts: an analysis of amphibole-rich high-temperature hydrothermal veins and dykelets hosted in olivine gabbro samples from Wadi Wariyah (Samail Ophiolite) with EPMA, Sr and O isotope analyses, and EBSD (chapter 2); and an experimental part including hydrothermal experiments with natural starting materials to simulate the processes that formed the hydrothermal amphibole found in the natural samples. The following two chapters of this PhD thesis have been submitted for publication in the peer-reviewed journal *Lithos* in a similar form.



## **2 Chlorine-rich amphibole in deep layered gabbros as evidence for brine/rock interaction in the lower oceanic crust: a case study from the Wadi Wariyah, Samail Ophiolite, Sultanate of Oman**

### **2.1 Introduction**

This chapter focuses on high temperature hydrothermal veins and gabbroic dykelets hosted in the layered gabbro section of the Samail Ophiolite that contain different types of amphibole. The main focus is to explore the influence of fluids on amphibole genesis at depth, as well as determine the origin of the fluids reacting with the lower oceanic crust by using Sr and O isotopic analysis.

Studies done on ophiolites associated to mid-ocean ridge systems can provide insight into processes analogous to those occurring in the oceanic crust. For instance, Nicolas et al. (2003) describe the infiltration pathways of seawater into gabbros of the lower crust of the Samail ophiolite (Oman) down to its base and at about 1 km off the ridge axis. The corresponding successive alteration sequence of these gabbros is described by Bosch et al. (2004), who concluded – supported by strontium and oxygen isotopic data – that the alteration followed deep penetration of seawater-derived fluids from very high temperatures at low water/rock ratios (3-5) at the transition between magmatic and metamorphic processes (starting above 975 °C), and well into subsolidus conditions (500 °C) with increasing hydrothermal activity (fluid/rock ratios >10).

### **2.2 Analytical techniques**

Polished thin sections of the rock samples were made of the hydrothermal veins and dykelets and areas around them. Mineral major element compositions were determined in situ using a Cameca SX100 electron microprobe equipped with 5 spectrometers and the “Peak Sight” software at the Institute of

Mineralogy of the Leibniz University Hannover, Germany. A focussed beam current of 15nA and an acceleration voltage of 15kV were used to analyse all minerals. Counting time for minerals was 10s for peak and 5s for background, but was longer for Cl and F (30s at peak). Elemental measurements were calibrated using the following natural and synthetic standards: albite (Na), wollastonite (Ca and Si), orthoclase (K), Durango apatite (P), Al<sub>2</sub>O<sub>3</sub> (Al), Mn<sub>2</sub>O<sub>3</sub> (Mn), TiO<sub>2</sub> (Ti), MgO (Mg), Fe<sub>2</sub>O<sub>3</sub> (Fe), NaCl (Cl), and SrF<sub>2</sub> (F). In order to monitor analytical precision, each measurement was checked against the following international mineral standards (reference materials): Lake County plagioclase (USNM 115900), Kakanui hornblende (USNM 143965), Kakanui augite (USNM 122142), San Carlos Olivine (NMNH 111312-44), (Jarosewich et al. 1980). Detection limits (in wt. %) in amphibole were: SiO<sub>2</sub>: 0.03; TiO<sub>2</sub>: 0.02; Al<sub>2</sub>O<sub>3</sub>: 0.03; FeO: 0.09, MnO: 0.05; MgO: 0.04; CaO: 0.04, NaO: 0.05; K: 0.015; Cr: 0.07; Cl: 0.007; F: 0.04. Representative values for measured amphiboles are listed in table 2.1.

<sup>87</sup>Sr/<sup>86</sup>Sr radiogenic isotope analyses of amphiboles, whole vein and whole dykelet samples were performed at the University of Southampton by thermal ionisation mass spectrometry (TIMS) using a ThermoFisher Scientific TritonPlus. Mineral separates were crushed and digested using a standard HF-HNO<sub>3</sub> acid attack, mother solutions were prepared (Zihlmann et al., this issue) and bulk trace element compositions were measured from diluted daughter solutions, using a ThermoScientific X-Series 2 ICP-MS adjusted for REE measurements prior to isotope analysis. Strontium spec<sup>™</sup> columns were then used to separate Strontium from dissolved samples (Harris et al., 2015). The Sr concentrate was loaded onto degassed tantalum filaments for analysis by TIMS. Good internal precision was ensured by measuring 150 ratios per sample and presented as given as two standard errors. The <sup>87</sup>Sr/<sup>86</sup>Sr ratio of standard reference material NBS987 was measured as a monitor of external precision. Over the duration of the analyses returned 0.710247 ± 0.000023 (2σ); n = 53).

The oxygen isotopic compositions of the same mineral separates as used for Sr-isotopes were determined by Actlabs (Activation Laboratories Ltd., Ancaster, Ontario, Canada). Oxygen was extracted from 5 mg samples at 550-600 °C according to the conventional BrF<sub>5</sub> procedure of Clayton and Mayeda (1963) and analyzed via dual inlet on a Thermo-Finnigan DeltaPlus XP Isotope-Ratio Mass Spectrometer (IRMS). Results are calibrated to certified reference materials, relative to the VSMOW and VSLAP international standards. Precision and accuracy (standard deviation) are of 0.1‰.

Electron backscattered diffraction (EBSD) analyses were performed at the facilities of Montpellier University, France using a CamScan X500FE CrystalProbe with an Oxford/HKL EBSD system. This equipment allows for high resolution EBSD measurements (10-50 nm) and includes Energy Dispersive Spectrometry (EDS). The EBSD software used is AZtecHKL by Oxford Instruments for data acquisition and the Matlab-based code MTEX for analysis (see Ferrando et al., 2018).

## **2.3 Results**

### **2.3.1 Outcrop description and Petrography**

The rocks cropping out in Wadi Wariyah (N 22°58'51.49", E 58°15'53.98") mainly consist of layered gabbro, crosscut by hydrothermal veins and cm-scale gabbroic dykelets, and are representative of deep oceanic crust, with rocks sampled ~ 100 m above the Moho transition zone (MTZ) (Fig. 2.1). Magmatic layering in the gabbros is approximately perpendicular to the strike of the overlying sheeted dykes in the area. The vein system displays a large variety of gabbroic dykelets and hydrothermal veins with different mineral fillings (Wolff, 2014), including dykelets of several cm in width, mostly cutting the gabbro layering at high angles. These dykelets connect to each other in a system of branches (branched

connectivity), and contacts, although sharp, do not show chilled margins. A second type of feature are thin, black to dark green veins up to 4 mm wide that probably formed from the filling of microcracks, parallel to the gabbroic dykelets. These veins have sharp contacts to the host gabbro. The gabbroic dykelets and dark veins are clustered in several cm-wide swarms with single dykelets and veins spaced every few cm within the swarms, and swarms are spaced up to several metres apart. A third type of hydrothermal veins are white veins dominated by epidote/clinozoisite and/or prehnite that formed at lower temperatures. These white veins cross-cut the aforementioned dark veins and gabbroic dykelets. For details of this outcrop including images see Wolff (2014) and Bosch et al. (2004). This study includes data from dark veins (2 samples; Fig. 2.2A, C) and gabbroic dykelets (5 samples; Fig. 2.2B, D).

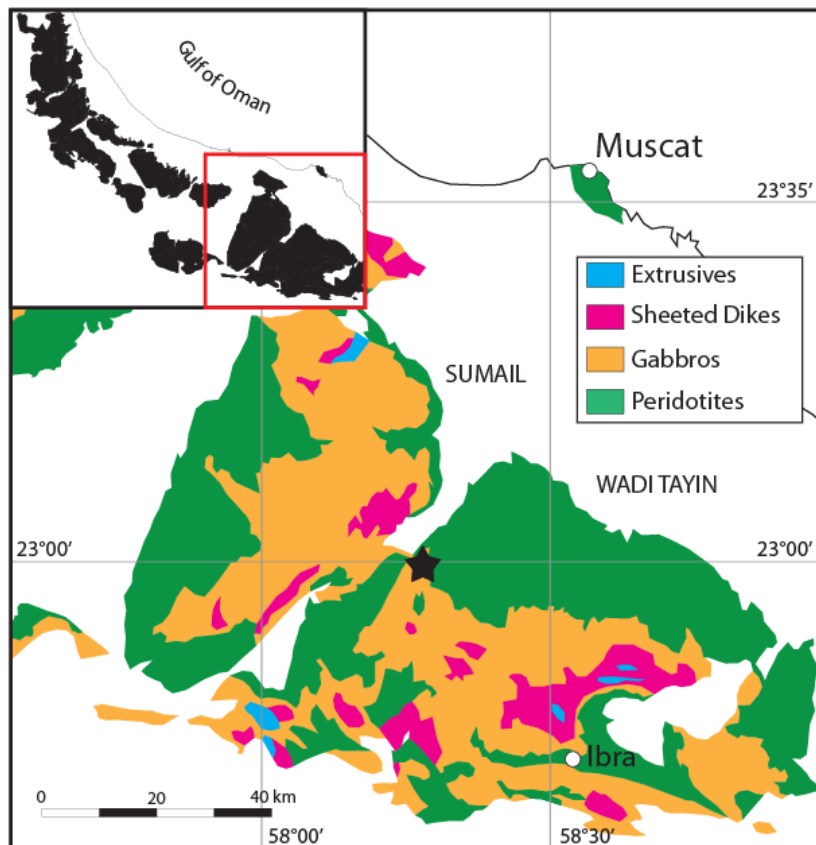


*Figure 2.1. Map of sampling location in Wadi Wariyah (star), in Wadi Tayin Massif, Samail Ophiolite, Sultanate of Oman, modified after Nicolas et al. (2000).*

### 2.3.1.2 Petrography

The host rock is a layered olivine gabbro displaying a magmatic foliation and comprising olivine, clinopyroxene, and plagioclase, with small amounts of Fe-Ti oxides and orthopyroxene. The average grain size of the host rock minerals is ~1.5 mm. The veins contain different types of amphiboles (pargasite, magnesiohastingsite, magnesiohornblende, actinolite, hastingsite and ferropargasite), and some of them are highly enriched in chlorine (table 2.1).

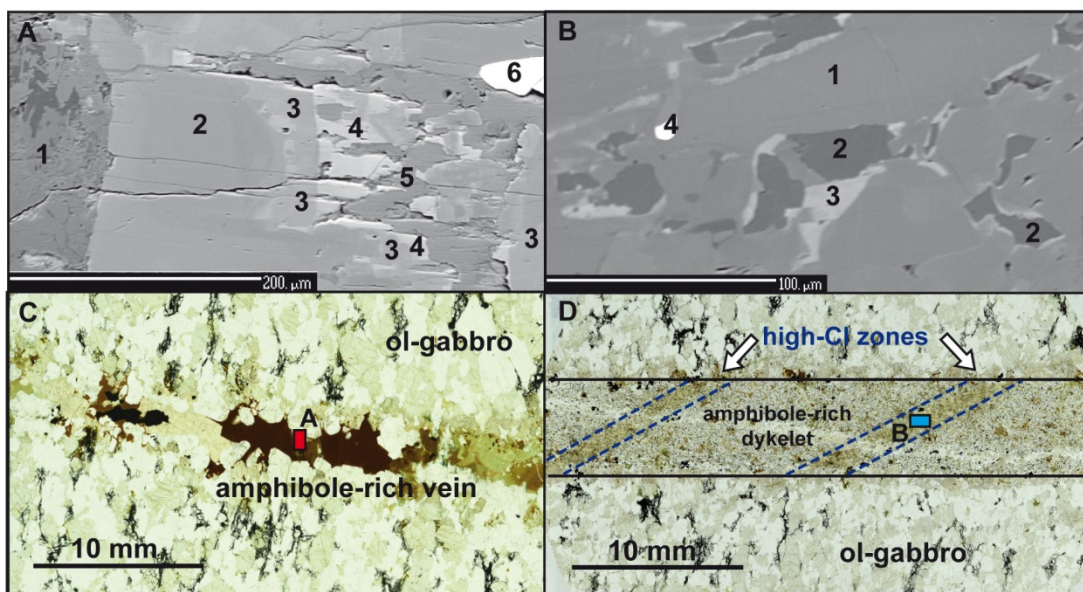


**Figure 2.2.** BSE image showing the area marked in red in thin section C (sample WA02) showing a zoned amphibole. This is the same area selected for a compositional profile (Fig. 2.4). 1: plagioclase, 2: high-Ti pargasite, 3: magnesiohornblende to actinolite, 4: Cl-rich ferropargasite, 5: secondary calcite, 6: Fe-Ti oxides. B: BSE image showing the area marked in blue in thin section D (sample WA42). 1: pargasite, 2: plagioclase, 3: Cl-pargasite, 4: Fe-Ti oxides. C: thin section of layered olivine gabbro crosscut by an amphibole-rich hydrothermal vein (sample WA02). D: thin section of layered olivine gabbro crosscut by a fine-grained amphibole-rich gabbroic dykelet that is, in turn, crosscut by two oblique Cl-rich pargasite zones (sample WA42).

Specimens WA02 and WA05 were sampled from a high temperature hydrothermal vein containing mainly high-Ti pargasite (Ti >4 wt. %). Some pargasite grains are zoned and show within a single grain the transition from magmatic pargasite via amphibolite-facies magnesiohastingsite and magnesiohornblende to greenschist facies actinolite, and locally, areas with Cl-rich ferropargasite and hastingsite with chlorine contents of up to 5.4 wt. % (1.2 a.p.f.u.; atoms per formula unit) (Fig. 2.3). In sample WA02, the grain size of the vein minerals is an average of 2 mm. The magmatic minerals that make up the gabbroic dykelet mainly have large grain sizes of about 2 to 3 mm. However, alteration zones within amphibole have grain sizes down to  $\sim 5 \mu\text{m}$ .

Specimens WA42, WA04, WA33, WA46, and WA32A are samples of gabbroic dykelets that cut the layering of the host rock layered olivine gabbros as high angles. The gabbroic dykelets display poikilitic to fine-grained granular textures. Typically, anhedral, mm-sized brown pargasitic amphibole forms poikilitic clusters, enclosing lath-shaped plagioclase chadacrysts and uncommon granular olivine, commonly associated with FeTi-oxides. Some plagioclase laths in the groundmass show swallowtail-shapes indicating a rapid cooling during formation. The amphiboles in these dykelets are of different types: Brown high-Ti pargasite and magnesiohastingsite (commonly poikilitic), green amphibole (mainly magnesiohornblende) replacing brown pargasite, and local occurrences of a distinctive bluish-green Cl-rich amphibole (WA04 & WA42: Cl-rich pargasite; WA32A: Cl-rich hastingsite). Microveins of green amphibole and amphibole overgrowths (hornblende and actinolite) in these dykelets are common. Sample WA42 displays chlorine-rich amphibole grains concentrated along two elongated and parallel amphibole-rich, high-Cl zones, formed oblique to the margins of the dykelet (Fig. 2.2). The high-Ti pargasites can have grain sizes of up to  $150 \mu\text{m}$  whereas the other amphiboles have grain sizes between 10 to  $50 \mu\text{m}$ . Serpentinite minerals occur locally as secondary phases reflecting a later stage of hydrothermal alteration.

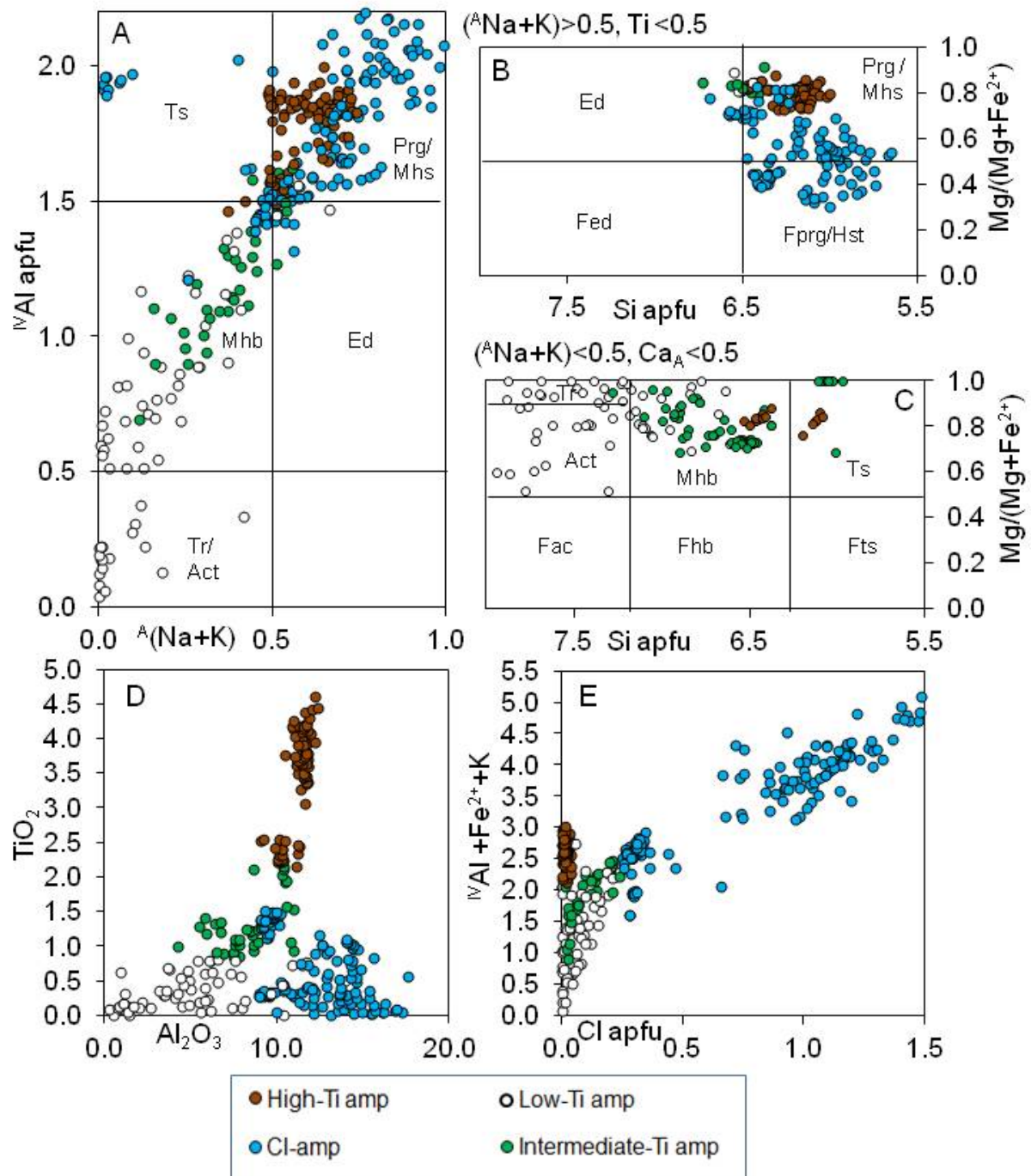


**Figure 2.3.** Compositional diagrams for measured amphiboles. A:  $(Na+K)$  vs.  $Al$ ; B: Si a.p.f.u. vs.  $Mg\#$  ( $Mg/(Mg+Fe^{2+})$ ), with  $(Na+K) > 0.5, Ti < 0.5$ ; C: Si a.p.f.u. vs.  $Mg\#$  ( $Mg/(Mg+Fe^{2+})$ ), with  $(Na+K) < 0.5, Ca_A < 0.5$ ; D:  $Al_2O_3$  vs.  $TiO_2$ ; E: Cl a.p.f.u. vs.  $Al+Fe^{2++K}$ . Abbreviations after Whitney et al. (2010): Ts, tschermakite; Mhs, magnesiohastingsite; Prg, pargasite; Mhb, magnesiohornblende; Tr, tremolite; Act, actinolite; Fed, ferro-edenite; Fprg, ferropargasite; Hst, hastingsite; Fac, ferro-actinolite; Fts, ferrotschermakite; Fhb, ferrohornblende.



Table 2.1. EPMA analyses of amphiboles from Wadi Wariyah (representative analyses).

Sample name	Temp. (°C) <sup>a)</sup>	Amph. Name <sup>b)</sup>	wt %													T position <sup>c)</sup>													C position						B position						A position						W position					
			SiO <sub>2</sub>	TiO <sub>2</sub>	Al <sub>2</sub> O <sub>3</sub>	Cr <sub>2</sub> O <sub>3</sub>	MnO <sup>d)</sup>	FeO <sup>d)</sup>	MgO	CaO	Na <sub>2</sub> O	K <sub>2</sub> O	Cl	F	Total	Si	Al	Ti	Al	Cr	Fe <sup>3+</sup>	Mn <sup>2+</sup>	Fe <sup>2+</sup>	Mg	Mg	Ca	Na	Na	K	Cl	OH	F	Mg#																			
WA02	545	Hs	39.74	0.3	9.35	0	0.15	23.17	7.09	11.67	1.9	1.05	4.33	0.22	98.97	6.37	1.63	0.04	0.14	0.60	0.02	2.51	1.70	0.00	2.00	0.00	0.59	0.22	1.18	0.71	0.11	40.3																				
WA02	660	Mhb	48.65	0.89	6.92	0.07	0.08	10.09	16.34	11.98	1.5	0.21	0.28	0.12	97.13	7.00	1.00	0.10	0.17	0.49	0.01	0.73	3.50	0.00	1.85	0.15	0.26	0.04	0.07	1.88	0.06	82.8																				
WA02	867	Ts	44.64	2.26	10.15	0	0.13	9.81	15.46	11.49	2.26	0.4	0.08	0.13	96.81	6.47	1.53	0.25	0.21	0.55	0.02	0.64	3.34	0.00	1.79	0.22	0.42	0.07	0.02	1.92	0.06	83.9																				
WA02	751	Mhb	44.79	1.43	9.48	0.06	0.08	13.89	13.22	11.77	2.05	0.25	1.19	0.16	98.37	6.58	1.42	0.16	0.22	0.01	0.53	0.01	1.17	2.90	0.00	1.85	0.15	0.44	0.05	0.30	1.63	0.07	71.2																			
WA02	1008	Mhs	42.74	3.96	12.17	0.06	0.13	10.67	14.27	11.64	2.62	0.24	0.06	0.08	98.64	6.15	1.86	0.43	0.21	0.01	0.43	0.02	0.86	3.06	0.00	1.79	0.21	0.52	0.05	0.01	1.95	0.04	78.1																			
WA05	716	Mhb	49.08	1.21	6.77	0.01	0.18	8.84	17.32	11.90	1.50	0.08	0.19	b.d.	97.08	6.99	1.02	0.13	0.12	0.00	0.58	0.02	0.48	3.67	0.00	1.81	0.19	0.23	0.01	0.05	1.95	88.5																				
WA05	768	Mhs	43.45	1.54	10.95	0.03	0.05	10.21	14.78	11.98	2.43	0.14	0.79	b.d.	96.35	6.41	1.59	0.17	0.31	0.00	0.43	0.01	0.83	3.25	0.00	1.89	0.11	0.59	0.03	0.20	1.80	79.7																				
WA04	488	Prg	40.66	0.03	12.11	0.00	0.10	16.93	9.84	11.96	1.86	0.68	4.04	b.d.	98.21	6.30	1.70	0.00	0.51	0.51	0.01	1.68	2.27	0.00	1.99	0.01	0.54	0.14	1.06	0.94	57.5																					
WA04	630	Mhs	44.14	0.73	11.51	0.10	0.12	9.69	15.36	12.45	2.35	0.06	0.96	b.d.	97.46	6.42	1.58	0.08	0.39	0.01	0.47	0.01	0.71	3.33	0.00	1.94	0.06	0.60	0.01	0.24	1.76	82.5																				
WA04	1013	Prg	42.00	4.07	11.95	0.43	0.18	9.45	14.18	11.65	2.84	0.20	0.03	0.07	97.07	6.16	1.84	0.45	0.22	0.05	0.17	0.02	0.99	3.10	0.00	1.83	0.17	0.64	0.04	0.01	1.96	0.03	75.8																			
WA32	537	Fe-Prg	38.23	0.26	12.14	0.05	0.09	22.12	6.31	12.22	2.16	0.84	5.18	b.d.	99.61	6.15	1.85	0.03	0.46	0.01	0.26	0.01	2.72	1.51	0.00	2.00	0.00	0.68	0.17	1.41	0.59	35.7																				
WA32	523	Mhb	50.45	0.19	5.46	0.05	0.23	12.54	14.80	12.78	0.62	0.03	0.32	b.d.	97.48	7.30	0.70	0.02	0.23	0.01	0.27	0.03	1.24	3.19	0.00	1.98	0.02	0.16	0.01	0.08	1.92	72.0																				
WA32	547	Mhb	46.82	0.31	9.67	0.00	0.04	8.99	17.17	11.58	2.13	0.10	0.26	b.d.	97.08	6.64	1.36	0.03	0.26	0.90	0.01	0.17	3.63	0.00	1.76	0.24	0.35	0.02	0.06	1.94	95.6																					
WA33	1025	Mhs	41.16	4.45	12.40	0.05	0.15	9.82	14.32	11.45	3.16	0.11	0.01	b.d.	97.08	6.02	1.98	0.49	0.16	0.01	0.33	0.02	0.87	3.12	0.00	1.80	0.21	0.69	0.02	0.00	2.00	78.1																				
WA42	582	Prg	38.85	0.48	14.60	0.06	0.09	16.79	9.21	11.97	2.43	0.61	4.18	b.d.	99.27	5.99	2.01	0.06	0.64	0.01	0.45	0.01	1.72	2.12	0.00	1.98	0.02	0.70	0.12	1.09	0.91	55.2																				
WA42	642	Mhb	48.64	0.79	7.60	0.07	0.09	7.05	18.91	12.71	1.58	0.08	0.30	0.07	97.91	6.84	1.16	0.08	0.10	0.01	0.60	0.01	0.23	3.97	0.00	1.92	0.08	0.35	0.02	0.07	1.90	0.03	94.6																			
WA42	672	Ts	42.77	0.96	14.68	0.13	0.11	11.82	14.77	10.67	0.59	0.08	1.22	0.12	97.90	6.07	1.93	0.10	0.52	0.02	1.40	0.00	2.95	0.18	1.62	0.16	0.00	0.01	0.29	1.66	0.05	100.0																				
WA42	982	Mhs	42.42	3.48	11.61	0.10	0.13	10.19	15.42	12.01	3.00	0.13	0.02	0.05	98.57	6.10	1.90	0.38	0.07	0.01	0.51	0.02	0.71	3.31	0.00	1.85	0.15	0.69	0.02	0.01	1.97	0.02	82.3																			
WA46	558	Mhb	52.34	0.37	5.54	0.00	0.23	11.89	16.44	12.10	0.57	0.04	0.08	b.d.	97.59	7.44	0.56	0.04	0.04	0.60	0.03	0.82	3.49	0.00	1.84	0.16	0.00	0.01	0.02	1.98	81.0																					
WA46	900	Ts	44.63	2.55	9.20	0.06	0.18	11.82	14.62	11.24	1.91	0.69	0.15	b.d.	97.04	6.50	1.50	0.28	0.08	0.01	0.68	0.02	0.76	3.17	0.00	1.75	0.25	0.29	0.13	0.04	1.96	80.8																				

<sup>a)</sup> Temperatures calculated with Ti-in-hornblende thermometry (Ernst and Liu, 1998)

<sup>b)</sup> According to mineral abbreviations by Whitney and Evans (2010). Prg: pargasite; Hst: hastingsite; Mhb: magnesio-hornblende; Mhs: magnesio-hastingsite; Ts: tschermakite.

<sup>c,d)</sup> FeO = FeO<sup>total</sup>; MnO = MnO<sup>total</sup>

<sup>e)</sup> Amphibole positions in the structure according to Leocock (2014).

<sup>f)</sup> b.d.: below limit of detection

Values for the structural formula are atoms per formula unit (a.p.f.u.), calculated using a sum of 13 cations excluding Ca, Na, K.



### 2.3.2 Amphibole compositions (major and minor elements)

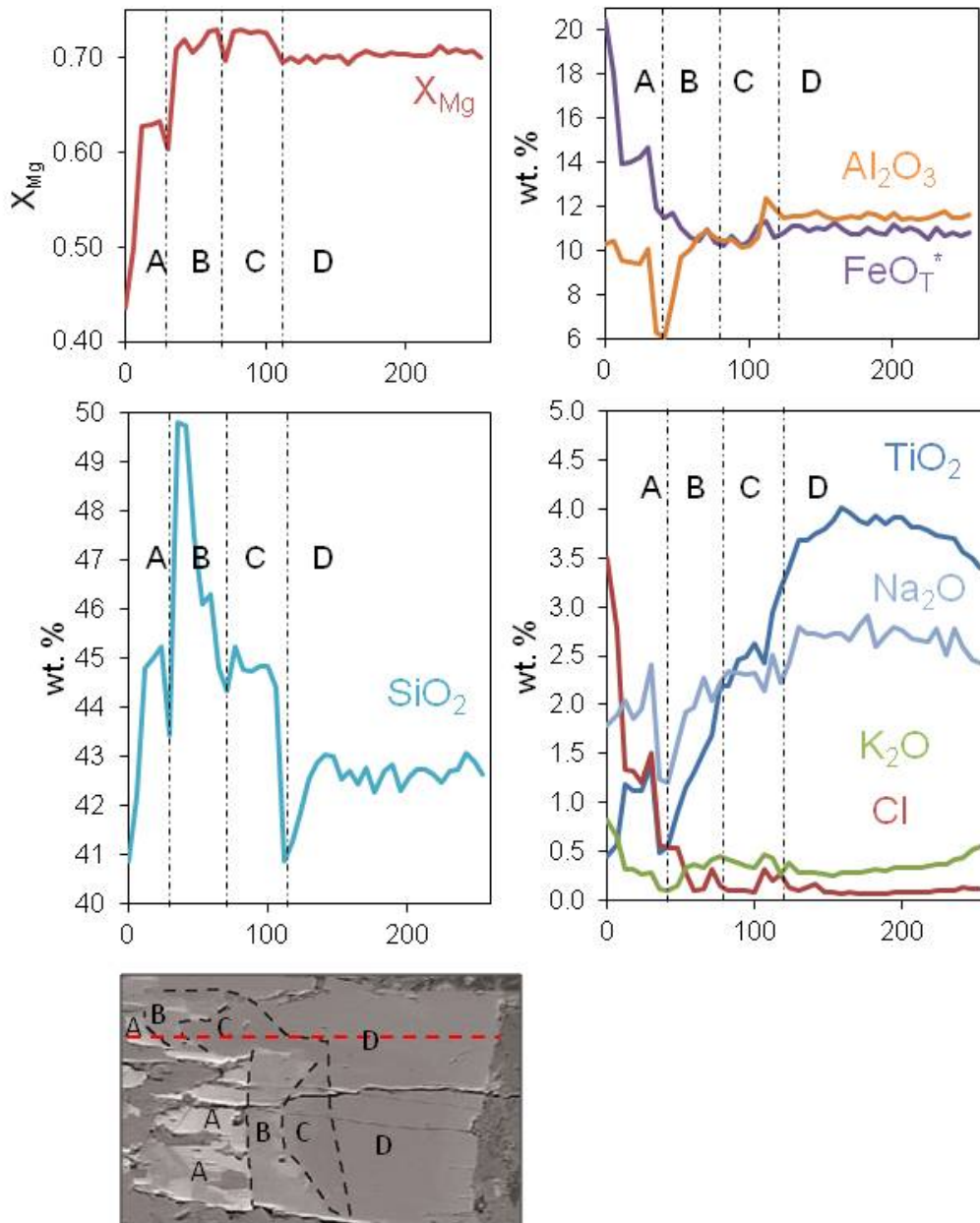
Major element and isotopic (Sr, O) data were obtained from the sampled hydrothermal veins and gabbroic dykelets cutting the gabbros from Wadi Wariyah. Amphiboles measured in both veins and dykelets display similar compositional characteristics, with their main differences being textural with the gabbroic dykelets generally having finer grained amphibole.

The analysis of different amphibole types including magmatic and hydrothermal amphibole shows a large range of compositions (table 2.1). High-Ti pargasites and magnesiohastingsites of magmatic origin have high <sup>iv</sup>Al contents (1.5 to 1.9 a.p.f.u). A-site occupancy (Na + K) in this group of amphiboles ranges from 0.37 to 0.74, with total Na of 0.5 to 0.9 a.p.f.u. and K < 0.1 a.p.f.u. TiO<sub>2</sub> contents are between 2.1 wt. % and 4.6 wt. %, and Cl contents range from 0.01 to 0.16 wt. % Cl (0.01 to 0.04 a.p.f.u.), with no apparent correlation between Cl content and <sup>iv</sup>Al, Fe<sup>2+</sup> and K (Fig. 2.3). Formation temperatures calculated for these amphiboles using Ti-in-amphibole thermometry (Ernst and Liu, 1998) range from 850 to 1030 °C.

Pargasite, magnesiohastingsite, and edenite occurring in the gabbroic dykelets and veins are light brown to green and formed by high temperature hydrothermal alteration. This group of amphiboles has <sup>iv</sup>Al contents ranging from 0.7 to 1.6 a.p.f.u. A-site occupancy (Na + K) ranges from 0.12 to 0.61, with total Na of 0.26 to 0.7 a.p.f.u. and K < 0.1 a.p.f.u. These amphiboles have TiO<sub>2</sub> contents between 0.75 and 2.5 wt. %, and Al<sub>2</sub>O<sub>3</sub> contents between 4 and 11 wt. %. Cl concentrations range from 0.05 to 1 wt. % (<0.25 a.p.f.u.). There's an overall trend of increasing <sup>iv</sup>Al, Fe<sup>2+</sup> and K with increasing Cl from a.p.f.u. 0.05 (0.2 wt. %) onwards. Below this Cl concentration there is no correlation between Cl content and <sup>iv</sup>Al, Fe<sup>2+</sup> and K (Fig. 2.3). Temperatures calculated for these amphiboles range from 650 °C to 850 °C (Ti in amphibole thermometer) corresponding to the transition between magmatic and amphibolites facies metamorphic conditions.

Blue-green amphiboles have high concentrations of Cl (contents above 1 wt. %) and occur as rims around other amphibole grains or as fine-grained crystals. They are low in Si and high in <sup>iv</sup>Al compared to other amphiboles with lower Cl contents. Tetrahedral Al contents range from 1.2 to 2.3 a.p.f.u. They are mainly classified as Cl-bearing pargasite, Cl-bearing magnesiohastingsite, Cl-bearing hastingsite and Cl-bearing ferropargasite (Fig. 2.3). A-site occupancy (Na + K) ranges from 0 to 1, with a total Na content of 0.16 to 0.85 a.p.f.u. and K of 0.01 to 0.24 a.p.f.u. TiO<sub>2</sub> contents are below 1.5 wt. %, and Al<sub>2</sub>O<sub>3</sub> above 9 wt. %. Cl contents in this group of amphiboles ranges from 1 wt. % up to 5.4 wt. % (1.5 a.p.f.u. Cl). There is an overall trend of increasing <sup>iv</sup>Al, Fe<sup>2+</sup> and K with increasing Cl. Formation temperatures for these amphiboles, calculated using Ti in amphibole thermometry, range from 484 to 765 °C. The higher Cl contents (> X wt% Cl) occur in grains formed at temperatures below 650 °C (see table 2.1) indicating that the Cl-rich amphiboles formed in the amphibolite to greenschist facies metamorphic conditions.

Green actinolite, tremolite and magnesiohornblende form overgrowths over pargasite and magnesiohastingsite. These overgrowths are high in Si and low in <sup>iv</sup>Al compared to other amphiboles described in this section. Tetrahedral Al contents range from 0 to 1.6 a.p.f.u. Total Na ranges from 0 to 0.7 a.p.f.u., with K < 0.04 a.p.f.u. TiO<sub>2</sub> contents are found below 1 wt. %, and Al<sub>2</sub>O<sub>3</sub> generally below 8 wt. %. Maximum Cl content is of 0.25 a.p.f.u. (1 wt. %). There is an overall trend of increasing <sup>iv</sup>Al, Fe<sup>2+</sup> and K with increasing Cl from a.p.f.u. 0.05 (0.2 wt. %) onwards. Below this value, there is no apparent trend (Fig. 2.3). Formation temperatures for these amphiboles are estimated between 484 °C and 646 °C from Ti in amphibole thermometry, indicating hydrothermal alteration at amphibolite to greenschist facies conditions.



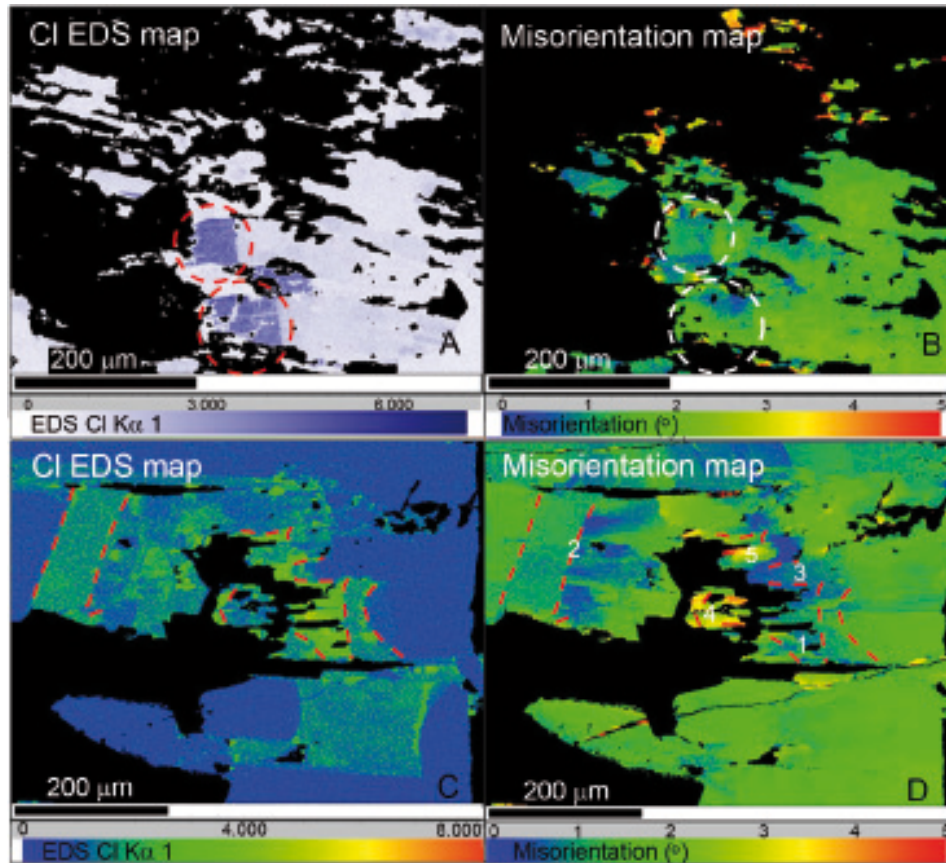
**Figure 2.4.** Profile through an amphibole grain in sample WA02, ranging from magmatic high-Ti pargasite (D), through magnesiohornblende (C) and actinolite (B) to Cl-rich ferropargasite (A). Dashed and dotted black lines showing changes in amphibole zoning.

Fig. 2.4 shows a typical situation of amphibole grain, displaying zoning, with each zone formed under different conditions. This compositional profile through a zoned amphibole grain from a hydrothermal vein hosted in layered gabbro (sample WA02) is an example of the stepwise alteration of an amphibole grain by different episodes of interaction with hydrothermal fluids or brines. This profile shows (A) a Cl-hastingsite zone (Cl contents up to 3.5 wt%) with low silica content and high aluminum, as well as noticeably high total Fe and low Ti, corresponding to metamorphic conditions (amphibolite to greenschist facies); (B) a low-T actinolite zone (greenschist facies); (C) a magnesiohornblende zone with intermediate Cl contents (0.2 to 1 wt%) with higher Si content and poor in Ti (amphibolites facies); and (D) a zone of brown high-Ti pargasite formed at magmatic conditions and resulting from hydrous partial melting.

### 2.3.3 EBSD analyses

To determine whether Cl-rich and Cl-poor amphiboles have the same orientation, we obtained EBSD maps of areas containing amphiboles with different compositions, and compared the misorientations in a chosen area with the Cl-concentration map (EDS) of the same area (Fig. 2.5). Misorientations observed in zoned amphibole in relation to a point selected in a Cl-rich area (>3 wt. % Cl) are of 1 to 2° (Fig. 2.5, Mis2Mean map). Area 1 in Fig. 2.5D shows a misorientation boundary line with the same shape as the boundary between different domains of high and low Cl concentrations (Fig. 2.5C). This is also the case of the area circled in figures 2.5A and B, where changes in Cl content coincide with misorientations.

Point 2 in Fig. 2.5D shows a misorientation boundary line that coincides with a change in Cl content in Fig. 2.5C. In contrast, point 3 in Fig. 2.5D shows only a gradual change in misorientation, but a more pronounced change in Cl content in Fig. 2.5C. Points 4 and 5 highlight areas where there is no relationship between the misorientation map (Fig. 2.5D) and distribution of Cl concentrations (Fig. 2.5C).



*Figure 2.5. Chlorine EDS maps (A & C) and EBSD misorientation maps of areas in sample WA02. Chlorine maps highlight the areas most enriched in Cl (A: purple, C: bright green). In contrast with EBSD misorientation maps (B & D) we can figure out if there are differences in orientation, grain boundaries or dislocations between Cl-rich areas and Cl-poor areas of the amphibole.*

## 2.3.4. Isotopic data

### 2.3.4 Isotope analyses

#### 2.3.4.1 Sr isotopes

$^{87}\text{Sr}/^{86}\text{Sr}$  radiogenic isotope analyses were carried out on amphiboles from both gabbroic dykelets and dark veins. We divided our samples into three groups: dark brown amphiboles (high-Ti pargasite and

magnesiohastingsite) formed at magmatic temperatures >850 °C, green and blue-green amphiboles (magnesiohornblende and actinolite, and Cl-rich ferropargasite and hastingsite) formed at subsolidus temperatures between 550 and 750 °C, and whole rock samples (dark vein and gabbroic dykelet samples) (Fig. 2.6; Table 2.2).

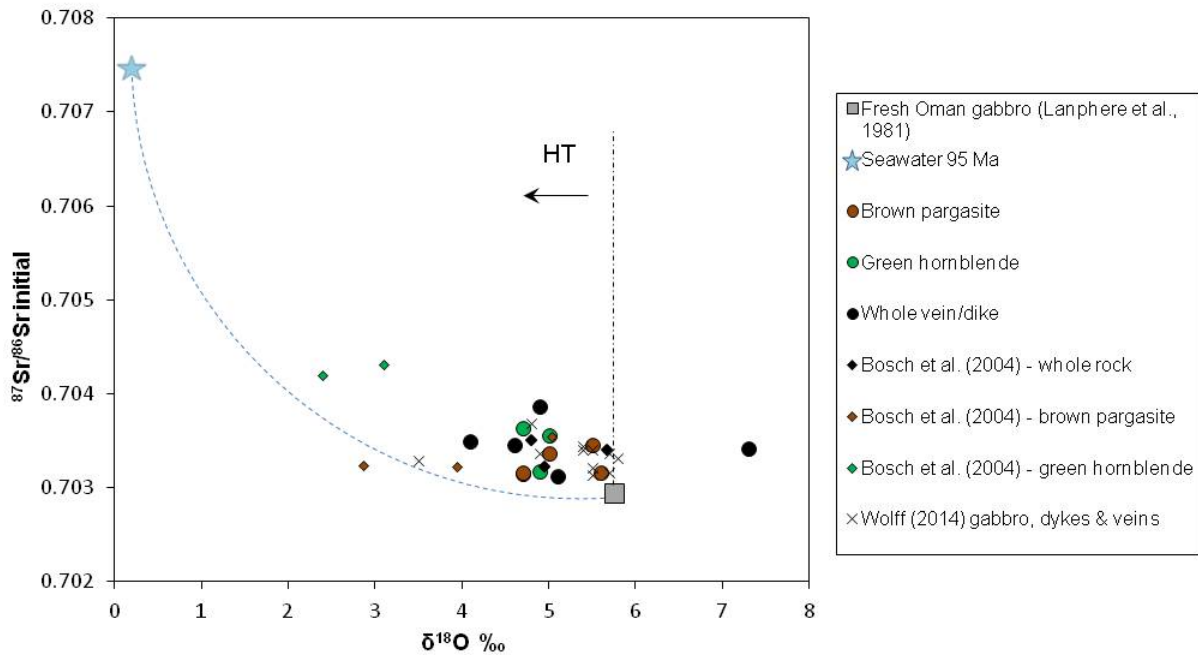


**Figure 2.6.** Initial  $^{87}\text{Sr}/^{86}\text{Sr}$  isotopic ratios plotted against  $\delta^{18}\text{O}$  for amphibole separates from high temperature veins and gabbroic dykelets of the Wadi Wariyah, Sultanate of Oman, as well as whole vein and dyke measurements. Values for Cretaceous seawater at 95 Ma are from McArthur et al. (2001), and MORB mantle, from Lanphere et al. (1981). Blue line: mixing curve fresh Oman gabbro to seawater. Results are compared to measurements done by Wolff (2014) and Bosch et al. (2004).

The dark brown amphiboles contain 60 to 150 ppm Sr and show  $^{87}\text{Sr}/^{86}\text{Sr}$  values between 0.7031 and 0.7035 (table 2.2), similar to the green and blue-green amphiboles in the second group (Sr between 80 to 105 ppm;  $^{87}\text{Sr}/^{86}\text{Sr} = 0.7032$  and  $0.7036$ ). Whole vein and dykelet analyses yield  $^{87}\text{Sr}/^{86}\text{Sr}$  ratios between 0.7031 and 0.7039 (Sr concentration from 111 to 160 ppm).



The  $^{87}\text{Sr}/^{86}\text{Sr}$  ratios of all the amphiboles measured are only slightly elevated compared to the range of fresh Oman rocks ( $^{87}\text{Sr}/^{86}\text{Sr} \sim 0.7030$ ; McCulloch et al., 1981) and there are no significant differences between the different amphibole groups. The slight increase in  $^{87}\text{Sr}/^{86}\text{Sr}$  indicates only a minor exchange with seawater-derived Sr even for amphiboles with high Cl concentrations, suggesting fluid-rock exchange with seawater-derived hydrothermal fluids that had already reacted with a large amount of rock at low fluid/rock ratios (Fig. 2.6).

**Table 2.2.**  $^{87}\text{Sr}/^{86}\text{Sr}$  and  $\delta^{18}\text{O}$  (‰) values for amphiboles and veins and dykelets from Wadi Wariyah, as well as Rb and Sr, and calculated W/R ratios.

Sample	Rb (ppm)	Sr (ppm)	$^{87}\text{Rb}/^{86}\text{Sr}$	$^{87}\text{Sr}/^{86}\text{Sr}$	$^{87}\text{Sr}/^{86}\text{Sr}_i$	$\delta^{18}\text{O}$ (‰)	W/R		
							8 ppm	38 ppm	
<b>WA02</b>									
Prg, mhs	A	0.784	64.26	0.0352	0.70317 ± 1	0.70313		1.11	0.18
	B	0.771	64.76	0.0344	0.70318 ± 1	0.70314	4.7	1.07	0.17
	C	0.764	73.09	0.0303	0.70323 ± 1	0.70318		1.32	0.23
Mhb, Act, Cl-Hst Vein		1.148	81.07	0.1505	0.70383 ± 1	0.70363	4.7	4.95	0.76
		0.525	138.2	0.0109	0.70347 ± 1	0.70346	4.6	2.65	0.54
<b>WA05</b>									
Prg, mhs	0.952	64.04	0.0429	0.70322 ± 1	0.70316	4.7	1.27	0.21	
Vein	0.376	159.5	0.0068	0.70350 ± 1	0.70349	4.1	2.84	0.59	
<b>WA42</b>									
Prg, mhs	1.571	120	0.0377	0.70321 ± 1	0.70316	5.6	1.22	0.20	
Mhb, Act, Cl-Hst Dykelet		1.396	101.3	0.0397	0.70323 ± 1	0.70318	4.9	1.34	0.23
		0.235	140.6	0.0048	0.70313 ± 1	0.70312	5.1	0.83	0.17
<b>WA04</b>									
Prg, mhs	0.786	116.5	0.0195	0.70348 ± 1	0.70345	5.5	2.70	0.54	
Mhb, Act, Cl-Hst Dykelet		0.337	91.37	0.0106	0.70357 ± 1	0.70356	5	3.25	0.67
		0.417	111.5	0.0108	0.70388 ± 1	0.70386	4.9	5.26	1.09
<b>WA33</b>									
Prg, mhs	0.418	152	0.0079	0.70342 ± 1	0.70341	5	2.18	0.43	
Dykelet	0.728	122.8	0.0171	0.70339 ± 1	0.70336	7.3	2.38	0.49	

<sup>a)</sup> According to the mineral abbreviations by Whitney and Evans (2010). Ed: Edenite; Fprg: ferro-pargasite; Hst: hastingsite;

Mhb: magnesio-hornblende; Mhs: magnesio-hastingsite; Ts: tschermakite.

<sup>b)</sup> Effective water/rock ratio mass balance calculation using the following equation (Taylor, 1977)

$$(W/R) = \frac{(^{87}\text{Sr}/^{86}\text{Sr}^{\text{rock}})_{\text{final}} - (^{87}\text{Sr}/^{86}\text{Sr}^{\text{rock}})_{\text{initial}}}{(^{87}\text{Sr}/^{86}\text{Sr}^{\text{seawater}})_{\text{initial}} - (^{87}\text{Sr}/^{86}\text{Sr}^{\text{rock}})_{\text{final}}} \times (C_{\text{initial}}^{\text{rock}} / C_{\text{initial}}^{\text{seawater}})$$

<sup>c)</sup> Using age-corrected  $^{87}\text{Sr}/^{86}\text{Sr}$  for 95 Ma, considering initial (95 Ma) of the rock (Lanphere et al., 1981) and initial seawater (McArthur et al., 2001), Sr concentration in the rock of 163 ppm (Kawahata et al., 2001) and initial concentration in seawater of 38 ppm (Coogan et al., 2009).

<sup>d)</sup> Using current (dynamic)  $^{87}\text{Sr}/^{86}\text{Sr}$ , considering initial (95 Ma) of the rock (Lanphere et al., 1981) and initial seawater (McArthur et al., 2001), Sr concentration in the rock of 163 ppm (Kawahata et al. (2001) and current concentration in seawater of 8 ppm (Coogan et al., 2009).

### **2.3.4.2. O isotopes**

$\delta^{18}\text{O}$  values obtained for amphiboles fall in a narrow range between 4.1 and 5.6 ‰ except for one sample with value of 7.3 ‰ (Fig. 2.6, table 2.2). Values obtained from veins fall between 4.1 and 4.7, and values from gabbroic dykelets range from 4.9 to 7.3. Using the amphibole formation temperatures estimated from Ti-in-amphibole thermometry we calculated the oxygen isotopic composition of the hydrothermal fluid in equilibrium with these minerals using the amphibole-water fractionation equation of Zheng (1993; supplementary table S1). If the formation temperatures are correct and the amphiboles have retained their original oxygen isotopic compositions and not been subject to low temperature isotopic exchange, they are in equilibrium with hydrothermal fluids with high  $\delta^{18}\text{O}$  between 6.9 and 7.5 ‰. This is very different from Late Cretaceous seawater ( $\delta^{18}\text{O} = -1$  ‰; Gregory and Taylor, 1981) or the composition of ancient black smoker fluids that are typically 1 to <4 ‰ higher than co-existing seawater (see Shanks et al., 1995). This suggests that oxygen isotopic exchange occurred in a very rock dominated system at low water/rock ratios. Alternatively, if the fluids are similar to Late Cretaceous seawater or a black smoker-like fluid derived from seawater, the analysed amphibole  $\delta^{18}\text{O}$  suggests formation temperatures between 90 and 130 °C (Appendix A1).

## **2.4 Discussion**

### **2.4.1 Formation of different amphibole types and various episodes of fluid/rock interaction**

It has been proposed that the gabbroic dykelets are products of hydrous partial melting of the host gabbro (Wolff, 2014), implied by the crystallization of amphiboles from a water-bearing fluid, marking the onset of hydrothermal fluid-rock interactions at very high to magmatic temperatures (850 – 1020 °C). In contrast, the green amphibole veins appear to have formed from high temperature fluid-rock reactions



occurring at upper amphibolite facies conditions (650 – 850 °C. In some samples, these dark veins retain relict amphibole cores that formed during the magmatic precursor stage (Wolff, 2014).

In addition to textural observations (poikilitic amphibole) and geothermometry, magmatically formed amphiboles and hydrothermal amphiboles formed at subsolidus temperatures from hydrothermal fluids can be distinguished by their Ti, Na, K, Si contents and Mg number, with hydrothermal amphiboles exhibiting higher Si contents and Mg numbers but lower Ti, Na and K contents (Gillis et al., 2003). The occurrence of different amphibole types from supra- and subsolidus reactions in an alteration parageneses in gabbros is also documented in other studies of oceanic (e.g. Vanko, 1986; Silantyev et al., 2008; Coogan et al., 2001) and continental rocks (Liu et al., 2009; Enami et al., 1999; McCormick & McDonald, 1999), and from experimental investigations (e.g., Currin et al., this issue; suprasolidus experiments: Khodorevskaya & Aranovich, 2016; Koepke et al., 2004; 2007; Chan et al., 2016). The passage of hydrothermal fluids through the crust in episodes of different temperatures and salinities is evidenced by the formation of different amphibole types, equilibrating at progressively lower temperatures. This provides evidence for the progressive cooling of the lower oceanic crust by involvement of hydrothermal fluids (Fig. 2.7).

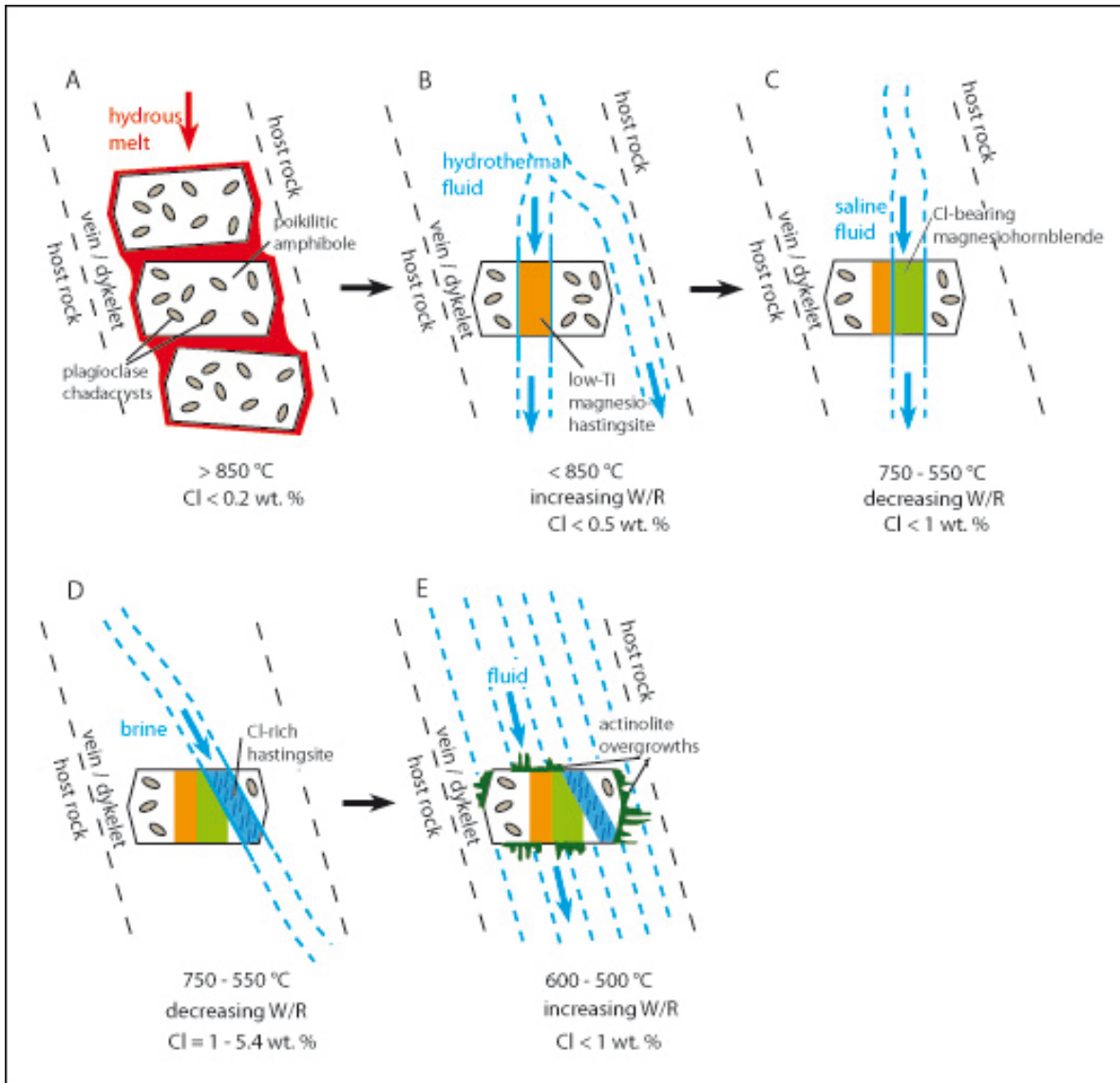


**Figure 2.7.** Sketch showing the evolution of amphibole in gabbroic dykelets and dark veins in Wadi Wariyah. A: hydrous partial melting, formation of poikilitic magmatic amphibole – pargasite and magnesiohastingsite – in gabbroic dykelets & dark veins – amphibole is part of a dykelet that cross-cuts the host rock; red: represents the fine-grained matrix of the dykelets consisting of plagioclase, olivine, clinopyroxene, orthopyroxene, Fe-Ti oxides; Wolff, 2014. B: Flushing of dykelet with the infiltration of a high-T hydrothermal fluid, heat removal and metamorphism of vein and dykelet minerals. Formation of magnesiohastingsite containing Cl > 0.2 wt. %. C: Flushing of dykelet with the infiltration of a hydrothermal seawater-derived fluid, cooling & progressive concentration of Cl & lower water/rock ratios. Formation of magnesiohornblende containing Cl < 1 wt. %. D: infiltration of highly concentrated saline fluid. formation of hastingsite and ferropargasite containing Cl > 1 wt. % up to 5.4 wt. %. E: new episode of fluid infiltration at lower temperature – Cl-poor fluid – and formation of actinolite overgrowths.

The presence of brown high-Ti pargasite and magnesiohastingsite with poikilitic texture indicates a magmatic origin of these amphiboles (Fig. 2.7A).  $^{87}\text{Sr}/^{86}\text{Sr}$  values only slightly above 0.703 indicate Sr-isotopic exchange with a very rock dominated fluid with only a hint of seawater derived Sr. Epitactic growth of Ti-poor and Cl-rich amphiboles (Fig. 2.7 B to D) provides evidence of sub-solidus fluid-rock interactions and metamorphism at amphibolite facies. The occurrence of Cl-rich amphibole domains (8D) record the reaction with high Cl hydrothermal fluids or brines, albeit at low water/rock ratios. Finally, further fluid-rock exchange at lower amphibolite to greenschist facies temperatures is deduced from the presence of actinolite overgrowths (8E). This sequence of processes identified at the mm-scale provides evidence for the transition from the suprasolidus regime to the subsolidus regime in the presence of hydrothermal fluids percolating through the lower oceanic crust.

The amphiboles from Wadi Wariyah are comparable to amphiboles equilibrated in high temperature experiments (900 °C; Fig. 2.8, and see Currin et al. this issue), and plot in the same area as high-Ti natural amphiboles formed magmatically (pargasite, magnesiohastingsite and tschermakite). Amphiboles formed experimentally at 650 °C (subsolidus, metamorphic conditions) also have similar compositions to the natural amphiboles analysed in this study (mainly magnesiohornblende, magnesiohastingsite, edenite). Experimental amphiboles formed at lower temperatures (600-500 °C) are higher in Si than amphiboles formed at higher temperatures, and approach actinolitic compositions (Currin et al., this issue), in contrast to the natural amphiboles that plot in the actinolite-tremolite field.

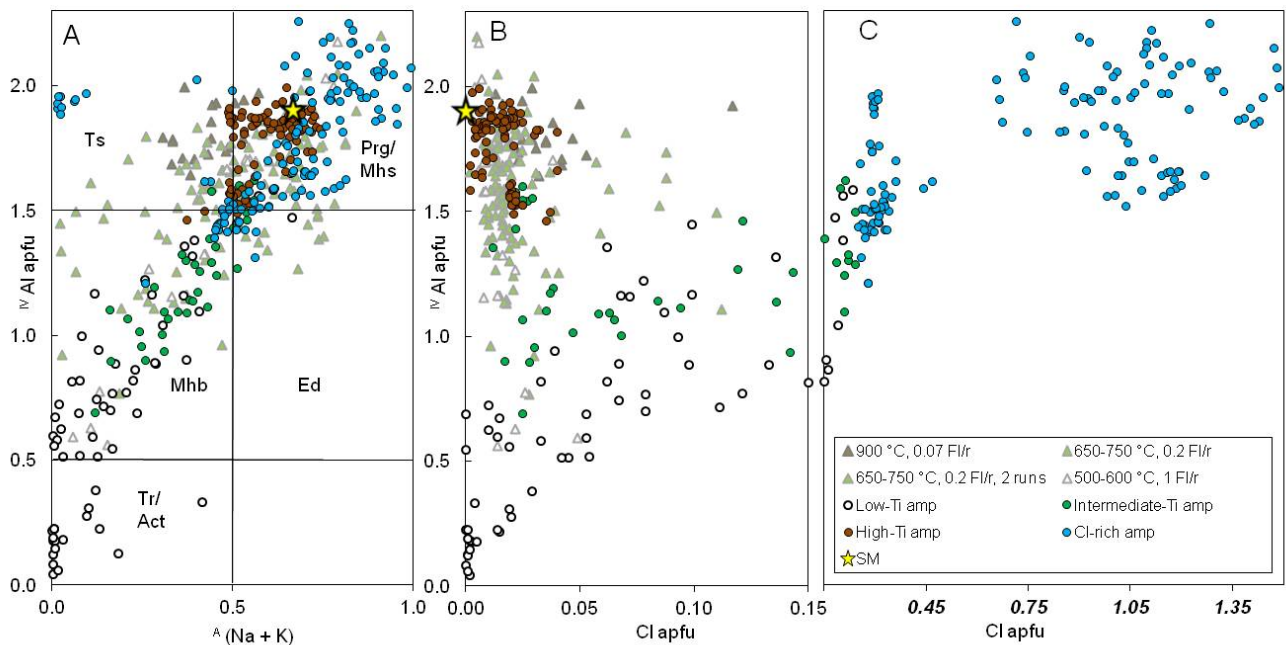


**Figure 2.8.** Composition of amphiboles from Wadi Wariyah plotted against experimental results from Currin et al. (this issue). Abbreviations after Whitney et al. (2010): Ts, tschermakite; Mhs, magnesiohastingsite; Prg, pargasite; Mhb, magnesiohornblende; Tr, tremolite; Act, actinolite.

#### 2.4.2 Cl incorporation into amphibole

Correlations between Cl concentrations in amphibole and  ${}^{\text{IV}}\text{Al}$ ,  $\text{Fe}^{2+}$  and K contents are observed in Cl-rich amphiboles (up to 5.4 wt. % Cl, Fig. 2.3E), due to constraints in the amphibole structure and the larger size of the Cl anion with respect to OH (Oberti et al., 1993). For natural amphiboles from Wadi Wariyah, this correlation starts to be apparent for Cl contents greater than 0.3-0.4 wt. %. In amphiboles containing less than 0.3 wt% Cl, the contents of  ${}^{\text{IV}}\text{Al}$ ,  $\text{Fe}^{2+}$  and K do not seem to be influenced by Cl incorporation. This also holds true for amphiboles obtained experimentally (Currin et al. (this issue)) that do not show any correlation between the aforementioned cations and Cl incorporation, since these amphiboles contain < 0.4 wt. % Cl (Fig. 2.8). This lack of correlation between Cl and certain cations (e.g. Al, Fe, K) when small amounts of Cl are measured in the amphibole (<0.3 wt. %) has also been reported in other natural

Cl-bearing amphiboles (Kullerud, 1996; Enami, 1999), as well as from experimental studies (Chan et al., 2016).

### **2.4.3 Relationship between Cl content in amphibole and microstructure**

The subtle intragrain misorientations illustrated in Fig. 2.5 are not large enough to account for different orientations at the time of mineral growth. Thus, the Cl-rich ferropargasite and hastingsite may be epitactic with the other amphibole compositional zones. This may suggest that low-Ti amphiboles formed from the interaction of pre-existing magmatic amphibole with an aqueous Cl-rich fluid. Small orientation changes may be related to structural changes in the amphibole lattice due to Cl incorporation, or may be unrelated to mineral composition – possibly due to deformation of unknown origin. In some amphibole grains the misorientation boundary (see Fig. 2.5C) is not exactly coincident with the change in Cl content. This may be due to the fact that only higher Cl contents cause significant changes in the amphibole lattice (as present in the right-hand side of Fig. 2.5). Consequently, the misorientation of the amphibole structure due to Cl incorporation is only visible at higher Cl contents.

### **2.4.4 Fluid evolution: changing water/rock ratios and salinity**

The occurrence of Cl-rich amphiboles is linked to the participation of brines in fluid/rock interaction (Manning and Aranovich, 2014). This has also been shown experimentally. Experiments performed with an NaCl with the aim of producing Cl-rich amphibole require supersaturated brines to succeed in producing amphiboles that contain Cl contents greater than 0.4 wt. % Cl (Chan et al., 2016). This may suggest that amphiboles formed in nature require Cl saturation in order to reach high Cl contents, and may be applied to the state of the fluid during equilibration with the rocks outcropping in Wadi Wariyah. Decrease of fluid/rock ratio is caused by the progressive reaction with host rocks and incorporation of water (OH) into hydrous minerals, with the subsequent concentration of Cl in the seawater-derived

hydrothermal fluid, leading to the formation of brines that react with the host rock to form Cl rich amphiboles.

Phase separation in saline fluids occurs below the critical curve that is found at different pressures for a given temperature – e.g. around 1.3 kbar for 750 °C and 20 wt. % NaCl (Driesner & Heinrich, 2007). By crossing this curve towards lower pressures, a fluid will undergo phase separation into a NaCl-free vapour and a NaCl-concentrated fluid (i.e. brine). Pressures in the lower oceanic crust (ca. 6 km deep in the crust) are estimated at 2 kbar (Iturrino et al., 2002), and may vary due to exhumation and faulting of the oceanic crust, affecting fluid circulation and changing fluid behaviour, locally resulting in phase separation.

Large measured Cl quantities in amphibole from Wadi Wariyah (< 5.4 wt. %) confirms reaction with a seawater-derived fluid, and the isotopic signature of the amphibole (being relatively close to fresh Oman gabbro) suggests the environment was mostly rock-dominated and water/rock ratios were low during equilibration between fluid and amphibole. This is consistent with the findings of Bickle & Teagle (1992) for the Troodos ophiolite, and Gregory and Taylor (1981) for the Samail ophiolite, who also report on fluid-rock exchange at low water/rock ratios near the base of the crust.

## **2.5 Conclusions**

The study of high temperature hydrothermal veins and gabbroic dykelets emplaced in layered gabbros from the Samail Ophiolite, Sultanate of Oman, has revealed complexly zoned amphibole areas with hastingsite containing more than 5 wt. % Cl. These amphibole zones are a sign of the passage of Cl-rich hydrothermal fluids through the lower oceanic crust at a range of temperatures, ranging from magmatic to hydrothermal in origin, and may suggest that the global cooling system of the oceanic crust reaches beyond depths of 5 km, starting in an on-axis environment.

This study gives evidence for hydrothermal circulation occurring in the deep oceanic crust formed at a fast-spreading rate. Variations in Cl content (from 0.1 to 5.4 wt. % Cl) and differences in Si, <sup>iv</sup>Al, Mg#, Na and K in amphibole, indicate equilibration with fluids of different salinities. These findings suggest an inhomogeneous distribution of hydrothermal fluid pathways in the lower oceanic crust near fast-spreading ridges, with stepwise fluid infiltration, and variations in fluid temperature and salinity. In addition, EBSD analyses show compositional differences within single amphibole grains, indicating alteration of pre-existing magmatic amphibole by interaction with hydrothermal fluids. Near MORB-like <sup>87</sup>Sr/<sup>86</sup>Sr and high  $\delta^{18}\text{O}$  isotopic compositions confirm the influence of a high-temperature seawater-derived fluid from magmatic (suprasolidus) to hydrothermal (subsolidus) temperatures, albeit in rock-dominated low fluid-rock ratio conditions.

Amphiboles with mild Cl enrichment (<0.5 wt. %) show heterogeneous Fe, Mg, Al and Si contents, suggesting that Cl-bearing amphiboles with Cl<0.5 wt. % may not be the structural constraints of Cl-bearing amphiboles with Cl> 1 wt. % (Oberti et al., 1993), although natural amphiboles with high to very high Cl-rich contents (up to 5.4 wt. % Cl) do in fact show good correlations between Cl and <sup>iv</sup>Al, Fe<sup>2+</sup>, and K.

EBSD studies showing the structural link between different amphibole zones reveal the lack of grain boundaries or misorientations between adjacent amphiboles with differing chlorine contents, and are therefore epitactic, despite very mild 1° intragrain misorientations.

Isotopic studies of <sup>87</sup>Sr/<sup>86</sup>Sr, show influence of seawater-derived fluids in the studied amphiboles. This further confirms the existence of hydrothermal circulation at depths above 5km in the oceanic crust. The proximity to <sup>87</sup>Sr/<sup>86</sup>Sr MORB values may be due to very small amounts of seawater-derived fluid interacting with the host rock, therefore overprinting the pre-existing magmatic signature of the rock only very slightly.

### 3 Interaction of highly saline fluid and olivine gabbro: experimental simulation of deep hydrothermal processes involving amphibole at the base of the oceanic crust

#### 3.1 Introduction

This chapter describes the experimental part of the study, done using cold seal pressure vessels (CSPV) and internally heated pressure vessels (IHPV) to illustrate the process by which gabbro-hosted amphibole-rich parageneses evolve in the presence of a hydrothermal saline fluid. The experiments run have the aim to simulate ongoing reactions in the deep oceanic crust near the Moho, where high-temperature hydrothermal activity takes place (Fig. 3.1).

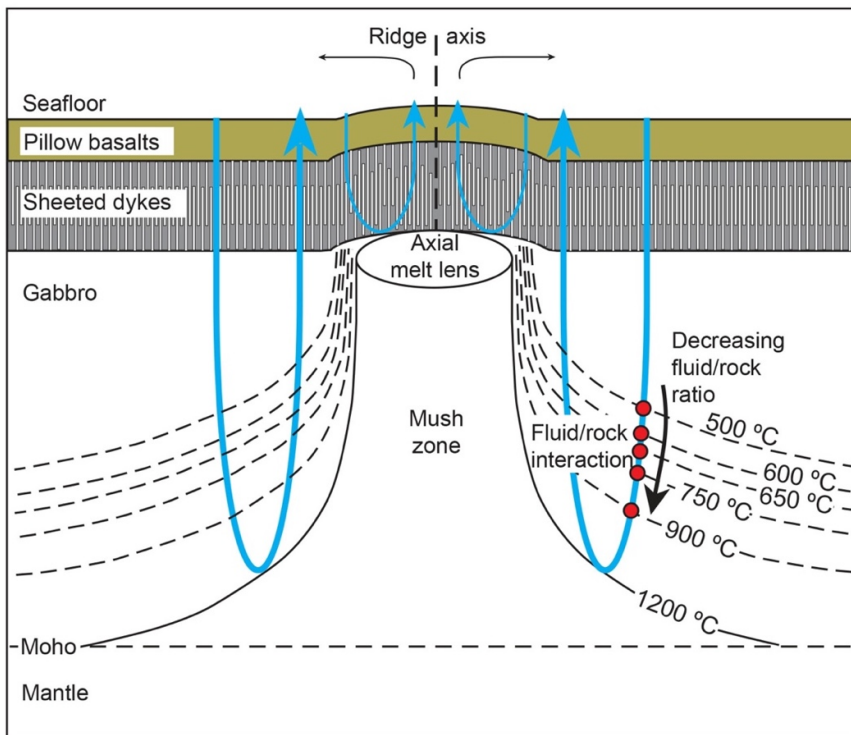


**Figure 3.1.** Schematic cross-section of the oceanic crust below fast-spreading mid-ocean ridges showing seawater-derived fluid/rock interaction in the lower oceanic crust. Arrows indicate extent of hydrothermal systems (e.g. Gregory and Taylor, 1981; Nicolas et al., 2003). Red dots illustrate the geological conditions simulated in the experiments presented in this work. Isotherms are from Dunn et al., 2000. Not to scale.



### 3.2 Experimental strategy and methods

The aim of this study is to simulate reactions that produce a variety of amphibole compositions in the deep oceanic crust beneath mid-ocean ridges as a result of the interaction of aqueous NaCl-rich fluids and olivine gabbro. Experiments were conducted at 200 MPa, corresponding to pressures at the base of the oceanic crust at ~ 5 to 6 km depth for typical oceanic crust (Canales et al., 2003). Experimental temperatures (900, 750, 650, 600 and 500 °C) were chosen to simulate reactions during successive cooling of the lower oceanic crust, from magmatic, suprasolidus (900 °C) conditions, to hydrothermal, subsolidus conditions (750-500 °C), following the transition from granulite over amphibolite to greenschist facies conditions. The fluid/rock mass ratios selected were 0.07 (900 °C), 0.2 (750-650 °C) and 1 (600 and 500 °C) consistent with the concept of clearly rock dominated conditions during fluid interactions with dense, deep gabbro at high temperature, and the increasing influence of hydrothermal fluids with increasing extent of brittle deformation upon cooling (e.g., Bosch et al., 2004). Moreover, an additional experimental approach was used in an attempt to simulate increasing of hydrothermal activity by small increments at a particular temperature (750 °C), by conducting additional experimental runs at the same temperature re-using the solids after the first experimental run with a new batch of saline fluid. Thus, the olivine gabbro was reacted twice: experiments were run once (run 1) and, after retrieving the solid products from the capsule, half of the material was analyzed and the other half was inserted into a new capsule with a new batch of fluid of the same NaCl concentration, and run a second time at the same fluid/rock ratio (0.2) (run 2). This procedure could potentially be reproduced multiple times, however, experiments often result in comminution of the solid material and loss during opening of the capsules and transfer to a clean jar, which constrains the number of times this operation can be replicated and analyzed successfully. As explained in the following section, the higher water/rock ratio of 1 at the hydrothermal experiments at the lowest temperature (600 and 500 °C) also intended to facilitate free growth of alteration minerals into the fluid and hence the attainment of clear local fluid-mineral equilibrium.

### 3.2.1 Starting material and sample preparation

In order to simulate the process by which olivine gabbro of the lower oceanic crust reacts with a saline fluid, we designed a strategy tailored to this specific case by using a natural oceanic olivine gabbro as starting material and added a fluid consisting of water and NaCl. In order to provide optimal conditions for the crystallization of amphibole, we used an olivine gabbro containing amphibole in its starting mineral assemblage, to serve as nucleation sites for new amphibole. The composition of the starting amphibole is unique, homogeneous, and easy to distinguish from newly-formed amphibole after experiments (see results section).

An amphibole-free olivine gabbro starting powder (ol + plg + px + mt) was used for setup A, and 3 to 4 compositionally homogeneous crystals of magnesiohastingsite were added (Cl content <0.07 Cl wt. %), with saline solutions of 6, 20 and 50 wt. % NaCl (0.02, 0.07 and 0.24  $X_{\text{NaCl}}$ ) in water (Fig. 3.2). The olivine gabbro used as starting material was sampled in the Wadi Gideah, Sultanate of Oman (sample OM10-Gid24A) and added magnesiohastingsite crystals are xenocrysts extracted from a diabase groundmass sampled in Loitsch (Thüringen) Germany. The gabbro used for setup B was an amphibole-bearing gneissic olivine gabbro from the lower crust of the Mid-Atlantic Ridge near the Kane fracture zone, drilled by ODP during Leg 153 (Hole 920B, Core 13, Section 4, 32-36 cm) consisting of olivine, plagioclase, clinopyroxene, small amounts of orthopyroxene (<2 vol. %), magnetite and Ti-rich magnesio-hastingsite in its original assemblage. This amphibole is of magmatic origin and extremely poor in Cl (<0.01 wt. % Cl). Rock cylinders of the starting olivine gabbro were used for experiments (diameter 3.5 mm; height: 3.8 mm). For experiments at lower temperature (500 and 600 °C, setup C in Fig. 3.2), larger cylinders of the same starting gabbro were used (7 mm in diameter and 10 mm in height). The aqueous starting solutions used ranged from moderately to highly saline with NaCl concentrations of 6, 20 and 50 wt. % (0.02, 0.07 and 0.24  $X_{\text{NaCl}}$ ) and therefore ~2-16 times richer in Cl than seawater (~3.2 wt. % NaCl; ~0.01  $X_{\text{NaCl}}$ ). These starting solutions were produced by dissolving reagent grade NaCl in distilled

water in appropriate proportions – or by mixing when exceeding NaCl saturation at ambient conditions (e.g. 50 wt. % NaCl). In the experimental pressure and temperature conditions used, all solutions were single phase fluids above critical pressure (Fig. 3.3) (Driesner and Heinrich, 2007; Driesner, 2007). The corresponding densities with respect to pure NaCl-H<sub>2</sub>O fluids were calculated using the equations of Driesner (2007), ranging from 0.55 to 1.06 g/cm<sup>3</sup> (table 3.1).

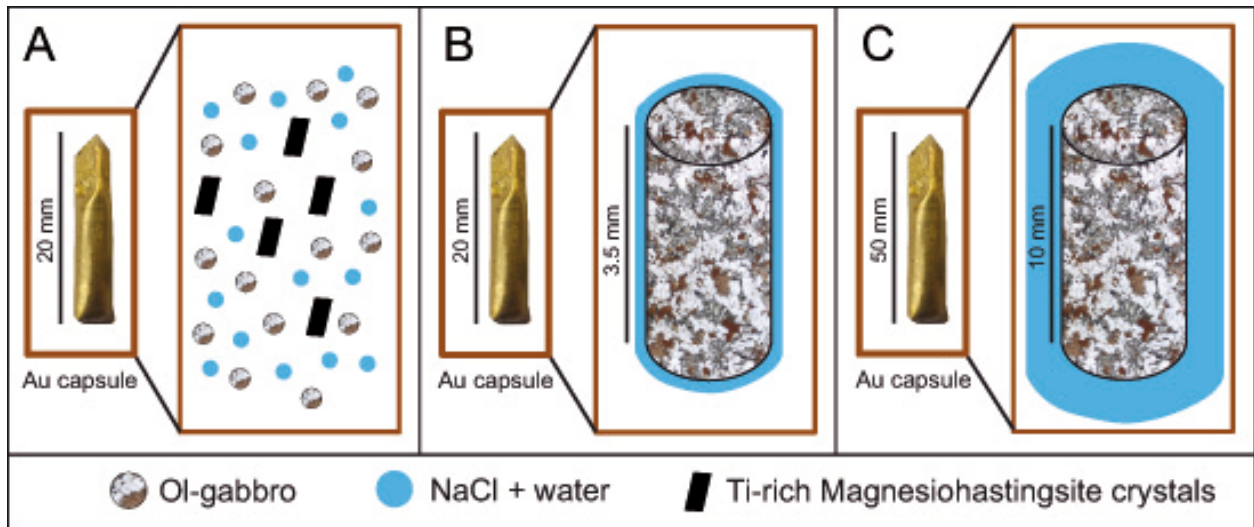


**Figure 3.2.** Capsule setup of the experiments performed. A: capsule contents of the set of experiments using olivine gabbro powder, 3 to 4 crystals of Ti-rich magnesiohastingsite (2 mm grain size), and water with added NaCl (50 wt% and 20 wt% NaCl in water), and fluid/rock ratio of 0.2. B: capsule contents of the set of experiments using an olivine gabbro core containing high-Ti pargasite/magnesiohastingsite and water with added NaCl (50 wt%, 20 wt% and 6 wt% NaCl in water), and fluid/rock ratio of 0.2. C: capsule contents of the set of experiments using an olivine gabbro core containing high-Ti pargasite/magnesiohastingsite and water with added 20 wt% NaCl in water, and fluid/rock ratio of 1. See Table 1 for list of experiments done with each capsule setup.

The approach used in experiments at 500 and 600 °C was intrinsically chosen to analyse both solid and fluid products. The intended fluid analyses by induced coupled optical emission spectroscopy require a minimum fluid volume recovery of ~ 500 ml. Although ex situ sampling involves uncertainties regarding possible precipitation and/or re-dissolution processes in the liquid composition, former studies on hydrothermal fluid-rock interaction experiments yielded reliable fluid compositions with respect to major

elements (Hajash and Archer, 1980; Hajash and Chandler, 1981) as well as major and trace elements (Beermann et al., 2017) correlating systematically with the experimental parameters in fluids that were thoroughly sampled at ambient conditions ~20-30 min run termination. The relatively large amount of starting fluid required (~1000  $\mu$ l) needed a correspondingly large starting rock sample (Fig. 3.2C). However, the starting rock absorbed most of the fluid during experimental runs, and fluid recovery was therefore too low for chemical analysis. Taking into account lower reaction kinetics expected from lower temperature experiments (500-600 °C), a longer run duration was chosen (101 days) to obtain secondary phases large enough for analysis.

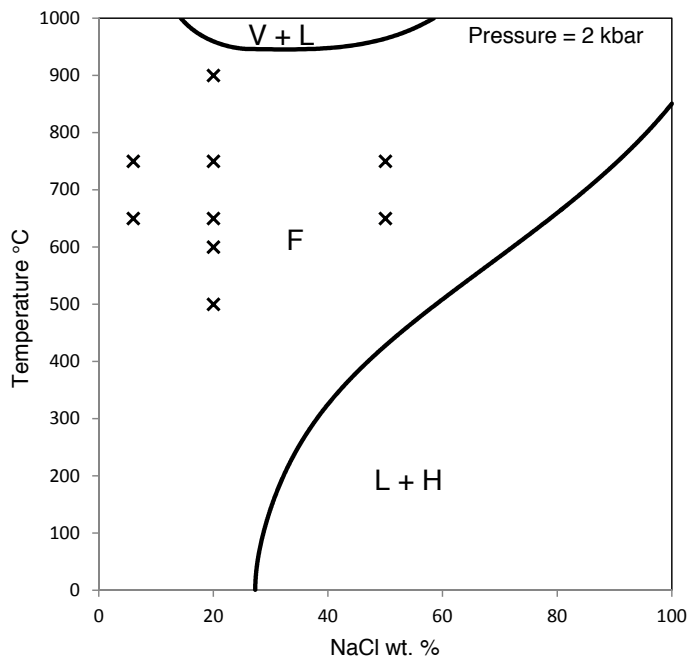


**Figure 3.3.** Phase diagrams of the NaCl-H<sub>2</sub>O system at 2 kbar. The different fields represented are: vapour and liquid (V + L), liquid and halite (L + H), and fluid (F), where – according to the terms used by Driesner and Heinrich (2007) – “F” denotes any type of fluid that can change properties from vapour to liquid-like without undergoing heterogeneous phase transitions. Experimental conditions shown by crosses. Curves calculated using the ‘SoWat’ model for fluid properties in the NaCl-H<sub>2</sub>O system (Driesner and Heinrich, 2007; Driesner, 2007).

Fluid and rock starting materials – and salt in experiments using 50 wt. % NaCl – were weighed and inserted into capsules made of gold tubing with 0.1 mm wall thickness and inner diameter of 3.8 mm and 20 mm length or, for the longer cylinders, of 7.6 mm inner diameter and 50 mm length. The charged capsules were closed by pulsed electric arc welding under argon gas using a LAMPERT® PUK3 welding station. This method keeps the capsules cool during sealing to avoid evaporation of the charge. Capsules

were then left in an oven at 110 °C for a few hours and subsequently weighed, to ensure they were properly sealed before proceeding to the experiments. For experimental details see table 3.1.

### 3.2.2 Experimental apparatuses and procedure

All experiments were conducted at a pressure of 200 MPa in different kinds of pressure vessels as described as follows.

The single partial melting, suprasolidus experiment (900 °C) was conducted in an Internally Heated Pressure Vessel (IHPV) with an argon-hydrogen mixture pressure medium at the Institute of Mineralogy, Leibniz University of Hannover. The accuracy in pressure and temperature monitored was better than  $\pm 1$  MPa and  $\pm 1$  °C. The experiment was started at constant temperature for one day, using the temperature cycling technique for 4 days of 900 °C  $\pm$  25 °C in order to increase the sizes of the experimental phases, and left at constant temperature for 6 days. More details on thermal cycling of experiments can be found in Erdmann and Koepke (2016) and Silva et al. (2017). The oxygen fugacity ( $fO_2$ ) was adjusted according to values of NNO ( $fO_2$  imposed by the Nickel-Nickel Oxide buffer reaction) by adding the desired amount of hydrogen to the argon gas. The partial hydrogen pressure in the running experiment was monitored using a Shaw membrane. The  $fO_2$  was determined using the dissociation reaction of H<sub>2</sub>O and the associated correlations between the H<sub>2</sub>O dissociation constant (Pitzer and Sterner, 1995) and the standard state fugacity of H<sub>2</sub>O (Robie et al., 1978) and of H<sub>2</sub> (Shaw and Wones, 1964). The experiment was stopped

Table 3.1. Experiments performed and experimental conditions used.

Run	Starting rock	Exp. apparatus	T (°C)	t (days)	NaCl Fl <sup>1</sup> (wt%)	ρ Fl <sup>2</sup> (g/cm <sup>3</sup> )	N. of runs	Fl/R <sup>3</sup>	Newly-formed phases
IHB20-9	Ol gabbro cylinder	IHPV	900	10	20	0.55	1	0.07	Amp, melt, Pl, Ol, (Ilm), (Mag)
CSA50-1	Ol gabbro pw + Amp	CSPV	750	10	50	0.99	1	0.2	Amp*
CSA50-2	Ol gabbro pw + Amp	CSPV	750	10	50	0.99	2	0.2	Amp*
CSA20-1	Ol gabbro pw + Amp	CSPV	750	10	20	0.66	1	0.2	Amp*
CSA20-2	Ol gabbro pw + Amp	CSPV	750	10	20	0.66	2	0.2	Amp*
CSB50-1	Ol gabbro cylinder	CSPV	750	10	50	0.99	1	0.2	Amp, (Chl), Pl, Cpx, (Ilm), (Mag)
CSB50-2	Ol gabbro cylinder	CSPV	750	10	50	0.99	2	0.2	Amp, (Chl), Pl, Cpx, (Ilm), (Mag)
CSB20-1	Ol gabbro cylinder	CSPV	750	10	20	0.66	1	0.2	Amp <sub>2</sub> (Chl), Pl, Ol, (Ilm), (Mag)
CSB20-2	Ol gabbro cylinder	CSPV	750	10	20	0.66	2	0.2	Amp, (Chl), Pl, Ol, Cpx, (Ilm), (Mag)
CSB6-1	Ol gabbro cylinder	CSPV	750	10	6	0.52	1	0.2	Amp, (Chl), Pl, Ol, (Ilm), (Mag)
CSBX50-1	Ol gabbro cylinder	CSPV	650	10	50	1.06	1	0.2	Amp, (Chl), Pl, Ol, Cpx, (Ilm), (Mag)
CSBX20-1	Ol gabbro cylinder	CSPV	650	10	20	0.74	1	0.2	Amp, (Chl), Pl, Ol, (Ilm), (Mag)
CSBX6-1	Ol gabbro cylinder	CSPV	650	10	6	0.60	1	0.2	Amp, (Chl), Pl, Ol, (Ilm), (Mag)
OB-600-C	Ol gabbro cylinder	CSPV	600	101	20	0.79	1	1	Amp, Chl, Pl, (Ilm), (Mag)
OB-500-C	Ol gabbro cylinder	CSPV	500	101	20	0.87	1	1	Amp, Chl, (Ilm), (Mag)

All experiments performed at pressures of 200 MPa and oxygen fugacity close to NNO. Number of runs indicates whether an experiment was run once (1), or whether solids were extracted after first run and run again adding a new batch of saline fluid (2).

<sup>1</sup>NaCl content of the starting fluid

<sup>2</sup>Density of the corresponding pure NaCl-H<sub>2</sub>O fluid at the experimental pressure and temperature conditions (calculated using equations of Driesner, 2007).

<sup>3</sup>N. (Number) of runs indicates whether an experiment was run once (1), or whether the solids of the first run were extracted and run again using a new batch of the same starting solution (2).

<sup>4</sup>Fl/R is the fluid-to-rock mass ratio.

Solids run twice at Fl/R of 0.2 and hence approximately at Fl/R of ~0.4

<sup>5</sup>Mineral name in brackets denotes small amounts (<~2 vol. %)

<sup>6</sup>Mineral abbreviations after Whitney and Evans (2010). Amp: amphibole; Pl: plagioclase; Ol: olivine; Ilm: ilmenite; Mag: magnetite; Chl: chlorite; cpx: clinopyroxene.

\*Other phases in the powder not analysed (see more details in chapter 3 on experimental design).

by rapid quenching ( $\sim 150$  °C/s) (details on the IHPV apparatus and applied techniques can be found in Berndt et al., 2002).

Subsolidus experiments were performed in two similar Cold Seal Pressure Vessel (CSPV) facilities, one at the Institute of Mineralogy in Hannover (750 and 650 °C), and the other at the Institute of Geosciences, Kiel University (600 and 500 °C), the latter with autoclaves constructed for large sample volumes. The accuracy in temperature and pressure of these experiments was better than  $\pm 1$  MPa and  $\pm 4$  °C for the runs at 650 to 750 °C and, given the larger temperature differences along the larger sample capsules,  $\pm 7$  °C at 500 and 600 °C. The oxygen fugacity in the hydrothermal environment of the vessel is imposed by the hydrogen fugacity along the water dissociation reaction in vicinity of the nickel-nickel oxide buffer (NNO) reaction from the Ni filler rods. However, due to the low permeability of 0.2 mm thick gold capsules to hydrogen (Chou, 1986), attainment of redox equilibrium of the experimental systems with the autoclave atmosphere – particularly for the run at 500 °C – is not ensured (Allen and Seyfried, 2003). Experiments were terminated by removing the vessels from the furnace and subsequently cooling them using a compressed air flow for approximately 15 minutes close to room temperature.

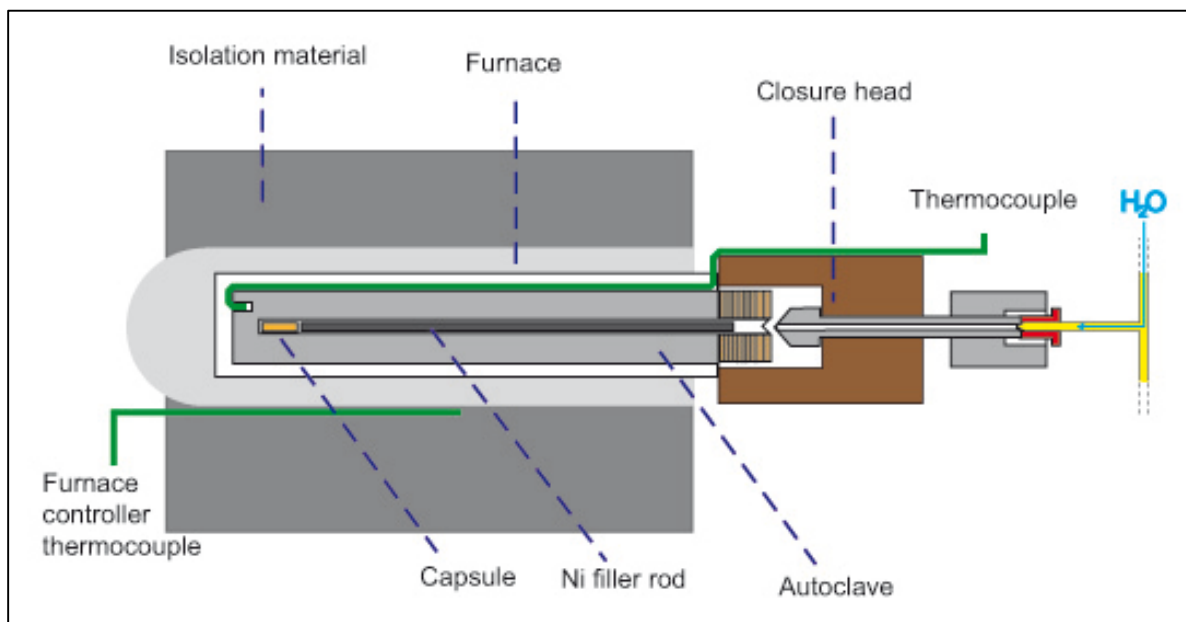


**Figure 3.4.** Schematic drawing of the Cold Seal Pressure Vessel (CSPV) apparatus used in setup B at 2 kbar of pressure and temperatures of 750 °C and 650 °C, and oxygen fugacity close to NNO.

Given the extent of suppression of the  $H_2O$  activity to be expected by the NaCl-rich fluids (Webster, 1992), the corresponding  $fO_2$  (in bar) of the most NaCl-rich experiments (50 wt. % NaCl or 0.24  $X_{NaCl}$  solutions) should be lowered roughly by  $\sim 0.3$  log units, but does not significantly affect  $fO_2$  at lower NaCl concentrations.

Experimental capsules were examined for any damage and weighed after each run to check for possible fluid leakages, in which case the contents of the capsule were discarded and the procedure was repeated again. When successful, the solid experimental products were then extracted from the capsules, mounted on epoxy and polished for analysis.

### **3.2.3 Analytical methods**

Analysis of amphibole minerals from experimental charges have been conducted in-situ with electron probe microanalysis (EPMA) for major elements (and trace Cr, Ti, Cl, F). A Cameca SX100 electron microprobe equipped with 5 spectrometers and the software “Peak Sight” was used at the Institute of Mineralogy of the Leibniz University in Hannover, Germany. A 15nA focussed beam current and a 15kV acceleration voltage were used for analysis. The peak counting times of 10s were used for all elements (5s background), except for Cl and F (30 s). For calibration of elemental measurements, the natural and synthetic standards used were albite (Na), wollastonite (Ca and Si), orthoclase (K), Durango apatite (P),  $Al_2O_3$  (Al),  $Mn_2O_3$  (Mn),  $TiO_2$  (Ti), MgO (Mg),  $Fe_2O_3$  (Fe), NaCl (Cl), and  $SrF_2$  (F). To monitor analytical precision, each measurement was checked against the international amphibole standard Kakanui hornblende (USNM 143965) as reference material (Jarosewich et al. 1980). Representative analyses from amphibole EPMA measurements are detailed in table 3.2, and supplementary tables S2 and S3). The amphibole formula calculation was done using a cation sum of 13 excluding Ca, Na, and K. Limits of



detection (in wt. %) in amphibole are: SiO<sub>2</sub>: 0.04; TiO<sub>2</sub>: 0.02; Al<sub>2</sub>O<sub>3</sub>: 0.04; FeO: 0.094, MnO: 0.06; MgO: 0.056; CaO: 0.06, NaO: 0.06; K: 0.014; Cr: 0.09; Cl: 0.003; F: 0.3.

### **3.3 Results**

#### **3.3.1 Preliminary experiments**

Preliminary runs were performed to test the experimental design. After trying experiments at various fluid/rock ratios, it was found that product amphiboles obtained at slightly higher water/rock ratios (>0.1) had a more consistent structural formula, and thus reached local equilibrium. Conversely, amphiboles obtained at lower water rock ratios resulted in many analyses with low totals, suggesting formation outside or partially outside equilibrium. For this reason, the results section is concentrated on the experiments performed at fluid/rock ratios of 0.2.

The amphibole compositions measured in hydrothermal amphiboles formed at low water/rock ratios show a wide range of A-site (Na+K) occupancies (0 to 0.9 a.p.f.u.), and plot on a continuum between actinolite-hornblende and edenite-pargasite domains in comparison to the starting material (similarly to experiments run at higher water/rock ratios), and plot on a continuum between actinolite-hornblende and edenite-pargasite domains in comparison to the starting material. Most Cl contents in amphibole are below 0.2 wt. % (0.05 a.p.f.u.). Representative analyses of amphiboles formed at fluid/rock ratios of 0.07 wt. % with totals above 96 are shown in the appendix (supplementary table S3).

Experiments were also performed using KCl instead of NaCl. However, the strategy was abandoned since it escaped the objective of simulating a seawater-derived fluid, i.e. a predominantly NaCl-rich fluid. In addition, experiments were run with only an amphibole crystal and a NaCl-rich fluid, however, again the issue was that the system to be simulated required the full host rock assemblage, containing other phases

as well. The latter experiments resulted in the formation of Na-rich hydrothermal amphibole on the rims of the starting amphibole, indicating the extraction of Na from the fluid, but not the Cl.

### 3.3.2 Suprasolidus experiments

Experiments run at a temperature of 900 °C (IHB20-9) at the lowest fluid/rock ratio (0.07) show the presence of a melt phase (Fig. 3.5D). New amphibole crystallized in melt pools (about 10 - 20 µm grain size), in contact with plagioclase and olivine, sometimes as rims (5 µm grain size) around olivine, classified as magnesio-hastingsite and tschermakite. Compositions of experimental amphiboles plotted in Figs. 3.7A and 3.8A show little departure from the starting amphibole's magnesio-hastingsitic composition, with only slightly lower <sup>v</sup>Al. TiO<sub>2</sub> contents of newly-crystallized amphibole show variations between 0.5 wt. % TiO<sub>2</sub> and ~ 2 wt. %, depending on local availability of Ti (i.e., local presence of a Fe-Ti oxide phase). These newly-crystallized amphiboles mostly show consistent Cl contents above 0.15, reaching maximum Cl contents of 0.48 wt. %. The coexisting melt phase is evolved and enriched in SiO<sub>2</sub>, very similar to the felsic melts produced by hydrous partial melting of oceanic gabbros (Koepke et al., 2004; 2007).

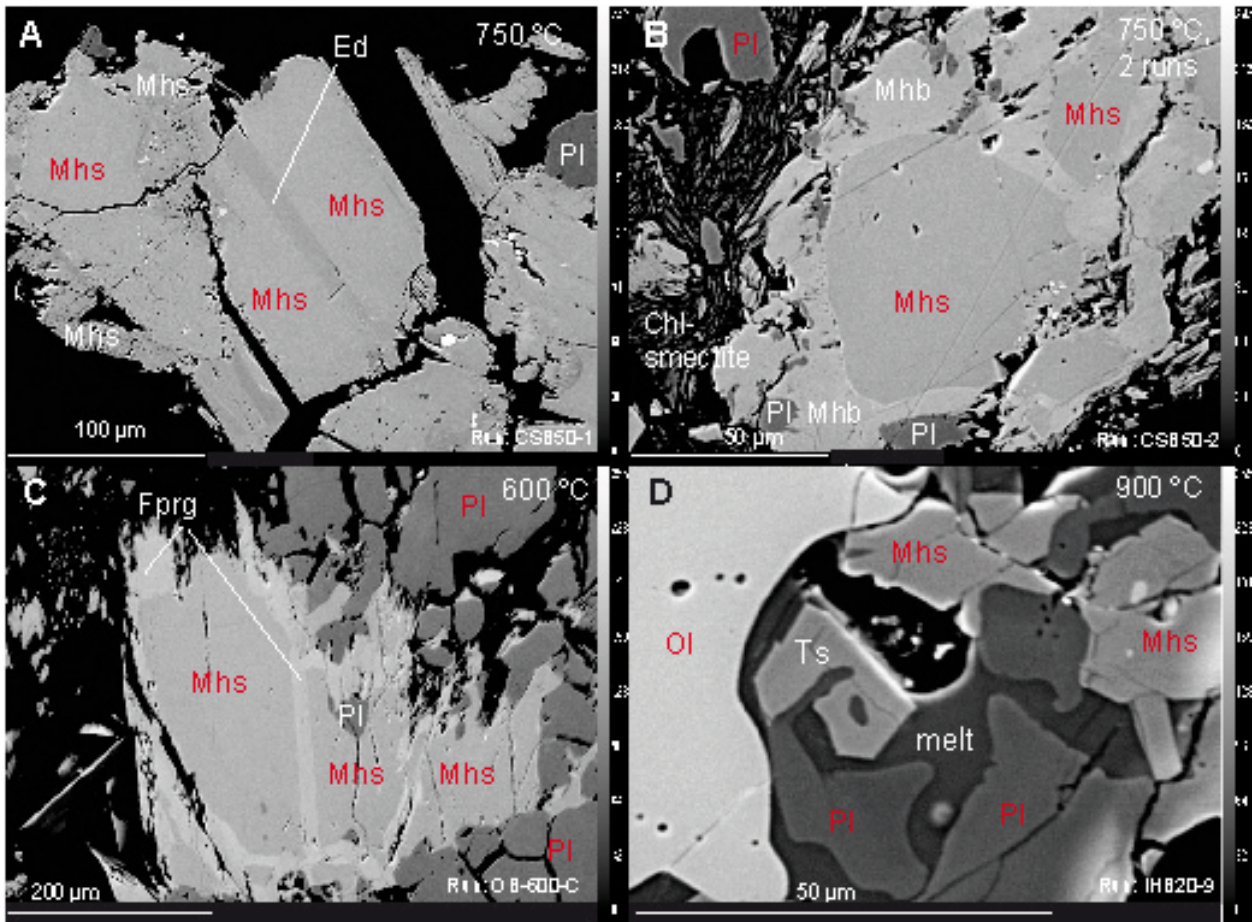


**Figure 3.5.** BSE images of experimental products. Pre-existing minerals such as the starting amphibole (Ti-rich magnesio-hastingsite) are indicated in red. A: Experiment performed at 750 °C, with 50 wt% NaCl fluid. Newly crystallized amphiboles (magnesio-hastingsite and edenite) form coherent domains within the starting amphiboles, corresponding to epitactic growth. B: Experiment performed at 750 °C, with 50 wt% NaCl fluid, run twice with an added batch of NaCl-rich fluid. Relatively large crystals of the starting amphibole are replaced by porous domains of magnesio-hornblende with plagioclase inclusions. Aggregates of chlorite/smectite mixed layer minerals are visible in the matrix. C: Experiment performed at 600 °C, with 20 wt% NaCl fluid. Note the overgrowth of new ferro-pargasite replacing the starting amphibole at the rim, showing features of crystal growth into an open space. D: Experiment performed at 900 °C, with 20 wt% NaCl in fluid, showing newly formed tschermakite amphibole and small melt pools, as well as relict plagioclase, olivine, and amphibole of the starting gabbro. Mineral abbreviations after Whitney and Evans (2010); Ed: Edenite; Fprg: ferro-pargasite; Hst: hastingsite; Mhb: magnesio-hornblende; Mhs: magnesio-hastingsite; Ts: tschermakite; Pl: plagioclase; Ol: olivine.

### 3.3.3. Subsolidus experiments

#### 3.3.3.2. *Experiments performed with setup A*

During experiments, new Cl-enriched magnesiohastingsite was formed around small pieces of Ti-rich magnesiohastingsite single crystals, which were added to the starting material. The Cl content of these rims do not exceed 0.3 wt% Cl.

In comparison to the starting material and core of the amphiboles, rims are generally poor in Ti, which is to be expected given the difference in formation temperature from starting Ti-rich magnesiohastingsite to newly-formed Ti-poor magnesiohastingsite. A decrease in Al content is observed, with a subsequent increase in Si. In addition, newly-formed rims are more enriched in Mg (>1wt%) than cores. The reactions taking place during experiments follow the hastingsite/edenite isomorphous substitution towards edenite (Fig. 3.6).

Most Cl-rich amphiboles (> 0.15 wt% Cl) found in reaction rims show slightly different cation compositions. Namely, the concentration of total Fe is higher than in other newly-formed amphibole rims, which is consistent with studies by Oberti et al. (1993) on the structural constraints on Cl acceptance in relation to certain cations in the amphibole structure (mainly Fe<sup>2+</sup>, Na, and K).

The changes observed in the A-site, if we compare core and rim, involve the incorporation of additional Na, coupled with the loss of K in the site, in equal amounts. We are thus able to extrapolate that an exchange took place between the Na in the saline solution added in the experimental capsule and the K in the A-site of the starting amphibole.

The main difference between experimental products of single-run experiments and those run a second time with a second batch of saline fluid is that, in the latter type, the hastingsite – edenite exchange reaction has gone further (i.e. cores and rims show both higher Si and Mg with respect to cores and rims

measured after single-run experiments). Compositions are shown in Fig. 3.6 and EPMA measurements are found in the appendix (supplementary table S2).

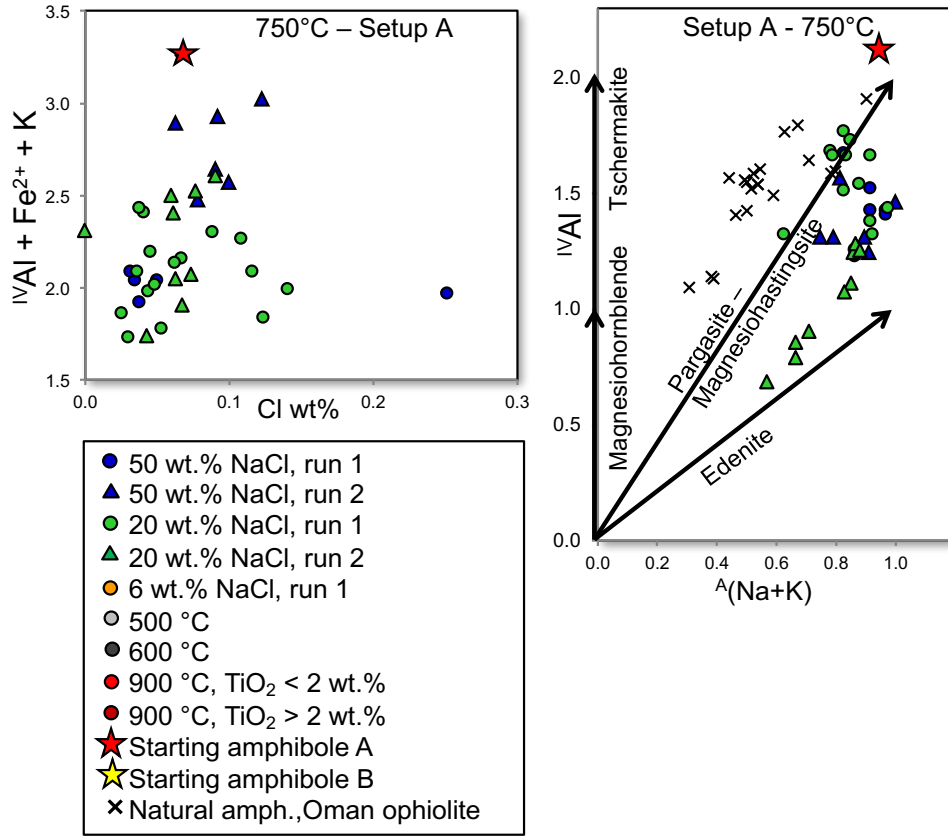


**Figure 3.6.** Figure 3.6. Compositional diagrams for amphiboles formed with setup A.

### 3.3.3.2. Experiments performed with setup B

After experiments, relics of the initial olivine gabbro assemblage were preserved in all runs. In general, a decrease in the amount of primary olivine, clinopyroxene, and magnetite in the starting gabbro can be observed, especially in multiple-run experiments, with a relative increase in plagioclase and amphibole in the newly formed phases.

Table 3.2. EPMA analyses of newly-formed amphibole from experimental products (representative analyses) and starting amphibole (average).

Run	Temp. (°C)	Amph. Name <sup>a,b</sup>	wt %													T position <sup>c</sup>													C position						B position						A position						W position					
			SiO <sub>2</sub>	TiO <sub>2</sub>	Al <sub>2</sub> O <sub>3</sub>	Cr <sub>2</sub> O <sub>3</sub>	MnO <sup>d</sup>	FeO <sup>e</sup>	MgO	CaO	Na <sub>2</sub> O	K <sub>2</sub> O	O-Cl	Total	Si	Al	Ti	Al	Cr	Fe <sup>2+</sup>	Mn <sup>2+</sup>	Fe <sup>3+</sup>	Mg	Mn <sup>3+</sup>	Mg	Ca	Na	Na	K	Cl	OH	Mg <sup>f</sup>																				
IHB20-9	900	Ts	43.28	0.40	11.68	0.00	0.17	11.77	15.24	10.59	3.02	0.03	0.03	-0.03	96.28	6.25	1.71	0.04	0.24	1.31	0.02	0.12	3.28	0.00	0.00	1.64	0.36	0.48	0.01	0.03	1.97	96.6																				
IHB20-9	900	Mhs	42.80	0.84	14.11	0.00	0.18	10.08	16.00	10.70	3.39	0.03	0.06	-0.01	98.18	6.03	1.97	0.09	0.37	1.19	0.00	0.00	3.33	0.02	0.03	1.62	0.36	0.57	0.01	0.01	1.99	100.0																				
IHB20-9	900	Ts	42.60	2.12	11.56	0.00	0.21	14.10	14.29	10.13	3.22	0.01	0.48	-0.11	98.61	6.08	1.92	0.23	0.02	1.45	0.03	0.23	3.04	0.00	0.00	1.55	0.45	0.44	0.00	0.11	1.88	92.9																				
CSB50-1	750	Mhs	42.91	0.19	11.71	0.00	0.10	13.20	15.63	10.66	3.98	0.02	0.07	-0.02	98.45	6.11	1.89	0.02	0.08	1.42	0.01	0.15	3.32	0.00	0.00	1.63	0.37	0.72	0.00	0.01	1.98	95.6																				
CSB50-1	750	Ed	45.67	0.92	8.79	0.05	0.14	12.40	14.93	10.63	3.51	0.00	0.04	-0.01	98.40	6.62	1.38	0.10	0.12	0.72	0.01	0.50	3.55	0.00	0.00	1.60	0.40	0.74	0.00	0.01	1.99	87.7																				
CSB50-1	750	Mhs	43.89	0.00	10.39	0.00	0.14	12.40	14.93	10.63	3.51	0.00	0.06	-0.06	96.30	6.41	1.59	0.03	0.20	1.03	0.02	0.49	3.25	0.00	0.00	1.66	0.34	0.66	0.00	0.06	1.94	87.0																				
CSB50-2	750	Mhs	43.00	1.08	11.84	0.22	0.15	11.78	15.10	10.62	3.68	0.01	0.26	-0.01	97.55	6.18	1.82	0.12	0.19	0.03	1.07	0.02	0.34	3.24	0.00	0.00	1.64	0.37	0.66	0.00	0.01	1.98	90.4																			
CSB50-2	750	Ed	45.74	0.92	8.96	0.10	0.05	11.67	15.99	10.37	4.01	0.00	0.07	-0.01	97.88	6.56	1.45	0.10	0.07	0.01	0.87	0.01	0.53	3.42	0.00	0.00	1.59	0.41	0.71	0.00	0.01	1.98	86.5																			
CSB50-2	750	Mhs	44.58	1.31	9.65	0.01	0.22	11.53	15.24	10.48	3.71	0.00	0.34	-0.08	97.00	6.48	1.52	0.14	0.13	0.00	0.80	0.03	0.60	3.30	0.00	0.00	1.65	0.37	0.68	0.00	0.08	1.97	84.6																			
CSB20-1	750	Mhs	42.67	0.81	12.63	0.03	0.25	11.16	14.46	10.56	3.62	0.01	0.11	-0.03	96.29	6.21	1.79	0.09	0.38	0.00	0.91	0.03	0.45	3.14	0.00	0.00	1.65	0.35	0.67	0.00	0.02	1.97	87.4																			
CSB20-1	750	Mhb	46.17	0.69	9.00	0.00	0.15	10.58	16.49	10.21	3.17	0.00	0.08	-0.02	96.53	6.61	1.39	0.08	0.13	0.00	1.11	0.02	0.16	3.52	0.00	0.00	1.57	0.44	0.45	0.00	0.02	1.98	95.8																			
CSB20-2	750	Ts	44.41	0.43	10.57	0.00	0.22	11.08	16.47	10.20	3.24	0.01	0.13	-0.03	96.71	6.35	1.65	0.05	0.13	0.00	1.32	0.00	0.00	3.48	0.03	0.03	1.56	0.41	0.49	0.00	0.03	1.97	100.0																			
CSB20-1	750	Ts	44.41	0.43	10.57	0.00	0.22	11.08	16.47	10.20	3.24	0.01	0.13	-0.03	96.71	6.35	1.65	0.05	0.13	0.00	1.32	0.00	0.00	3.48	0.03	0.03	1.56	0.41	0.49	0.00	0.03	1.97	100.0																			
CSB20-2	750	Mhs	43.77	0.48	11.36	0.00	0.23	11.81	15.05	9.95	3.68	0.00	0.07	-0.02	96.39	6.32	1.68	0.05	0.25	1.21	0.03	0.22	3.24	0.00	0.00	1.54	0.46	0.57	0.00	0.01	1.98	93.7																				
CSB20-2	750	Mhs	45.18	0.09	4.99	0.00	0.24	8.63	18.40	10.98	1.90	0.01	0.12	-0.03	96.51	7.23	0.77	0.01	0.07	0.83	0.03	0.19	3.88	0.00	0.00	1.66	0.34	0.18	0.00	0.02	1.97	95.4																				
CSB20-2	750	Ed	45.46	0.94	9.65	0.00	0.28	11.65	15.08	9.98	3.48	0.00	0.08	-0.02	96.58	6.57	1.43	0.10	0.21	0.96	0.04	0.45	3.25	0.00	0.00	1.54	0.46	0.52	0.00	0.01	1.98	87.8																				
CSB20-2	750	Mhs	43.47	2.10	10.69	0.09	0.20	12.80	13.54	10.77	3.47	0.01	0.35	-0.08	97.40	6.37	1.63	0.23	0.21	0.59	0.02	0.98	2.96	0.00	0.00	1.69	0.31	0.67	0.00	0.08	1.91	75.1																				
CSB6-1	750	Mhs	38.48	0.47	15.73	0.00	0.21	17.54	9.41	12.11	3.24	0.04	0.02	0.00	97.25	5.80	2.20	0.05	0.59	0.63	0.03	1.58	2.12	0.00	0.00	1.96	0.04	0.90	0.01	0.00	2.00	57.3																				
CSB6-1	750	Ts	43.50	0.02	11.55	0.00	0.14	14.19	14.54	10.25	3.30	0.03	0.06	-0.01	97.57	6.23	1.77	0.00	0.18	1.52	0.02	0.18	3.10	0.00	0.00	1.57	0.43	0.49	0.01	0.01	1.99	94.5																				
CSB6-1	750	Mhs	45.85	0.26	9.02	0.00	0.19	12.98	15.21	10.17	2.60	0.01	0.07	-0.01	96.36	6.60	1.41	0.03	0.13	1.36	0.02	0.20	3.26	0.00	0.00	1.44	0.56	0.26	0.00	0.01	1.89	97.7																				
CSB6-1	750	Mhb	50.61	0.08	6.21	0.00	0.15	9.77	18.52	9.94	1.39	0.16	0.13	-0.03	96.93	7.08	0.92	0.01	0.10	1.14	0.00	0.37	3.02	0.00	0.00	1.70	0.30	0.44	0.00	0.01	1.99	82.5																				
CSB50-1	650	Mhs	42.64	1.55	10.95	0.00	0.14	13.67	13.23	10.73	3.24	0.01	0.07	-0.02	96.22	6.30	1.70	0.17	0.21	0.82	0.02	0.87	2.91	0.00	0.00	1.70	0.30	0.63	0.00	0.01	1.98	77.0																				
CSB50-1	650	Mhb	44.10	0.51	9.88	0.00	0.16	18.94	10.57	10.82	2.48	0.00	0.15	-0.03	97.57	6.53	1.48	0.06	0.25	0.98	0.02	1.37	2.33	0.00	0.00	1.72	0.29	0.43	0.00	0.03	1.96	63.0																				
CSB50-1	650	Ts	45.49	0.06	11.34	0.00	0.22	11.34	16.13	10.99	2.79	0.03	0.08	-0.02	98.45	6.18	1.82	0.01	0.09	1.27	0.03	0.06	3.37	0.00	0.00	1.65	0.35	0.41	0.01	0.01	1.98	98.1																				
CSB50-1	650	Ts	45.75	0.68	9.82	0.00	0.19	13.20	15.01	9.48	2.95	0.00	0.46	-0.10	97.44	6.51	1.50	0.07	0.15	1.50	0.02	0.70	2.75	0.00	0.00	1.69	0.31	0.59	0.00	0.02	1.99	79.8																				
CSB20-1	650	Ts	44.26	1.36	10.74	0.07	0.26	12.76	14.03	10.97	2.64	0.00	0.06	-0.01	96.82	6.30	1.70	0.06	0.22	1.55	0.03	0.03	3.12	0.00	0.00	1.60	0.40	0.02	0.00	0.00	1.99	97.7																				
CSB20-1	650	Mhs	42.58	0.45	11.17	0.00	0.33	15.36	13.02	10.78	2.99	0.00	0.04	-0.01	96.71	6.25	1.75	0.05	0.18	1.24	0.04	0.65	2.85	0.00	0.00	1.69	0.31	0.54	0.00	0.01	1.99	81.5																				
CSB20-1	650	Mhb	47.27	0.41	6.99	0.01	0.29	14.14	14.52	10.91	2.01	0.01	0.07	-0.02	96.60	6.86	1.14	0.05	0.06	1.02	0.04	0.69	3.14	0.00	0.00	1.70	0.30	0.26	0.00	0.01	1.98	81.9																				
CSB20-1	650	Mhs	41.95	0.05	11.03	0.00	0.18	17.28	12.52	10.70	3.16	0.02	0.10	-0.02	96.99	6.18	1.82	0.01	0.09	1.43	0.02	0.70	2.75	0.00	0.00	1.69	0.31	0.59	0.00	0.02	1.99	79.8																				
CSB20-1	650	Mhs	46.93	0.22	9.14	0.00	0.36	13.11	15.06	10.50	1.54	0.02	0.04	-0.01	96.91	6.66	1.34	0.02	0.19	1.48	0.04	0.07	3.19	0.00	0.00	1.60	0.40	0.02	0.00	0.00	1.99	97.7																				
CSB6-1	650	Ts	44.07	0.51	11.44	0.00	0.25	13.17	14.64	10.53	2.16	0.01	0.05	-0.01	96.82	6.30	1.70	0.06	0.22	1.55	0.03	0.03	3.12	0.00	0.00	1.61	0.39	0.21	0.00	0.01	1.99	99.2																				
CSB6-1	650	Mhs	41.13	0.27	13.67	0.03	0.17	14.46	12.83	12.03	2.83	0.01	0.04	-0.01	97.45	6.02	1.98	0.03	0.38	0.97	0.02	0.81	2.80	0.00	0.00	1.89	0.11	0.69	0.00	0.01	1.99	77.7																				
CSB6-1	650	Ts	42.84	0.17	12.71	0.05	0.26	16.26	12.03	10.58	2.20	0.01	0.07	-0.02	97.17	6.21	1.80	0.02	0.38	1.48	0.03	0.50	2.60	0.00	0.00	1.64	0.36	0.26	0.00	0.01	1.98	84.0																				
OB-600-C	600	Mhs	40.81	1.02	12.31	0.03	0.18	17.30	10.82	11.12	2.97	0.01	0.03	-0.01	96.60	6.11	1.89	0.12	0.28	1.12	0.28	0.00	0.95	0.02	1.22	0.41	0.00	0.78	0.22	0.65	0.00	0.00	1.99	66.5																		
OB-600-C	600	Ms	39.76	0.29	13.98	0.10	0.15	21.77	7.87	11.16	3.30	0.00	0.03	-0.01	98.40	5.97	2																																			

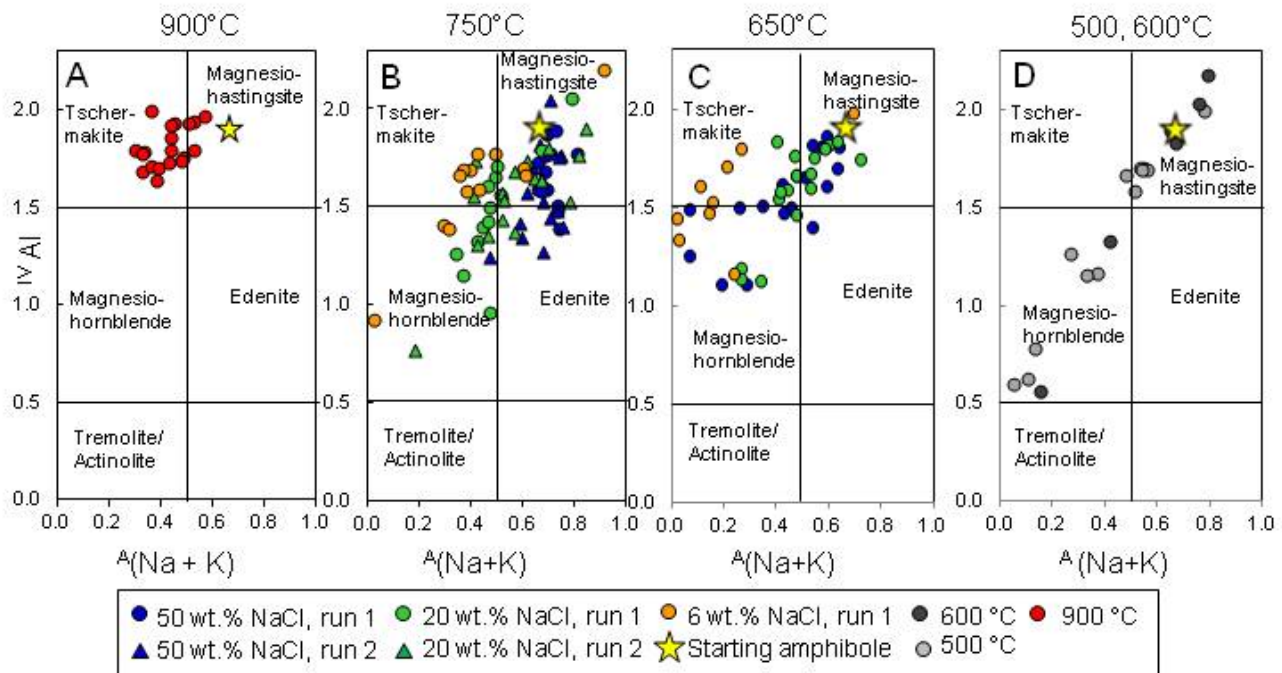


**Figure 3.7.** Diagrams showing  $^{\text{Al}}$  vs.  $^{\text{A}}(\text{Na}+\text{K})$  of product amphibole formed during experiments. Formula calculated using a sum of 13 cations excluding Ca, Na and K. Fields and classification after Leake et al. (1997). Stars denote starting amphibole composition (magnesio-hastingsite). A corresponds to experiment IHB20-9, B to experiments CSB50-1, CSB50-2, CSB20-1, CSB20-2, CSB6-1, C to experiments CSBX50-1, CSBX20-1, CSBX6-1, and D to experiments OB-600-C and OB-500-C.

a) Experimental runs performed at 750°C

The growth of new amphibole has been found on both on rims of the starting amphibole and as outward-growing prismatic crystals (Fig. 3.7). Secondary plagioclase, olivine, and clinopyroxene have been identified in equilibrium with the newly-formed amphibole. Interstitially, we observe the growth of chlorite-smectite (Fig. 3.5).

The newly-formed calcium amphibole crystals measured in experiments run at 750 °C are classified as magnesio-hastingsite, magnesio-hornblende, tschermakite and edenite (Leake et al., 1997) ranging from significantly higher Si (>7 atoms per formula unit (a.p.f.u.)) to lower Si (~5.2 a.p.f.u.) than the starting

amphibole (Fig. 3.7B).  $\text{TiO}_2$  contents are below 1.5 wt. %, and Mg# ( $100 * \text{Mg}/(\text{Mg}+\text{Fe}^{2+})$ ) ranges from 57 to 100. A-site occupancy (mainly Na), is variable, from 0.2 to 0.9 a.p.f.u. (table 3.2).

Effect of salinity is reflected in the Na content and A-site occupancy of the newly-formed amphiboles (Fig. 3.7B). Higher NaCl concentration in experimental fluid resulted in higher Na contents in amphiboles formed during experiments with 50 wt. % NaCl (0.9 – 1.15 total Na a.p.f.u.) in relation to experiments run with a fluid with 20 wt.% NaCl (0.5 – 1 total Na a.p.f.u.), and likewise, experiments with 20 wt. % NaCl have higher Na contents than experiments performed with a 6 wt. % NaCl fluid (0.38 – 0.95 total Na a.p.f.u.). In addition, in terms of Cl content, experiments performed with 50 wt. % result in higher Cl contents (0.26 wt. % Cl) than experiments performed at 20 wt. % NaCl (0.13 wt. % Cl), this difference, however is not observed in experiments run a second time. Experiments run with 6 wt. % Cl also reach a maximum of 0.13 wt.% Cl (Fig. 3.8B).

Experiments run a second time (CSB50-2, CSB20-2) result in higher Cl contents (0.34 and 35 wt. % Cl, respectively) than experiments of the same characteristics run a single time (0.26 wt. % Cl for CSB50-1, and 0.13 wt. % Cl for CSB20-1).



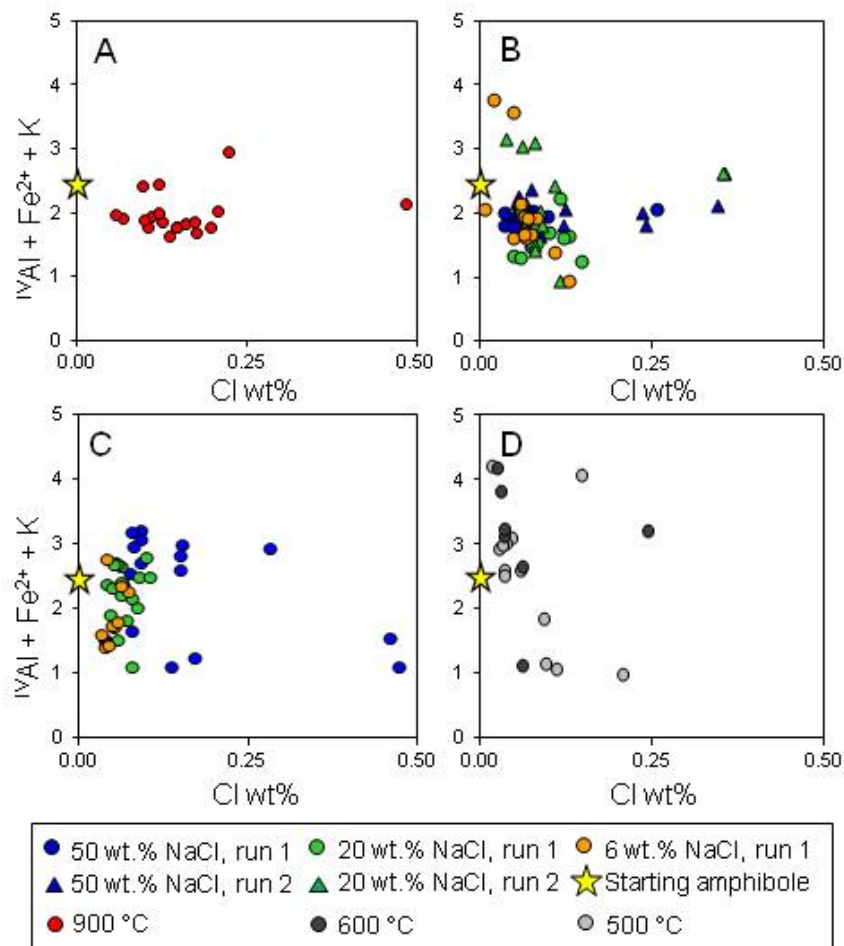


**Figure 3.8.** Diagrams showing the relationships between  $|Al| + Fe^{2+} + K$  vs.  $Cl$  wt% measured in amphiboles of the experimental products. Formula calculated using a sum of 13 cations excluding  $Ca$ ,  $Na$  and  $K$ . Fields and classification after Leake et al. (1997). Stars denote starting amphibole composition (magnesio-hastingsite). A corresponds to experiment IHB20-9, B to experiments CSB50-1, CSB50-2, CSB20-1, CSB20-2, CSB6-1, C to

*b) Experimental runs performed at 650 °C*

The experimental paragenesis found after runs at 650 °C is integrated by newly-formed amphibole, plagioclase, olivine, and small amounts of clinopyroxene.

Experimental amphiboles measured in experiments run at 650 °C correspond to magnesio-hastingsite, magnesio-hornblende, tschermakite and edenite (Leake et al., 1997), with a range of Si contents between 6 and 6.9 a.p.f.u. (Fig. 3.7C).  $TiO_2$  contents are below 1.6 wt. %, and Mg # is between 63 and 98. A-site occupancy in newly-formed amphiboles is generally below that of the starting amphibole (0.63 a.p.f.u.).

Effect of fluid salinity is reflected in significantly higher maximum Cl contents (0.47 wt. %) measured in experiments run with a 50 wt. % NaCl, vs. 0.10 and 0.07 wt. % Cl in experiments run at 650 °C with a 20 wt. % and a 6 wt. % starting solution, respectively (Fig. 3.8C). Additionally, total Na and A-site occupancy are lowest in experiments run with a concentration of 6 wt. % NaCl in fluid (total Na: 0.4-0.8).

*c) Experimental runs performed at 600 and 500 °C*

In experiments run at 600 and 500 °C at a water/rock ratio of 1 the growth of new amphibole can be observed in equilibrium with secondary plagioclase (Figs. 3.5, 3.9C). As evident in Fig. 3.9, needle-like shaped phases are found crystallizing on the surface of the gabbro cylinder and interstitially. Accurate analysis with EPMA was not possible due to their small size, though most of the analyses show relatively high amounts of MgO and Al<sub>2</sub>O<sub>3</sub>, with totals of ~86 to 88 wt%, implying the presence of chlorite – smectite mixed layers. The experiment performed at 500 °C, with a higher proportion of hydrous minerals and replacement of the original assemblage than the experiment at 600 °C.

Measured amphiboles are classified as hastingsite, magnesio-hastingsite, magnesio-hornblende, ferro-pargasite, and tschermakite (Leake et al., 1997). These amphiboles show a wide range of Si content, from <6 to 7.5 a.p.f.u., TiO<sub>2</sub> contents below 2 wt. %, and Mg# between 36 and 91. A-site occupancy ranges from 0 to 0.8 a.p.f.u (Fig. 3.7D).

Maximum Cl contents obtained at 600 °C are measured in magnesio-hastingsite (0.24 wt. % Cl) and in Si-rich magnesio-hornblende at 500 °C (0.20 wt. % Cl) (Fig. 3.8D).

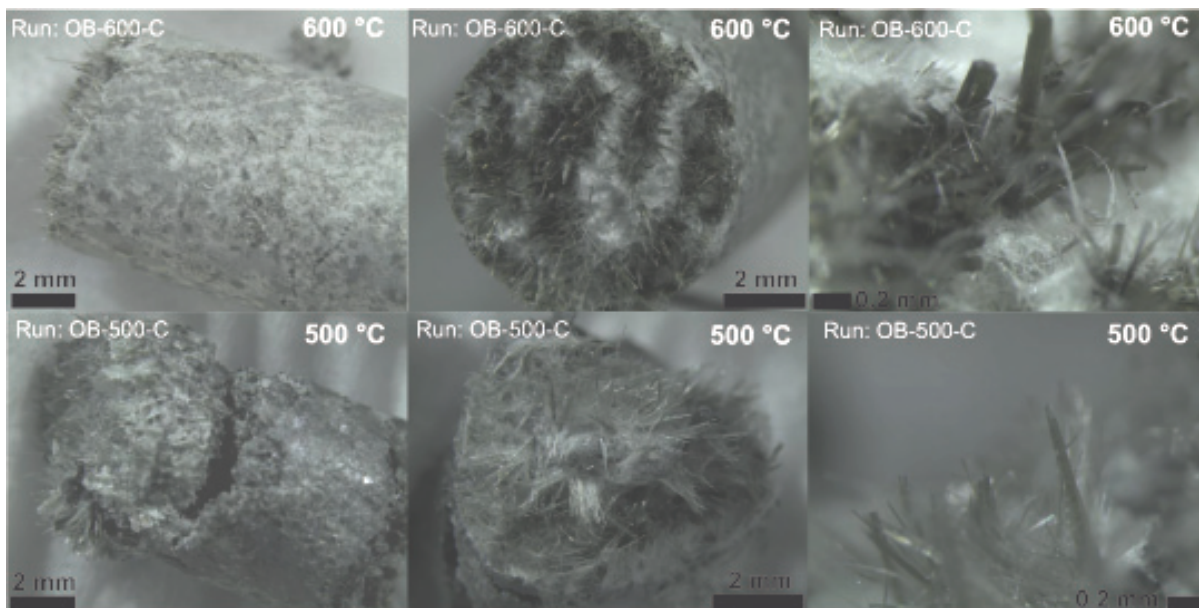


**Figure 3.9.** Microscope images from experiments performed in cold seal pressure vessels at 600 °C and 500 °C (OB-600-C and OB-500-C) with a fluid/rock ratio of 1 and a duration of 101 days (image acquisition by Leica M205 C stereo microscope equipped with Leica DFC 295 camera system). In both experiments the growth of new amphibole, as prismatic crystals on the surface of the gabbro cylinder, and mineralization of chlorite and smectite with needle-like shape are observed.

### 3.4 Discussion

#### 3.4.1 Compositional variations of newly-formed amphiboles

It is a characteristic feature of our experiments that the newly-formed amphiboles show a rather large variation in compositions. Depending on temperature, they vary from magnesio-hastingsite, through tschermakite or edenite, to magnesio-hornblende with  $Si \sim 7.5$  (close to actinolitic compositions) (Fig. 3.7). In terms of metamorphic facies, the chosen experimental temperatures correspond to a variation from granulite facies (900°C), via higher amphibolite facies (750°C), lower amphibolite facies (650 and 600°C) down to greenschist facies (500°C). An interesting outcome of this study is that although experiments were conducted under a given temperature, amphiboles do not cluster in one specific field, but show a large variation, which increases with decreasing temperature. This variation is largest in the

500 and 600°C runs where amphibole compositions vary from high-Si magnesio-hornblende (close to actinolite) up to magnesio-hastingsite. Even in the run simulating greenschist facies at 500°C, some newly-formed amphiboles show the composition of magnesio-hastingsite, which is normally not considered typical for greenschist facies assemblages. Only in the suprasolidus run, the experimental amphiboles cluster in a relatively small area in comparison to the other runs under subsolidus conditions – between the tschermakite and magnesio-hastingsite fields – high Al amphiboles being typically formed under high temperatures. In 750°C runs, at the transition between granulite and higher amphibolite facies, it is surprising that some of the amphiboles show compositions of magnesio-hornblende that are relatively low in  $^{23}\text{Na}+^{39}\text{K}$  and  $^{27}\text{Al}$  in the tetrahedral site, which is unexpected at such high temperatures.

The presence of amphiboles with different Si contexts in settings of high temperature hydrothermal alteration in association with Cl-bearing amphiboles is not uncommon and is mostly associated with hydrothermal fluids that have cooled significantly, down to approximately 500 °C and below. Actinolite has been documented in association to higher-temperature Cl-bearing amphiboles in gabbroic rocks. Ito & Anderson (1983) reported the presence of actinolite and chlorite, as a result of the alteration of anorthite and hornblende at a temperature of 450 °C. Similarly, Silantyev et al. (2008) reported actinolite in assemblage with chlorite forming fibrous aggregates in contact with olivine and plagioclase, and as rims on relics of olivine, at low formation temperatures. Along these lines, Enami et al. (1999) described Cl-rich hastingsite with chlorine contents of 1 to 2.7 wt. %, intergrown with actinolites with less than 0.5 wt. % Cl, and suggest formation during shallow metamorphism at 300-400 °C. Manning (1993) reports actinolite forming outside equilibrium in the context of contact metamorphism of basaltic rocks. Due to disequilibrium caused by reaction kinetics, a whole mineral zone of the contact aureole corresponding to the amphibolites facies is not present altogether, involving a sharp transition from a 900-800 °C zone to a 300-500 °C zone with a total absence of hornblende nucleation. All these studies present phase situations where amphiboles of theoretically different thermal stabilities apparently coexist, which leads to an

apparent contradiction. However, in our experimental runs conducted under isothermal conditions, we observe the same situation, i.e., the apparent coexistence of near-actinolitic compositions and magnesio-hastingsite in the 600°C run. These situations have in common that there are different domains in close association corresponding to a local equilibrium with the reacting fluid, while there is no global equilibrium with the host rock. Our experiments show that the main factor constraining the composition of amphibole is not the temperature, but the local mineralogy of the starting material and the local equilibrium with the fluid. For instance this is reflected in the amphiboles of the run at the highest temperature in the partly molten system: here, TiO<sub>2</sub> in amphibole varies between 0.19 and 2.29 wt. % which is obviously related to local equilibrium, whether a Fe-Ti oxide is present or not. The formation temperature of experimental amphiboles high in TiO<sub>2</sub> (>2 wt. %) coincides with the temperature given by the Ti-in-amphibole geothermometer of Ernst and Liu (1998) – e.g., amphiboles with the highest TiO<sub>2</sub> concentration reveal 870°C (900°C run temperature). In this case, Ti saturation is given, a requirement for the application of this semi-quantitative thermometer. However, experimental amphiboles in the same run with relatively low TiO<sub>2</sub> contents (<1 wt. %) reveal much lower temperatures when using the aforementioned geothermometer (522°C for the amphibole with the lowest TiO<sub>2</sub>). This lack of correspondence between experimental and calculated temperature is due to the absence of a Fe-Ti oxide in the reacting local assemblage preventing TiO<sub>2</sub> saturation.

### **3.4.2 Suprasolidus conditions**

Suprasolidus experiments resulted in more homogeneous amphibole compositions than subsolidus experiments, both in terms of Cl concentration and cation distribution in amphibole (Figs. 3.7A and 3.8A). The presence of small pockets of melt in our experiments at 900 °C evidence the presence of residual hydrous melts during the last stages of suprasolidus conditions during cooling of the lower oceanic crust.

In the crystal mush, the melt migrates along grain boundaries and reacts with phases, forming new minerals (Coogan et al., 2001). As seen in relevant partial melting experiments in gabbros (Koepke et al., 2004), the melt generated is evolved and enriched in  $\text{SiO}_2$ . Since there is little melt volume, volatile elements such as Cl concentrate in the melt and a hydrothermal fluid may exsolve from this melt during degassing (Coogan et al., 2000; 2001, and references therein). In the context of a shallower volcanic system, Sato et al. (2005) attribute changes of Cl content in amphibole to input-output processes of hydrous fluids in magma chambers, and discuss different models of degassing in detail. They report Cl contents in amphibole up to 0.1 wt%. Chlorine content in melt decreases strongly when approaching solidus, probably due to exsolution of the aqueous fluid from the melt (Zhang et al., 2012).

### 3.4.3 Application to nature

Fig. 3.10 shows the occurrence of a magmatic pargasite on the boundary between a layered olivine gabbro and a gabbroic dikelet reflecting a fossilized melt at a very high temperature fluid pathway, sampled in the layered gabbro section of the Oman Ophiolite in the vicinity of the crust/mantle boundary. It illustrates the result of interaction between a gabbro and several pulses of hydrothermal fluid at different temperatures ranging from magmatic to amphibolite facies. We can observe that the pargasite is zoned, with different Cl contents in each of the amphibole zones from <0.2 to >5 wt. % Cl (magmatic pargasite, hydrothermal magnesio-hornblende, hydrothermal super Cl-rich hastingsite). These compositional variations indicate the passage of fluids at different temperatures and with varying Cl concentrations. The hastingsite with the highest Cl content evidences equilibrium with a fluid saturated in NaCl, while the magnesio-hornblende with Cl <0.4 wt. % Cl formed in equilibrium with a fluid below NaCl saturation, such as the fluid used in our experiments. The amphibole labelled as high-Ti pargasite is comparable to the amphibole formed in experiment IHB20-9, at suprasolidus conditions, and the amphibole labelled as magnesio-hornblende is analogous to some of the products of experiments at 650 and 750 °C. Our

experiments did not simulate the reaction that formed the super-Cl-rich hastingsite, since we used a saline aqueous fluid that was not saturated in NaCl (see Chan et al., 2016).

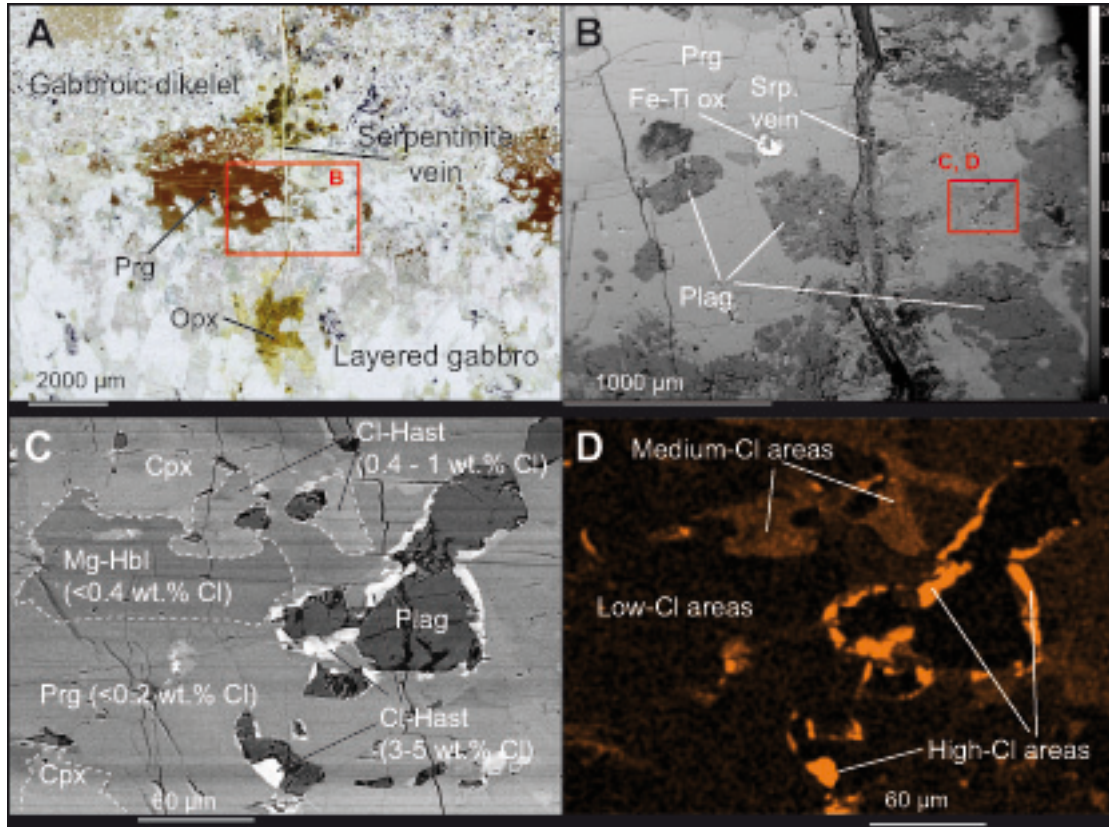


**Figure 3.10.** Microphotograph of thin section of sample WA32A showing the boundary between layered gabbro and a gabbroic dikelet affected by the action of hydrothermal fluids. **B:** BSE images of the same area in more detail. **C:** Detail of alteration of pargasite and plagioclase to super Cl-rich hastingsite, and magnesio-hornblende zone. **D:** Cl map produced by SEM/EDX of area C, brightness denotes high Cl contents, and dark areas are Cl-poor. Mineral abbreviations after Whitney and Evans (2010); Hst: hastingsite; Mhb: magnesio-hornblende; Prg: pargasite; Srp: serpentine; Pl: plagioclase; Opx: orthopyroxene; Cpx: clinopyroxene.

In Fig. 3.11, we compare our experimental results with amphiboles from natural rocks from the oceanic crust at different settings (fast- and slow-spreading systems) focussing on large datasets provided in several studies: from samples drilled at the ocean floor, and ophiolites: Silantsev et al. (2008), Ito and

Anderson (1983), Vanko (1986), Alt et al. (2010), Gillis et al. (2003), Coogan et al. (2001), Wolff (2014), Bosch et al. (2004), and Koepke et al. (2008; 2011).

The dataset from Silantyev et al. (2008) includes amphiboles from dolerite dyke samples drilled from the Mid-Atlantic Ridge at 15° 44' N at sites 1275B at a depth of 108.7 m (Leg 209, ODP), formed at temperatures 400-600 °C at slow spreading rates. Ito and Anderson (1983) include amphiboles from the Mid-Caiman Rise formed at temperatures between 550 and 750 °C that become less aluminous at decreasing temperatures, which is consistent with the results of our experimental study. Ito and Anderson (1983) report on the incipient formation of actinolite at 450 °C, similarly to the formation of magnesio-hornblende close to actinolitic compositions at 500 °C in our experiments. Vanko (1986) measured amphiboles in gabbroic rocks sampled from the Mathematician Ridge (East Pacific Ocean) including actinolite (greenschist facies) and hornblende (amphibolite facies). Coogan et al. (2001) measured amphiboles formed in the temperature range of 600 to 900 °C, MARK area (Mid-Atlantic Ridge south of the Kane Fracture Zone, ODP Hole 923A, and 922B). Studies by Koepke et al. (2008; 2011) include amphiboles from rocks sampled at the dike/gabbro transition at the East Pacific Rise (EPR) in IODP Site 1256D. The study of Alt et al. (2010) includes amphiboles also from the East Pacific Rise (EPR) formed at 350 to 600 °C (IODP Site 1256, Hole 504B) in the upper crust including uppermost gabbros. Gillis et al. (2003) studied amphiboles formed at high (850-925 °C) and intermediate hydrothermal temperatures (610-814 °C), found in rocks also sampled at the East Pacific Rise (ODP Site 894, Leg 147). The dataset of Kullerud (1996) includes amphiboles with 0.1 to 1 a.p.f.u. Cl in metamorphosed gabbroic rocks (norite) from obducted oceanic crust from Lofoten, north Norway, with hydrothermal fluid infiltration at 580 °C. The amphiboles from the datasets of Bosch et al. (2004) and Wolff (2014) were formed at a range between 500 and 975 °C, from dikelets and high temperature veins in the layered gabbro section of the Samail Ophiolite, Sultanate of Oman.



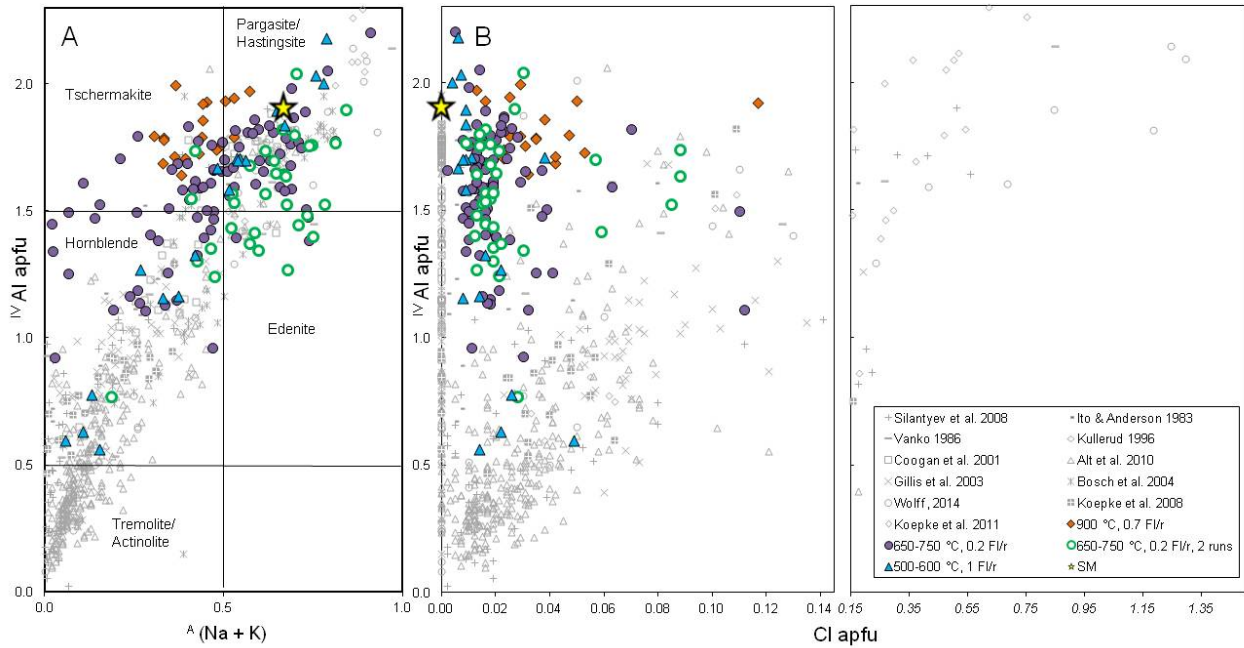


**Figure 3.11.** Diagram showing  ${}^{\text{IV}}\text{Al}$  vs.  ${}^{\text{A}}(\text{Na}+\text{K})$  of experimentally-formed amphiboles. Names of fields after Leake *et al.* (1997), hornblende field includes magnesio-hornblende and ferro-hornblende, tschermakite field includes tschermakite and ferro-tschermakite, pargasite/hastingsite field includes magnesio-hastingsite and ferro-pargasite. **B:**  ${}^{\text{IV}}\text{Al}$  vs.  $\text{Cl}$  a.p.f.u. (atoms per formula unit). Amphiboles formed at suprasolidus conditions (900 °C) and low water/rock ratios (0.07) are denoted by diamonds (incipient hydrothermal activity), amphiboles formed at high temperature subsolidus conditions (650 to 750 °C) and a fluid/rock ratio of 0.2 are denoted by circles (full circles: experiments run once; open circles: experiments run a second time with a new batch of fluid), amphiboles formed at intermediate temperature subsolidus conditions (500 to 600 °C) with a higher fluid/rock ratio (1) are denoted by

Experimental amphiboles from all runs clearly overlap with amphiboles occurring in nature (Fig. 3.11), implying that our experimental approach is relevant for the natural processes of interaction between rock and hydrothermal fluid. In Fig. 3.11 we can see that both our experimental amphiboles and the plotted data from studies of natural samples follow a trend that reflects a gradual increase in hydrothermal activity and decreasing metamorphic temperatures, going from amphiboles rich in tetrahedral Al (<2.3 a.p.f.u.) with high A-site occupancy ( ${}^{\text{A}}(\text{Na}+\text{K}) < 0.9$ ) (e.g. pargasite, magnesio-hastingsite, hastingsite, or ferro-pargasite) down to amphiboles with tetrahedral Al < 0.5 and close to empty A-sites. We can observe that the experimental samples covering the widest range are those performed with highest water/rock ratios (1) at the lowest temperatures (500 – 600 °C), suggesting varying degrees of interaction with the

saline fluid. Amphiboles from Alt et al. (2010), Silantyev et al. (2008), Wolff (2014) plot into the actinolite/tremolite field, and correspond to the stage of greenschist facies metamorphism alteration.

In terms of Cl incorporation in amphibole, the amphiboles from studies that measured relatively high Cl contents ( $>0.3$  a.p.f.u. Cl) (Wolff, 2014; Vanko, 1986; Silantyev et al., 2008; Kullerud, 1996) show a correlation between  ${}^{\text{v}}\text{Al}$  and increasing Cl content. Conversely, all studies of natural samples shown in Fig. 3.11 (and the present experimental study) also measured amphiboles with far lower Cl contents, including chlorine-absent hydrothermal amphiboles. This variability in Cl content is probably due to local changes in Cl activity in the fluid.

#### **3.4.4 Cl incorporation in amphiboles**

As reported by studies on the crystal structure of Cl-bearing amphibole (Volfinger et al., 1985), Oberti et al., 1993; Makino & Tomita, 1993), the incorporation of Cl, being a large anion in comparison to OH and F, involves the deformation of part of the amphibole crystal structure and therefore constrains the cation configuration in the amphibole. This involves preferentially incorporating larger cations like  $\text{Fe}^{2+}$  instead of Mg,  ${}^{\text{v}}\text{Al}$  instead of Si, and K instead of Na when accommodating Cl into the OH site. Several experimental investigations and studies on natural occurrences of Cl-bearing amphibole have supported these findings (Kullerud, 1996; Léger et al., 1996; McCormick & McDonald, 1999). However, though this mainly holds true for Cl-saturated environments, constraints on the incorporation of certain cations are not observed in every case of Cl-enriched amphibole. If availability of chlorine in the hydrothermal system coexisting with the rock is low, the incorporation of Cl in amphibole will be more sensitive to small increases in chlorinity, i.e. to the Cl activity in the fluid, than to structural constraints (Kullerud, 1996; Enami, 1999; Chan et al., 2016).

In our experimental results, the lack of correlation between incorporation of up to 0.5 wt. % Cl in amphibole and cations such as Fe<sup>3+</sup>, K, Na and <sup>iv</sup>Al, may suggest that at low levels of Cl acceptance, such compositional characteristics may not be relevant or pose constraints on Cl incorporation. Chan et al. (2016, pg. 343) reported a threshold of about 0.2 wt. % (0.05 a.p.f.u.) after which an increase in salinity of the reacting fluid is only marginally influential in increasing Cl incorporation in Cl, if below halite saturation point. The lack of correlation between Cl and <sup>iv</sup>Al, K, and Fe<sup>3+</sup> cations in our experimental products may indicate that mild Cl enrichment of amphibole (<0.5 wt. %) may not require fulfilling such structural constraints.

Cl contents obtained in amphiboles from all our experiments have been plotted against NaCl wt. % of the fluid used in each experiment (Fig. 3.12A) and against experimental temperature (Fig. 3.12B), in order to assess the influence of these two variables in Cl incorporation in amphibole. Results from other experimental studies were plotted alongside ours for comparison (Sato et al., 2005; Wolff et al., 2013; Khodorevskaya & Aranovich, 2016; Chan et al., 2016). Sato et al. (2005) studied zoning of Cl in hornblende by doing experiments to find out partition coefficients of Cl/OH between melt and amphibole. Khodorevskaya and Aranovich (2016) conducted experiments by reaction of pargasite and NaCl-rich fluid (0 to 72 wt. % NaCl) at 900 °C. Wolff et al. (2013) performed partial melting experiments with gabbro in the presence of a fluid with 3.3 wt. % NaCl (seawater analogue). Chan et al. (2016) performed experiments at 700 °C with a NaCl brine and different reagents (oxides, carbonates, metal, chloride) to study the incorporation of Cl in synthetic amphibole, and found that increasing the concentration of NaCl in the fluid would influence Cl incorporation in the amphibole up to about  $X_{\text{NaCl}} = 0.03$  in water – obtaining amphiboles with 0.045 a.p.f.u. Cl (<0.2 wt. % Cl) – after which the increase in Cl incorporation in amphibole slowed down, finally obtaining Cl >0.4 wt. % in amphibole only above NaCl saturation (i.e. a brine).

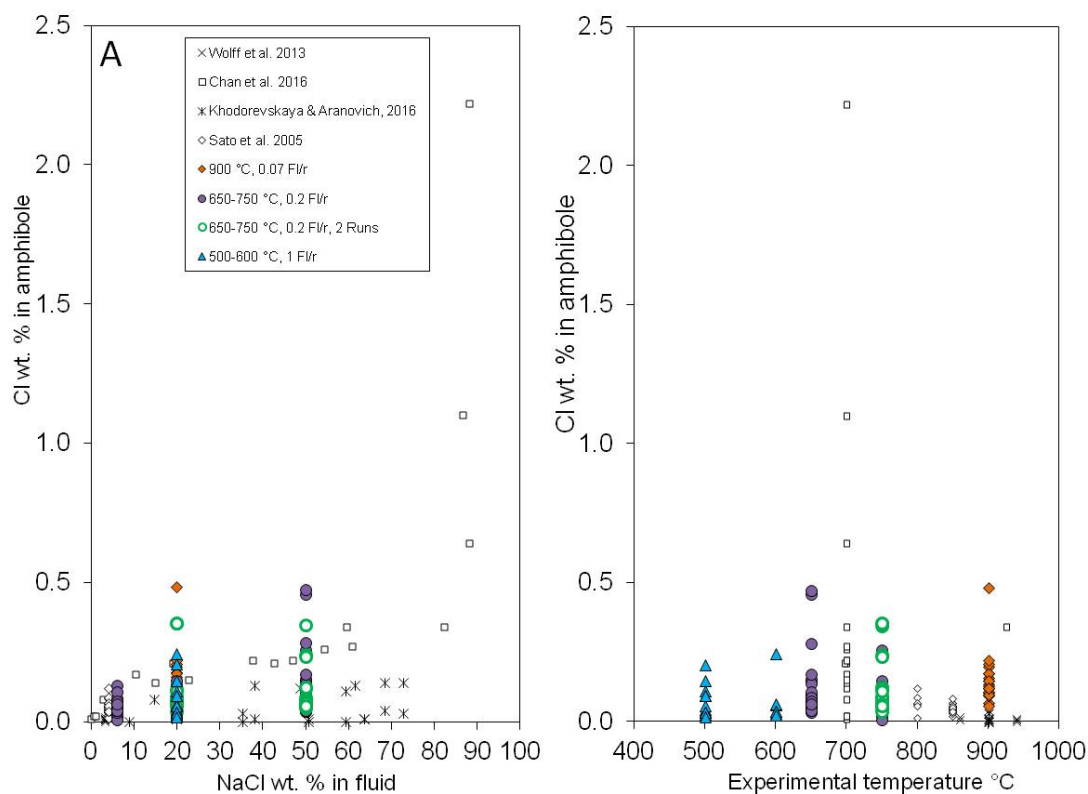


**Figure 3.12.** Cl concentration in experimental amphiboles versus experimental parameters. **A:** Cl wt. % of newly formed amphibole for each experiment, plotted against NaCl wt. % in aqueous fluid used in the experiment. **B:** Cl wt. % in experimental amphiboles for each experiment, plotted against experimental temperature. Data from previous experimental studies has been plotted against our experimental results for comparison: Wolff et al. (2013), Chan et al. (2016), Sato et al. (2005), Khodorevskaya and Aranovich (2016).

Fig. 3.12A shows significantly higher Cl contents in experiments done with 20 and 50 NaCl wt. % in fluid than in experiments done with a fluid containing 6 wt. % NaCl. This may suggest that the maximum Cl incorporated into amphibole is strongly dependent on the presence of a Cl-rich fluid. On average, analyses measured in experiments done with a 50 wt. % NaCl fluid are higher than in those measured in 20 w. % NaCl experiments, but the maximum Cl content obtained (0.47 wt.% Cl) is the same at both experimental fluid NaCl concentrations. Trends resulting from our study are consistent with data from the literature, e.g. amphiboles obtained by Khodorevskaya and Aranovich (2016) show little difference in Cl content between those formed in equilibrium with a fluid containing 35 wt. % NaCl and 70 NaCl wt. %.

Amphiboles measured by Chan et al. (2016) show a gradual increase in Cl content between 15 wt. % and 60 wt. % NaCl in fluid, and only start to show sharp increases in amphibole Cl content after a fluid NaCl concentration of 85 wt. %. In addition, it is hard to determine whether temperature exerts an influence on Cl incorporation in amphibole (Fig. 3.12B) within the range evaluated (500 °C to 900 °C). Higher fluid/rock ratios – such as in experiments performed at 600 °C and 500 °C at fluid/rock ratios of 1 – have not been found to play a large role on the significant increase in Cl content of the amphibole. In addition, the approach of running the reacted rock in a second experiment at the same temperature with a new batch of saline fluid resulted in increased Cl in amphibole for experiments performed with a fluid with 20 wt. % NaCl, and 50 wt. % Cl at 750 °C, with respect to experiments run only once at the same conditions. However, experiments performed at 650 °C and 900 °C yielded higher maximum Cl contents, thus a better comparison should be made by using the same approach at different temperatures in order to assess the effect of our experimental approach of reacting the rock with added fluid multiple times.

### **3.4.5 Considerations on the experimental setup**

Since it is difficult to determine the exact nature of the hydrothermal fluids, other fluid compositions and thermodynamic variables could be changed.

Further experiments could be done at slightly lower oxygen fugacities than those experimented with in this study (Chan et al., 2016; Mueller et al., 2017). In addition, the use of methods to further ensure the oxygen fugacity of the experimental vessel is kept as desired may be useful to avoid large changes in Fe oxidation state and therefore in the Fe-Mg content in amphibole. This can be attained, for instance, with the use of the double capsule technique in CSPV, or the use of the Shaw Membrane in IHPV.

The experimental setup with a large piece of amphibole and olivine gabbro powder, as opposed to the setup of a solid rock cylinder used earlier, results in more uniform rim compositions and is therefore a

more satisfactory option in terms of rim analysis by EPMA. In addition, by recharging the sample with a new batch of saline fluid, we are able to partially simulate the passage of a continuous fluid flux.

The approach of running experiments a second time and recharging the sample with a new batch of saline fluid allows for the simulation of a multiple step hydrothermal fluid infiltration. The results obtained show different tendencies according to the different experimental setups used. In setup A (gabbro powder + amphibole crystal), experiments run a second time with a new batch of fluid did not form higher-Cl amphiboles than single-run experiments. In contrast, in setup B (amphibole-containing gabbro cylinder), experiments run a second time did yield higher Cl contents in amphibole. The difference between the results of the two setups may be due to several factors. Most probably, in setup B, where a cylinder of solid rock with cracks and spaces between grain boundaries was used, reveal a better possibility for adsorption of salt in grain boundaries of minerals, therefore acting as traps for highly saline fluid. Conversely, in setup A, free flowing fluid around the crystal and the absence of a trap may lead to locally higher fluid/rock ratios, and therefore more likeliness of partitioning of Cl into the fluid.

When using a natural rock (whole or crushed) with an assemblage of several different mineral phases, the different compositions and local heterogeneities may account for a range of different mineral reactions involving amphibole. Obviously, different local equilibria were dominating the overall reaction, instead of achieving global equilibrium. Considering the wide range of amphibole compositions obtained, causality of results is difficult to trace back to the minerals involved in the different reactions occurring. Therefore, the approach of using natural rocks is probably not the best for producing homogeneous amphibole compositions. On the other hand, this approach is close to nature, where in gabbros of the deeper oceanic crust also amphiboles of different compositions occur in mutual contact with each other. It is obvious that these systems never reached a global equilibrium, since the individual reactions that take place are defined by a local equilibrium created by an inhomogeneous system of different mineral phases, varied distribution of fluid pathways, and changing fluid activity.

### 3.5 Conclusions

After testing the influence of different experimental variables on the resulting mineral products, we conclude that the reaction of gabbro with a hydrothermal fluid indeed leads to the formation of different amphibole types due to interaction with different minerals of the host rock and equilibration with a saline fluid. When comparing the results of the different experimental conditions used, there is a clear correlation between extent of hydrothermal activity and variability of amphibole compositions, with the narrowest range of compositions produced in suprasolidus experiments (900 °C), and the widest compositional variations produced in experiments at the lowest temperatures (subsolidus conditions: 500 and 600 °C). In terms of Cl enrichment in amphibole, fluid saturation in NaCl is the most influential variable on Cl incorporation for the conditions used, and therefore fluid salinity may be one of the main driving forces governing the Cl contents in the new amphiboles. In terms of structural controls on the incorporation of Cl into amphibole, the comparison of cation variations in our experimental products with those of natural and experimental samples from other studies has shown similarities in the lack of correlation between Cl in amphibole and cations such as Fe<sup>2+</sup>, <sup>iv</sup>Al and K in specimens with Cl wt. % < 1.

## 4 Concluding remarks

Amphiboles occurring in high-temperature veins and hydrothermal dykelets crosscutting layered gabbro in the Samail ophiolite record a wide range of formation conditions from magmatic to hydrothermal, and reveal a complex history of interactions between rock and hydrothermal fluid or brine in a lower oceanic crustal setting. These amphiboles show a conspicuous compositional variation from high-Ti magnesiohastingsite and pargasite via magnesiohornblende and edenite, to Cl-rich ferropargasite and hastingsite (up to 5.4 wt% Cl) and actinolite. Large variations in Cl content and cation configurations in amphibole suggest formation in equilibrium with fluids of different salinities at variable fluid/rock ratios. Moreover, the presence of subsolidus amphibole extremely enriched in chlorine implies phase separation and brine/rock interactions. Sr and O isotope analyses confirms the influence of a seawater-derived fluid, however, in a rock-dominated environment – i.e. fluid/rock ratios were extremely low during hydrothermal alteration and subsequent formation of Cl-rich amphiboles.

The comparison of cation variations in experimental and natural samples has shown some similarities between amphiboles of similar Cl contents. However, the experimental approach has had limitations in achieving highly Cl-rich amphiboles, but has been valuable to understand part of the alteration process and form Cl-bearing amphiboles with Cl < 0.4 wt. %. In addition, the isotopic study has helped to confirm the seawater origin of the fluid that influenced the studied rocks.

Cation changes in natural amphiboles show an increase of K, Al, and Fe<sup>2+</sup> when approaching very high Cl contents (> 1 wt. %), and Fe-Cl or Al-Cl correlations are not seen in amphiboles that are only mildly Cl-rich. This indicates, as seen by other authors (Oberti et al., 1993; Chan et al., 2016) that in order to incorporate small amounts of Cl into the amphibole structure, we do not require a major deformation of the amphibole structure, only for amounts > 1 wt. %. For this reason, Mg-Cl avoidance or Fe-Cl and Al-



Cl positive correlations are not observed in the experimental amphiboles obtained, where Cl contents are not large enough to deform the structure of the crystal.

## 5 References

- Abily, B., Ceuleneer, G., Launeau, P., 2011. Synmagmatic normal faulting in the lower oceanic crust: Evidence from the Oman ophiolite. *Geology* 39, 391-394.
- Allen, D.E., Seyfried, W.E., 2003. Compositional controls on vent fluids from ultramafic-hosted hydrothermal systems at mid-ocean ridges: An experimental study at 400°C, 500 bars. *Geochimica Et Cosmochimica Acta*, 67(8): 1531-1542.
- Alt, J.C., 2004. Alteration of the upper oceanic crust: mineralogy, chemistry, and processes
- in: *Hydrogeology of the Oceanic Lithosphere*, eds. E. E. Davis and H. Elderfield. Cambridge University Press.
- Alt, J.C., Bach, W., 2006. Oxygen isotope composition of a section of lower oceanic crust, ODP Hole 735B. *Geochemistry, Geophysics, Geosystems*, 7 (12), Q12008, doi:10.1029/2006GC001385.
- Alt, J.C., Laverne, C., Coggon, R.M., Teagle, D.A.H., Banerjee, N.R., Morgan, S., Smith-Duque, C.E., Harris, M., Galli, L., 2010. Subsurface structure of a submarine hydrothermal system in ocean crust formed at the East Pacific Rise, ODP/IODP Site 1256. *Geochemistry Geophysics Geosystems*, 11 (10), 2010GC003144.
- Almeew, R. R., Koepke, J., Silantyev, S. S., Strube, N., Portnyagin, M. V., Garbe-Schönberg, D., Botcharnikov, R. E., Holtz, F. Partial melting of gabbro in the presence of NaCl-rich fluid - Implications for the genesis of oceanic plagiogranites. *Lithos*, this issue.
- Aranovich, L.Y., Zakirov, I.V., Sretenskaya, N.G., Gerya, T.V., 2010. Ternary system H<sub>2</sub>O-CO<sub>2</sub>-NaCl at high T-P parameters: an empirical mixing model. *Geochemistry International*, 48; 446-55.
- Bach W, Jöns N & Klein F (2013): Metasomatism within the Ocean Crust. in: *Metasomatism and the chemical transformation of rock: the role of fluids in terrestrial and extraterrestrial processes* (ed. Harlov D, Austrheim H), *Lecture Notes in Earth System Sciences*, Springer, p. 253-288.
- Berermann, O., Garbe-Schönberg, D., Bach, W., Holzheid, A., 2017. Time-resolved interaction of seawater with gabbro: An experimental study of rare-earth element behavior up to 475 °C, 100 MPa. *Geochimica et Cosmochimica Acta*, 197: 167-192.
- Berndt, J., Liebske, C., Holtz, F., Freise, M., Nowak, M., Ziegenbein, D., Hurkuck, W., and Koepke, J., 2002. A combined rapid-quench and H<sub>2</sub>-membrane setup for internally heated pressure vessels: Description and application for water solubility in basaltic melts. *American Mineralogist*, 87(11-12), 1717-1726.
- Bosch, D., Jamais, M., Boudier, F. and Nicolas, A., 2004. Deep and High-temperature Hydrothermal Circulation in the Oman Ophiolite - Petrological and Isotopic Evidence. *Journal of Petrology*, 45(6), 1181-1208.
- Boudier F, Nicolas A, Ildefonse B (1996) Magma chambers in the Oman ophiolite: Fed from the top or from the bottom? *Earth and Planetary Science Letters* 144: 239-250.
- Canales, J.P., Detrick, R.S., Toomey, D.R., Wilcock, W.S.D., 2003. Segment-scale variations in the crustal structure of 150-300 kyr old fast spreading oceanic crust (East Pacific Rise, 8 degrees 15 ' N-10 degrees 5 ' N) from wide-angle seismic refraction profiles. *Geophysical Journal International*, 152,766-794
- Chan, A., Jenkins, D.M., and Dyar, M.D., 2016. Partitioning of Chlorine Between NaCl Brines and Ferro-Pargasite: Implications For the Formation of Chlorine-Rich Amphiboles In Mafic Rocks. *The Canadian Mineralogist*, 54(1), 337-351.
- Chou, I.M., 1986. Permeability of precious metals to hydrogen at 2kb total pressure and elevated temperatures. *American Journal of Science*, 286(8): 638-658.
- Clayton, R.N. and Mayeda, T.K., 1963. The Use of Bromine Pentafluoride in the Extraction of Oxygen from Oxides and Silicates for Isotopic Analysis. *Geochimica et Cosmochimica Acta*, 27, 43-52. [http://dx.doi.org/10.1016/0016-7037\(63\)90071-1](http://dx.doi.org/10.1016/0016-7037(63)90071-1)
- Coogan, L.A., Saunders, A.D., Kempton, P.D. and Norry, M.J., 2000. Evidence from oceanic gabbros for porous melt migration within a crystal mush beneath the Mid-Atlantic Ridge. *Geochemistry Geophysics Geosystems*, 1, 2000GC000072.
- Coogan, L. A., Wilson, R. N., Gillis, K. M., and MacLeod, C. J., 2001. Near-solidus evolution of oceanic gabbros: Insights from amphibole geochemistry. *Geochimica et Cosmochimica Acta*, 65(23), 4339-4357.
- Coogan, L.A., Howard, K.A., Gillis, K.M., Bickle, M.J., Chapman, H., Boyce, A.J., Jenkin, G.R.T., Wilson, R.N., 2006. Chemical and thermal constraints on focussed fluid flow in the lower oceanic crust. *American Journal of Science* 306, 389-427.
- Coogan, L.A., Manning, C.E., Wilson, R.N., 2007. Oxygen isotope evidence for short-lived high-temperature fluid flow in the lower oceanic crust at fast-spreading ridges. *Earth and Planetary Science Letters*, 260, 524-536.
- Coumou, D., Driesner, T., Weis, P., and Heinrich, C.A., 2009. Phase separation, brine formation, and salinity variation at Black Smoker hydrothermal systems. *Journal of Geophysical Research*, 114, B03212, doi:10.1029/2008JB005764.

- Currin, A., Wolff, P.E., Koepke, J., Almeev, R., Zhang, C., Teagle, D., Ildefonse, B., Zihlmann, B. Chlorine-rich amphibole in deep layered gabbros as evidence for brine/rock interaction in the lower oceanic crust: a case study from the Wadi Wariyah, Oman Sultanate. *Lithos*, (submitted).
- Currin, A., Koepke, J., Almeev, R., Beermann, O. Interaction of highly saline fluid and olivine gabbro: experimental simulation of deep hydrothermal processes involving amphibole at the base of the oceanic crust. *Lithos*, (submitted).
- Driesner, T., 2007. The System H<sub>2</sub>O-NaCl. II. Correlations for molar volume, enthalpy, and isobaric heat capacity from 0 to 1000 degrees C, 1 to 5000 bar, and 0 to 1 XNaCl. *Geochimica et Cosmochimica Acta*, 71(20), 4902–4919.
- Driesner, T., and Heinrich, C., 2007. The system H<sub>2</sub>O–NaCl. Part I: Correlation formulae for phase relations in temperature–pressure–composition space from 0 to 1000°C, 0 to 5000bar, and 0 to 1 XNaCl. *Geochimica et Cosmochimica Acta*, 71(20), 4880–4901.
- Dunn, R.A., Toomey, D.R., Solomon, S.C., 2000. Three-dimensional seismic structure and physical properties of the crust and shallow mantle beneath the East Pacific Rise at 9°30'N. *Journal of Geophysical Research*, 105 (B10), 23537–23555.
- Enami, M., Liou, J.G., Bird, D.K., 1999. Cl-bearing amphibole in the Salton Sea Geothermal System, California. *Canadian Mineralogist*, 30, 1077–1092.
- Erdmann, M., and Koepke, J., 2016. Experimental temperature cycling as a powerful tool to enlarge melt pools and crystals at magma storage conditions. *American Mineralogist*, 101 (4), 960–969. doi: <https://doi.org/10.2138/am-2016-5398>
- Ernst, W.G. and Liu, J., 1998. Experimental phase-equilibrium study of Al- and Ti- contents of calcic amphibole in MORB. A semiquantitative thermobarometer. *American Mineralogist*, 83, 952-969.
- Ferrando C., Godard M., Ildefonse B., Rampone E., 2018. Melt transport and mantle assimilation at Atlantis Massif (IODP Site U1309): Constraints from geochemical modeling. *Lithos*. doi: 10.1016/j.lithos.2018.01.012
- Filiberto, J., and Treiman, A.H., 2009. Martian magmas contained abundant chlorine, but little water. *Geology*, 37(12): 1087-1090.
- Gillis, K.M., Coogan, L.A., Chaussidon, M., 2003. Volatile element (B, Cl, F) behaviour in the roof of an axial magma chamber from the East Pacific Rise. *Earth and Planetary Science Letters*, 213, 447–462.
- Gregory, R. T., and Taylor, H.P., 1981. An oxygen isotope profile in a section of Cretaceous oceanic crust, Samail Ophiolite, Oman: Evidence for δ18O buffering of the oceans by deep (>5 km) seawater-hydrothermal circulation at mid-ocean ridges. *Journal of Geophysical Research: Solid Earth*, 86(B4): 2737–2755.
- Hajash, A., and Archer, P., 1980. Experimental seawater/basalt interactions: effects of cooling. *Contributions to Mineralogy and Petrology*, 75(1): 1–13.
- Hajash, A., and Chandler, G.W., 1981. An experimental investigation of high-temperature interactions between seawater and rhyolite, andesite, basalt and peridotite. *Contributions to Mineralogy and Petrology*, 78(3): 240–254.
- Harlov, D.E., Aranovich, L.Y., 2017. The Role of Halogens in Terrestrial and Extraterrestrial Geochemical Processes: Surface, Crust, and Mantle. Chapter 1. In: Harlov, D.E., Aranovich, L.Y. (Eds.), *The role of halogens in terrestrial and extraterrestrial geochemical processes: surface, crust, and mantle*. SpringerNature, pp. 1-19, DOI: 10.1007/978-3-319-61667-4\_1.
- Harlov, D.E., Förster, H-J, Nijland, T.J, 2002. Fluid-induced nucleation of (Y + REE)-phosphate minerals within apatite: Nature and experiment. Part I. Chlorapatite. *American Mineralogist* ; 87 (2-3): 245–261. doi: <https://doi.org/10.2138/am-2002-2-306>
- Harris, M., Coggon, R.M, Smith-Duque, C.E., Cooper, M.J., Milton, J.A., Teagle, D.A.H., 2015. Channelling of hydrothermal fluids during the accretion and evolution of the upper oceanic crust: Sr isotope evidence from ODP Hole 1256D. *Earth and Planetary Science Letters*, 416, 56-66.
- Harris, M., Coggon, R.M., Wood, M., Smith-Duque, C.E., Henstock, T.J., Teagle, D.A.H., 2017. Hydrothermal cooling of the ocean crust: Insights from ODP Hole 1256D. *Earth and Planetary Science Letters*, 462, 110-121.
- Hasenclever, J., Theissen-Krah, S., Rüpke, L.H., Morgan, J.P., Iyer, K., Petersen, S., Devey, C.W., 2014. Hybrid shallow on-axis and deep off-axis hydrothermal circulation at fast-spreading ridges. *Letters to nature*, 508, 508-512, doi:10.1038/nature13174.
- Henstock, T.J., Woods, A.W., White, R.S., 1993. The accretion of oceanic crust by episodic sill intrusion. *Journal of Geophysical Research*, 98, 4143-4161.
- Hopson, C.A., Coleman, R.G., Gregory, R.T., Pallister, J.S., Bailey, E.H., 1981. Geologic section through the Samail ophiolite and associated rocks along a Muscat–Ibra transect, southeastern Oman Mountains. *Journal of Geophysical Research* 86, 2527–2544.
- Ito, E., and Anderson, Jr., A.T., 1983. Submarine metamorphism of gabbros from the Mid-Cayman Rise: petrographic and mineralogic constraints on hydrothermal processes at low-spreading ridges. *Contributions to Mineralogy and Petrology*, 82, 371–388.
- Ito, E., and Clayton, R.N., 1983. Submarine metamorphism of gabbros from the Mid-Cayman rise: An oxygen isotopic study. *Geochimica et Cosmochimica Acta*, 47(3): 535–546.
- Iturrino, G.J., Ildefonse, B., and Boitnott, G., 2002. Velocity structure of the lower oceanic crust: results from Hole

- 735B, Atlantis II Fracture Zone. In Natland, J.H., Dick, H.J.B., Miller, D.J., and Von Herzen, R.P. (Eds.), *Proceedings of the Ocean Drilling Program, Scientific Results*, 176, 1–71.
- Jarosewich, E., Nelen, J., Norberg, J. A., 1980. Reference samples for electron microprobe analysis, *Geostandards Newsletter*, 4(1), 43–47.
- Kelemen PB, Koga KT, Shimizu N (1997) Geochemistry of gabbro sills in the crust/mantle transition zone of the Oman ophiolite: Implications for the origin of the oceanic lower crust. *Earth and Planetary Science Letters* 146: 475–488.
- Kendrick M.A. (2018) Halogens in Seawater, Marine Sediments and the Altered Oceanic Lithosphere. In: Harlov D., Aranovich L. (eds) *The Role of Halogens in Terrestrial and Extraterrestrial Geochemical Processes*. Springer Geochemistry. Springer, Cham, p. 591–648.
- Khodorevskaya, L. I., and Aranovich, L. Y., 2016. Experimental study of amphibole interaction with H<sub>2</sub>O–NaCl Fluid at 900°C, 500 MPa: toward granulite facies melting and mass transfer. *Journal of Petrology*, 24(3), 215–233.
- Koepke, J., Feig, S.T., Snow, J., Freise, M., 2004. Petrogenesis of oceanic plagiogranites by partial melting of gabbros: An experimental study. *Contributions to Mineralogy and Petrology*, 146, 414–432.
- Koepke, J., Berndt, J., Feig, S.T., Holtz, F., 2007. The formation of SiO<sub>2</sub>-rich melts within the deep oceanic crust by hydrous partial melting of gabbros. *Contributions to Mineralogy and Petrology*, 153, 67–84.
- Koepke, J., Christie, D.M., Dziony, W., Holtz, F., Lattard, D., MacLennan, J., Park, S., Scheibner, B., Yamasaki, T., Yamasaki, S., 2008. Petrography of the Dike/Gabbro Transition at IODP Site 1256D (Equatorial Pacific): The evolution of the Granoblastic Dikes. *Geochemistry Geophysics Geosystems*, 9, 2008GC001939.
- Koepke, J., France, L., Müller, T., Faure, F., Goetze, N., Dziony, W., Ildefonse, B., 2011. Gabbros from IODP Site 1256 (Equatorial Pacific): Insight into axial magma chamber processes at fast-spreading ocean ridges. *Geochemistry Geophysics Geosystems*, 12, 2011GC003655.
- Kullerud, K., 1996. Chlorine-rich amphiboles: interplay between amphibole composition and an evolving fluid, *European Journal of Mineralogy*, 8(2), 355.
- Kullerud, K., 2000. Occurrence and origin of Cl-rich amphibole and biotite in the Earth's crust - implications for fluid composition and evolution. In: Stober, I., and Bucher, K. (eds.). *Hydrogeology of Crystalline Rocks*. Kluwer Academic Publishers, 205–225.
- Kullerud, K., Flaatt, K., Davidsen, B., 2001. High-pressure fluid-rock reactions involving Cl-bearing fluids in Lower-Crustal Ductile shear zones of the Flakstadøy Basic Complex, Lofoten, Norway. *Journal of Petrology*, 42 (7), 1349–1372.
- Lanphere, M., R. Coleman, and C. Hopson, 1981. Sr isotopic tracer study of the Samail ophiolite, Oman, *Journal of Geophysical Research*, 86(B4), 2709–2720.
- Leake, B.E., Woolley, A.R., Arps, C.E.S., Birch, W.D., Gilbert, M.C., Grice, J.D., Hawthorne, F.C., Kato A., Kisch, H.J., Krivovichev, V.G., Linthout, K., Laird, J., Mandarino, J., Maresch, W.V., Nickel, E.H., Rock, N.M.S., Schumacher, J.C., Smith, D.C., Stephenson, N.C.N., Ungaretti, L., Whittaker, E.J.W. and Youzhi, G., 1997. Nomenclature of amphiboles: Report of the subcommittee on amphiboles of the International Mineralogical Association Commission on New Minerals and Mineral Names. *The Canadian Mineralogist*, 35, 219–246.
- Lecuyer, C., Reynard, B., 1996. High-temperature alteration of oceanic gabbros by seawater (Hess Deep, Ocean Drilling Program Leg 147): Evidence from oxygen isotopes and elemental fluxes. *Journal of Geophysical Research: Solid Earth*, 101(B7): 15883–15897.
- Léger, A., Rebbert, C., Webster, J., 1996. Cl-rich biotite and amphibole from Black Rock Forest, Cornwall, New York. *American Mineralogist*, 81, 495–504.
- Liu, J., Liu, W., Ye, K., Mao, Q., 2009. Chlorine-rich amphibole in Yangkou eclogite, Sulu ultrahigh-pressure metamorphic terrane, China. *European Journal of Mineralogy*, 21, 1265–1285.
- Locock, A.J., 2014. An Excel spreadsheet to classify chemical analyses of amphiboles following the IMA 2012 recommendations. *Computers and Geosciences*, 62, 1–11.
- MacLennan, J., Hulme, T., Singh, S.C., 2005. Cooling of the lower oceanic crust. *Geology*, 33(5), 357–360, doi: 10.1130/G21207.1.
- Makino, K., Tomita, K., 1993. Effect of chlorine on the crystal structure of a chlorine-rich hastingsite. *Mineralogical Magazine*, 57, 677–685.
- Manning, C.E., MacLeod, C.J., Weston, P.E., 2000. Lower Crustal Cracking Front at Fast Spreading Ridges: Evidence from the East Pacific Rise and Oman ophiolite. In: Dilek, Y., Moores, E., Elthon, D., Nicolas, A. (Eds.), *Special Paper*, vol. 349. Geological Society of America, pp. 261–272.
- Manning, C.E., Aranovich, L.Y., 2014. Brines at high pressure and temperature: Thermodynamic, petrologic and geochemical effects. *Precambrian Research*, 253, 6–16.
- Manning, C., Ingebritsen, S.E., Bird, D.K., 1993. Missing mineral zones in contact metamorphosed basalts. *American Journal of Science*, 293, 894–938.
- Manning, C., and MacLeod, C., 1996. Fracture-controlled metamorphism of Hess Deep gabbros, Site 894: constraints on the roots of mid-ocean-ridge hydrothermal systems at fast-spreading centers. In: C. Mével, K. M. Gillis, J. F. Allan and P. S. Meyer (Eds.), *Proceedings ODP, Scientific Results, Ocean Drilling Program, College Station, TX*, 189–212.

- Manning, C., Weston, P., and Mahon, K., 1996. Rapid high temperature metamorphism of East Pacific Rise gabbros from Hess Deep, *Earth and Planetary Science Letters*, 144, 123–132.
- McArthur, J.M., Howarth, R.J., and Bailey, T.R., 2001. Strontium isotope stratigraphy: LOWESS version 3: best fit to the marine Sr-isotope curve for 0–509 Ma and accompanying look-up table for deriving numerical age. *The Journal of Geology*, 109, 155–170.
- McCormick, K.A., and McDonald, A.M., 1999. Chlorine-bearing amphiboles from the fraser mine, Sudbury, Ontario, Canada: description and crystal chemistry. *The Canadian Mineralogist*, 37, 1385–1403.
- McCulloch, M.T., Gregory, R.T., Wasserburg, G.J., Taylor, H.P., 1981. Sm-Nd, Rb-Sr, and <sup>180</sup>/16O isotopic systematics in an oceanic crustal section: Evidence from the Samail Ophiolite. *Journal of Geophysical Research: Solid Earth*, 86(B4): 2721–2735.
- Morrison, J., 1991. Compositional constraints on the incorporation of Cl into amphiboles. *American Mineralogist*, 76, 1920–1930
- Mueller, B. L., Jenkins, D. M., and Dyar, M. D., 2017. Chlorine incorporation in amphiboles synthesized along the magnesio-hastingsite–hastingsite compositional join. *European Journal of Mineralogy*, 29 (2), 167–180.
- Munoz, J.L., 1984. F-OH and Cl-OH exchange in micas with applications to hydrothermal ore deposits. *Mineralogical Society of America, Reviews in Mineralogy*, 13, 469–493.
- Munoz, J.L., Swenson, A., 1981. Chloride-hydroxyl exchange in biotite and estimation of relative HCl/HF activities in hydrothermal fluids. *Economic Geology*, 76, 2212–2221.
- Nehlig, P., 1991. Salinity of oceanic hydrothermal fluids: a fluid inclusion study, *Earth Planet. Sci. Lett.* 102: 310–325.
- Nehlig, P. and Juteau, T., 1988. Deep crustal seawater penetration and circulation at oceanic ridges: evidence from the Oman ophiolite, *Marine Geology* 84: 209–228.
- Newton, R. C., and Manning, C. E., 2010. Role of saline fluids in deep-crustal and upper-mantle metasomatism: insights from experimental studies. *Geofluids*, v. 10, p. 58–72.
- Nicolas, A., F. Boudier, B. Ildefonse, and E. Bali, 2000. Accretion of Oman and United Arab Emirates ophiolite – Discussion of a new structural map. *Marine Geophysical Research*, 21, 147–179.
- Nicolas, A., Mainprice, D., Boudier, F., 2003. High temperature seawater circulation throughout crust of oceanic ridges. A model derived from the Oman ophiolite. *Journal of Geophysical Research* 108, No. B8, Art. No. 2371.
- Oberti, R., Ungaretti, L., Cannillo, E., Hawthorne, F., 1993. The mechanism of Cl incorporation in amphibole. *American Mineralogist*, 78, 746–752.
- Phipps Morgan, J., and Y. J. Chen (1993), The genesis of oceanic crust: Magma injection, hydrothermal circulation, and crustal flow, *J. Geophys. Res.*, 98(B4), 6283–6297, doi: 10.1029/92JB02650.
- Pitzer, K.S., Sterner, S.M., 1995. Equations of state valid continuously from zero to extreme pressures with H<sub>2</sub>O and CO<sub>2</sub> as examples. *International Journal of Thermophysics*, 16(2): 511–518.
- Robie, R.A., Hemingway, B.S., Fischer, J.R., 1978. Thermodynamic properties of minerals and related substances at 298.15 K and 1 bar (10<sup>5</sup> Pascals) pressure and at higher temperature. *U.S. Geological Survey Bulletin*, 1452: 456.
- Sato, H., Holtz, F., Behrens, H., Botcharnikov, R., and Nakada, S., 2005. Experimental Petrology of the 1991–1995 Unzen Dacite, Japan. Part II: Cl/OH Partitioning between Hornblende and Melt and its Implications for the Origin of Oscillatory Zoning of Hornblende Phenocrysts. *Journal of Petrology*, 46 (2), 339–354. doi:10.1093/petrology/egh078
- Sautter, V., Jambon, A., and Boudouma, O., 2006. Cl-amphibole in the nakhlite MIL 03346: Evidence for sediment contamination in a Martian meteorite. *Earth and Planetary Science Letters*, 252(1), 45–55.
- Shanks, W. C., Bohlke, J.K., Seal, R.R., II, 1995. Stable isotopes in mid-ocean ridge hydrothermal systems: Interactions between fluids, minerals, and organisms. Washington DC American Geophysical Union Geophysical Monograph Series. 194–221. 10.1029/GM091p0194.
- Shaw, H.R., Wones, D.R., 1964. Fugacity coefficients for hydrogen gas between 0° and 1000°C, for pressures to 3000 atm. *American Journal of Science*, 262(7): 918–929.
- Silantyev, S.A., Kostitsyn, Yu.A., Cherkashin, D.V., Dick, H.J.B., Kelemen, P.B., Kononkova, N.N., and Kornienko, E.M., 2008. Magmatic and Metamorphic Evolution of the Oceanic Crust in the Western Flank of the MAR Crest Zone at 15° 44' N: Investigation of Cores from Sites 1275B and 1275D, JOIDES Resolution Leg 209. *Petrology*, 16(4), 353–375.
- Silva, M. M., Holtz, F., Namur, O. (2017). Crystallization experiments in rhyolitic systems: The effect of temperature cycling and starting material on crystal size distribution. *American Mineralogist*; 102 (11): 2284–2294. doi: <https://doi.org/10.2138/am-2017-5981>
- Straub, S. M. and Layne, G. D., 2003. The systematics of chlorine, fluorine, and water in Izu arc front volcanic rocks: Implications for volatile recycling in subduction zones. *Geochimica et Cosmochimica Acta*, 67, 4179–4203.
- Taylor, H. P., 1977. Water/rock interactions and the origin of H<sub>2</sub>O in granitic batholiths, *J Geol Soc London*, 133(6), 509–558.
- Taylor, G.J., Boynton, W.V., McLennan, S.M., Martel, L.M.V., 2010. K and Cl concentrations on the Martian surface determined by the Mars Odyssey Gamma Ray Spectrometer: Implications for bulk halogen abundances in

- Mars. *Geophysica.*, 2017. Crystallization experiments in rhyolitic systems: The effect of temperature cycling and starting material on crystal size distribution. *American Mineralogist* ; 102 (11): 2284–2294. doi: <https://doi.org/10.2138/am-2017-59811> Research Letters, 37(12): n/a-n/a.
- Vanko, D., 1986. High-chlorine amphiboles from oceanic rocks: product of highly saline hydrothermal fluids, *American Mineralogist*, 71, 51–59.
- Volfinger, M., Robert, J.L., Vielzeuf, D., Neiva, A.M.R., 1985. Structural control of the chlorine content of OH-bearing silicates (micas and amphiboles). *Geochimica et Cosmochimica Acta*, 49(1): 37–48.
- Webster, J.D., 1992. Fluid-melt interactions involving Cl-rich granites: Experimental study from 2 to 8 kbar. *Geochimica et Cosmochimica Acta*, 56(2): 659–678.
- Whitney, D.L., and Evans, B.W., 2010. Abbreviations for names of rock-forming minerals. *American Mineralogist*, 95, 185–187.
- Wolff, P.E., Koepke, J., Feig, S.T., 2013. The reaction mechanism of fluid-induced partial melting of gabbro in the oceanic crust. *European Journal of Mineralogy*, 25, 279–298.
- Wolff, P.E., 2014. Hydrothermal circulation from very high to low temperatures in the lower oceanic crust - Evidence from layered gabbros from the Oman Ophiolite and from partial melting experiments on oceanic gabbros. PhD Thesis. Leibniz Universität Hannover, 167 pp.
- Zhang, C., Holtz, F., Changqian, M., Wolff, P.E., and Li, X., 2012. Tracing the evolution and distribution of F and Cl in plutonic systems from volatile-bearing minerals: a case study from the Liujiawa pluton (Dabie orogen, China). *Contributions to Mineralogy and Petrology*, 164, 859–879.
- Zhang, C., Koepke, J., Kirchner, C., Götze, N., Behrens, H., 2014. Rapid hydrothermal cooling above the axial melt lens at fast-spreading mid-ocean ridge. *Scientific Reports* 4, No. 6342. DOI: 10.1038/srep06342.
- Zhang, C., Koepke, J., Albrecht, M., Horn, I., Holtz, F., 2017a. Apatite in the dike-gabbro transition zone of mid-ocean ridge: Evidence for brine assimilation by axial melt lens. In: Harlov, D, and Hughes, J. (Eds.). *Apatite: a common mineral, uncommonly versatile*. *American Mineralogist*, 102, 558-570.
- Zhang, C., Wang, L.-X., Marks, M. A. W., France, L., Koepke, J., 2017b. Volatiles (CO<sub>2</sub>, S, F, Cl, Br) in the dike-gabbro transition zone at IODP Hole 1256D: Magmatic imprint versus hydrothermal influence at fast-spreading mid-ocean ridge. *Chemical Geology*, 459, 43-60.

## 6 Appendix (supplementary data)

**Table S1.** Fractionation factor between amphibole and water ( $\Delta^{18\text{O}}$  amphibole-water) was calculated for each of the amphibole samples analyzed for oxygen isotopes (magmatic and hydrothermal amphiboles), using the fractionation equation from the calibration of Zheng (1993) ( $A= 3.89$ ,  $B= -8.56$ ,  $C= 2.43$ ) for oxygen isotope fractionation between hornblende and water, and inserting temperatures calculated from Ti-in-amphibole thermometry. The  $\delta^{18\text{O}}$  value for water was obtained by subtracting measured  $\delta^{18\text{O}}$  values for amphibole to calculated values for the fractionation factor ( $\Delta^{18\text{O}}$  amphibole-water).  $\delta^{18\text{O}}$  values calculated for water range between 6.9 and 7.5 ‰. The result of this calculation suggests that, assuming temperatures from thermometry to be true, the fluid that equilibrated with the analysed amphiboles was very different from Cretaceous seawater (values of -1 ‰; Gregory & Taylor, 1981) or typical hydrothermal fluids derived from Cretaceous seawater (0 to 3 ‰; e.g. Shanks et al., 1995).

**Table S1. Hydrothermal fluid temperature calculations with oxygen isotopes.**

*Zheng, Y.-F., 1993. Calculation of oxygen isotope fractionation in hydroxyl-bearing silicates. EPSL, 120, 247-263*

**A**  $3.89$   
**B**  $-8.56$   
**C**  $2.43$   
 Temperature (°C)  $1198.15$   
 $1000 \ln \alpha$   $-2.00 \%$   
 $\Delta^{18}O_{\text{amph-water}} = 1000 \ln \alpha = (A \cdot 10^6/T^2) + (B \cdot 10^3/T) + C$   
 $\Delta^{18}O_{\text{amph-water}} = \delta^{18}O_{\text{amph}} - \delta^{18}O_{\text{water}}$

**Fractionation factor ( $\Delta^{18}O$ ) Calculated from temperatures from thermometry**

Sample	$1000 \ln \alpha$ $\Delta^{18}O_{\text{amph-water}}$	$\delta^{18}O$ measured $\delta^{18}O_{\text{amph}}$	Calc. $\delta^{18}O_{\text{water}}$	Avg. of thermometry T (Ernst & Liu, 1998) T (thermometry (K))	T (°C)	T Ernst & Liu (1998) (°C)
WA02-high-Ti pargasite	-2.2	4.7	6.9	1023.2	750	650-850
WA02-hornblende (hydrothermal)	-2.3	4.7	7.0	873.2	600	550-650
WA42-high-Ti pargasite	-1.93	5.6	7.5	1248.2	975	950-1000
WA42-hornblende (hydrothermal)	-2.3	4.9	7.2	848.2	575	500-650
WA04-high-Ti pargasite	-1.9	5.5	7.4	1273.2	1000	1000
WA04-hornblende (hydrothermal)	-2.3	5	7.3	923.2	650	650
WA05-high-Ti pargasite	-2.2	4.7	6.9	788.2	515	480-550
WA33-high-Ti pargasite	-2.0	5	7.0	1198.2	925	850-1000
WA02-whole rock (dark vein)		4.6				
WA05-whole rock (dark vein)		5.1				
WA42-whole rock (gabbroic dykelet)		4.9				
WA04-whole rock (gabbroic dykelet)		4.1				
WA33-whole rock (gabbroic dykelet)		7.3				

$\delta^{18}O_{\text{water}} = 6.9 - 7.5$

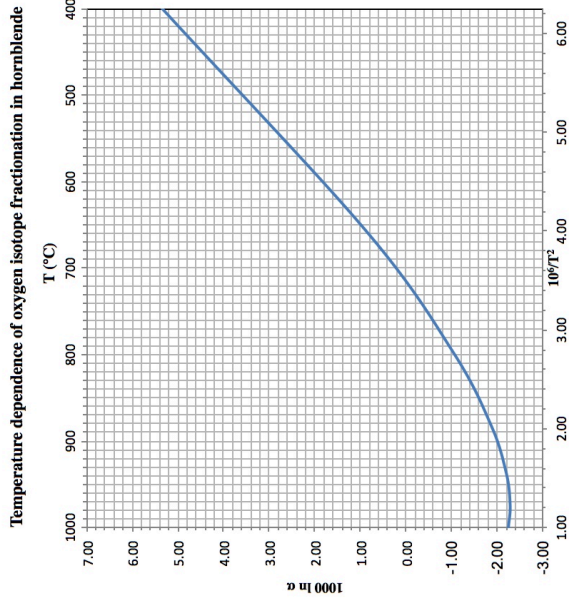




**Table S1 (continued). Hydrothermal fluid temperature calculations with oxygen isotopes.**  
 Zheng, Y.-F., 1993. Calculation of oxygen isotope fractionation in hydroxyl-bearing silicates. *EPSL*, 120, 247-263

**Input T**  
**A** 3.89  
**B** -8.56  
**C** 2.43  
 Temperature (°C) 395  
 1000 ln  $\alpha$  5.69 %

$$\Delta \delta^{18}\text{O}_{\text{amph-water}} = 1000 \ln \alpha = (A * 10^6 / T^2) + (B * 10^3 / T) + C$$

$$\Delta \delta^{18}\text{O}_{\text{amph-water}} = \delta^{18}\text{O}_{\text{amph}} - \delta^{18}\text{O}_{\text{water}}$$

Fractionation factor ( $\Delta \delta^{18}\text{O}$ ) Calculated assuming  $\delta^{18}\text{O}_{\text{water}} = 0$

Sample	1000 ln $\alpha$	$\delta^{18}\text{O}_{\text{amph-water}}$	$\delta^{18}\text{O}_{\text{amph}}$	$\delta^{18}\text{O}_{\text{water}}$	T calc isot	T in °C
WA02-high-Ti pargasite	5.7	4.7	395	6.4	121.9	121.9
WA02-hornblende (hydrothermal)	5.7	4.7	395	6.4	121.9	121.9
WA42-high-Ti pargasite	6.6	5.6	383	6.8	109.9	109.9
WA42-hornblende (hydrothermal)	5.9	4.9	392.1	6.5	119.0	119.0
WA04-high-Ti pargasite	6.5	5.5	384.2	6.8	111.1	111.1
WA04-hornblende (hydrothermal)	6	5	390.7	6.6	117.6	117.6
WA05-high-Ti pargasite	5.7	4.7	395	6.4	121.9	121.9
WA33-high-Ti pargasite	6	5	390.7	6.6	117.6	117.6
WA02-whole rock (dark vein)	5.6	4.6	396.3	6.4	123.2	123.2
WA05-whole rock (dark vein)	6.1	5.1	389.4	6.6	116.3	116.3
WA42-whole rock (gabbroic dykelet)	5.9	4.9	392.1	6.5	119.0	119.0
WA04-whole rock (gabbroic dykelet)	5.1	4.1	403.6	6.1	130.5	130.5
WA33-whole rock (gabbroic dykelet)	8.3	7.3	363.7	7.6	90.6	90.6

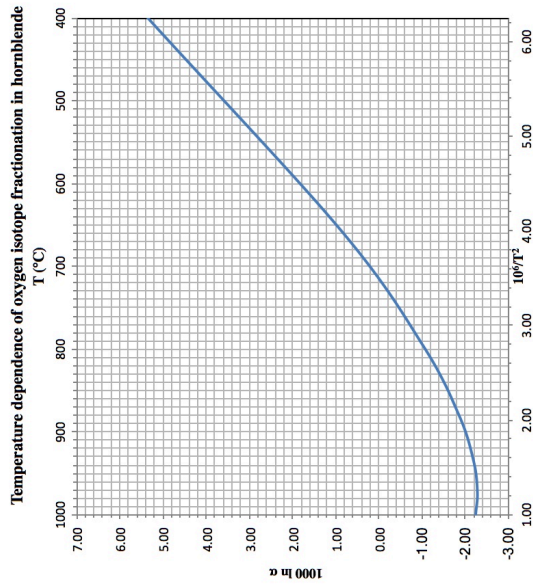


Table S1 (continued). Hydrothermal fluid temperature calculations with oxygen isotopes.

Input T  
Zheng, Y.-F., 1993. Calculation of oxygen isotope fractionation in hydroxyl-bearing silicates. *EPSL*, 120, 247-263

<b>A</b>	3.89	
<b>B</b>	-8.56	$\Delta^{18}\text{O}_{\text{amph-water}} = 1000 \ln \alpha = (A \cdot 10^3/T^2) + (B \cdot 10^3/T) + C$
<b>C</b>	2.43	$\Delta^{18}\text{O}_{\text{amph-water}} = \delta^{18}\text{O}_{\text{amph}} - \delta^{18}\text{O}_{\text{water}}$
Temperature (°C)	396	
1000 ln $\alpha$	5.62 %	

Fractionation factor ( $\Delta^{18}\text{O}$ ) Calculated assuming  $\delta^{18}\text{O}_{\text{water}}=0$

Sample	1000 ln $\alpha$	$\delta^{18}\text{O}_{\text{amph}}$	$\delta^{18}\text{O}_{\text{water}}$	T calc isot x (10 <sup>3</sup> 6/T <sup>2</sup> )	T in °C
WA02-high-Ti pargasite	4.7	4.7	0	410	136.9
WA02-hornblende (hydrothermal)	4.7	4.7	0	410	136.9
WA42-high-Ti pargasite	5.6	5.6	0	396	122.9
WA42-hornblende (hydrothermal)	4.9	4.9	0	407	133.9
WA04-high-Ti pargasite	5.5	5.5	0	397	123.9
WA04-hornblende (hydrothermal)	5	5	0	405	131.9
WA05-high-Ti pargasite	4.7	4.7	0	410	136.9
WA33-high-Ti pargasite	5	5	0	405	131.9
WA02-whole rock (dark vein)	4.6	4.6	0	440	166.9
WA05-whole rock (dark vein)	5.1	5.1	0	418	144.9
WA42-whole rock (gabbroic dykelet)	4.9	4.9	0	407	133.9
WA04-whole rock (gabbroic dykelet)	4.1	4.1	0	420	146.9
WA33-whole rock (gabbroic dykelet)	7.3	7.3	0	375	101.9

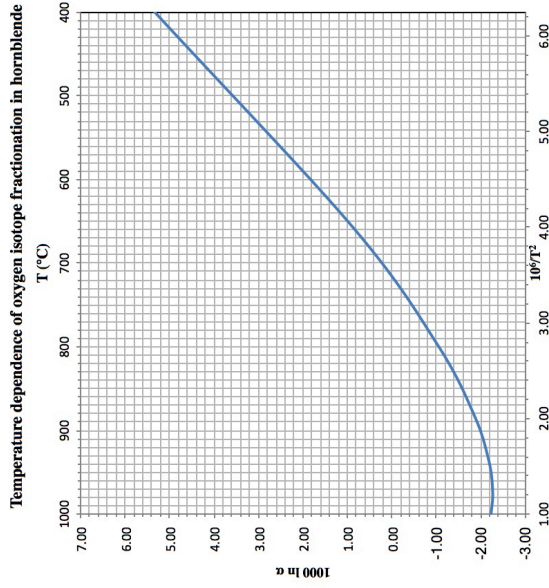


**Table S1 (continued). Hydrothermal fluid temperature calculations with oxygen isotopes.**  
 Zheng, Y.-F., 1993. Calculation of oxygen isotope fractionation in hydroxyl-bearing silicates. *EPSL*, 120, 247-263

**A** Input T  
3.89  
**B**  $\Delta^{18}\text{O}_{\text{amph-water}} = 1000 \ln \alpha = (A * 10^6 / T^2) + (B * 10^3 / T) + C$   
-8.56  
**C**  $\Delta^{18}\text{O}_{\text{amph-water}} = \delta^{18}\text{O}_{\text{amph}} - \delta^{18}\text{O}_{\text{water}}$   
2.43  
Temperature (°C)  
386.8  
1000 ln  $\alpha$   
6.30 ‰

**Fractionation factor ( $\Delta^{18}\text{O}$ ) Calculated assuming  $\delta^{18}\text{O}_{\text{water}}=1$**

Sample	1000 ln $\alpha$ $\Delta^{18}\text{O}_{\text{amph-water}}$	$\delta^{18}\text{O}$ measured $\delta^{18}\text{O}_{\text{amph}}$	$\delta^{18}\text{O}$ water	T calc isot x (10 <sup>6</sup> /T <sup>2</sup> )	T ln °C
WA02-high-Ti pargasite	3.7	4.7	1	427.3	5.5
WA02-hornblende (hydrothermal)	3.7	4.7	1	427.3	5.5
WA42-high-Ti pargasite	4.6	5.6	1	411.5	5.9
WA42-hornblende (hydrothermal)	3.9	4.9	1	423.6	5.6
WA04-high-Ti pargasite	4.5	5.5	1	413.2	5.9
WA04-hornblende (hydrothermal)	4	5	1	421.8	5.6
WA05-high-Ti pargasite	3.7	4.7	1	427.3	5.5
WA33-high-Ti pargasite	4	5	1	421.8	5.6
WA02-whole rock (dark vein)	3.6	4.6	1	429.2	5.4
WA05-whole rock (dark vein)	4.1	5.1	1	420	5.7
WA42-whole rock (gabbroic dykelet)	3.9	4.9	1	423.6	5.6
WA04-whole rock (gabbroic dykelet)	3.1	4.1	1	439.4	5.2
WA33-whole rock (gabbroic dykelet)	6.3	7.3	1	386.8	6.7

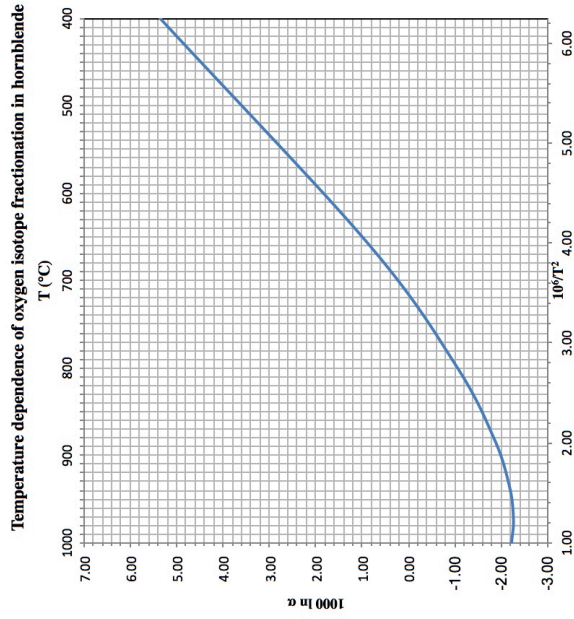
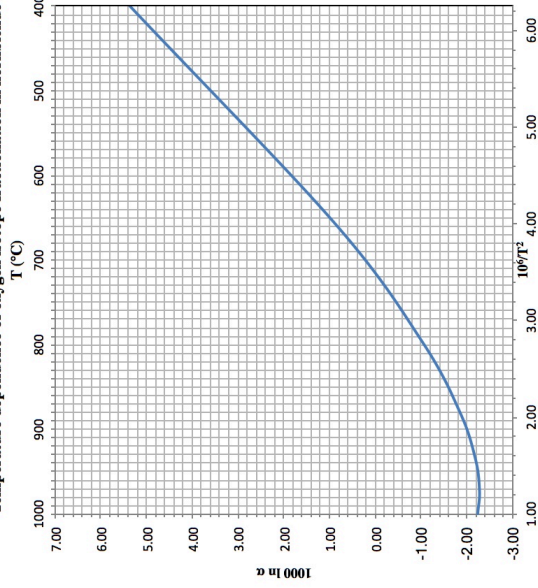


Table S1 (continued). Hydrothermal fluid temperature calculations with oxygen isotopes.

Input T Zheng, Y.-F., 1993. Calculation of oxygen isotope fractionation in hydroxyl-bearing silicates. *EPSL*, 120, 247-263

A	3.89
B	-8.56
C	2.43
Temperature (°C)	400.7
1000 ln $\alpha$	5.30 ‰



Fractionation factor ( $\Delta^{18}\text{O}$ ) Calculated assuming  $\delta^{18}\text{O}$  water=2

Sample	$\Delta^{18}\text{O}$ amphib-water	$\delta^{18}\text{O}$ amphib	$\delta^{18}\text{O}$ water	T calc isot x (10 <sup>6</sup> /T <sup>2</sup> )	T in °C
WA02-high-Ti pargasite	2.7	4.7	2	448	174.9
WA02-hornblende (hydrothermal)	2.7	4.7	2	448	174.9
WA42-high-Ti pargasite	3.6	5.6	2	429.2	156.1
WA42-hornblende (hydrothermal)	2.9	4.9	2	443.6	170.5
WA04-high-Ti pargasite	3.5	5.5	2	431.2	158.1
WA04-hornblende (hydrothermal)	3	5	2	441.4	168.3
WA05-high-Ti pargasite	2.7	4.7	2	448	174.9
WA33-high-Ti pargasite	3	5	2	441.4	168.3
WA02-whole rock (dark vein)	2.6	4.6	2	450.5	177.4
WA05-whole rock (dark vein)	3.1	5.1	2	439.4	166.3
WA42-whole rock (gabbroic dykelet)	2.9	4.9	2	443.6	170.5
WA04-whole rock (gabbroic dykelet)	2.1	4.1	2	462.6	189.5
WA33-whole rock (gabbroic dykelet)	5.3	7.3	2	400.7	127.6

Table S1 (continued). Hydrothermal fluid temperature calculations with oxygen isotopes.

Input T

Zheng, Y.-F., 1993. Calculation of oxygen isotope fractionation in hydroxyl-bearing silicates. *EPSL*, 120, 247-263

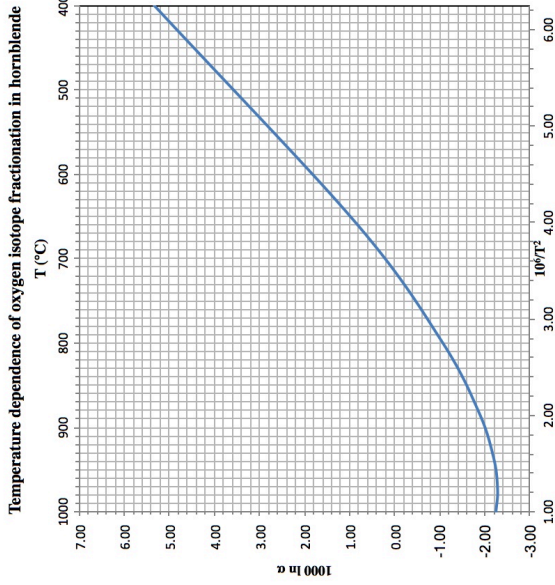
**A** 3.89  
**B** -8.56  
**C** 2.43  
 452.8  
 2.50 ‰  
 Temperature (°C)  
 1000 ln α

$$\Delta^{18}\text{O}_{\text{amph-water}} = 1000 \ln \alpha = (A * 10^3/T^2) + (B * 10^3/T) + C$$

$$\Delta^{18}\text{O}_{\text{amph-water}} = \delta^{18}\text{O}_{\text{amph}} - \delta^{18}\text{O}_{\text{water}}$$

Fractionation factor (Δ<sup>18</sup>O) Calculated assuming δ<sup>18</sup>O water=3

Sample	1000 ln α Δ <sup>18</sup> O <sub>amph-water</sub>	δ <sup>18</sup> O measured δ <sup>18</sup> O <sub>amph</sub>	δ <sup>18</sup> O water	T calc isot x (10 <sup>3</sup> /T <sup>2</sup> )	T in °C
WA02-high-Ti pargasite	1.7	4.7	3	473.5	200.4
WA02-hornblende (hydrothermal)	1.7	4.7	3	473.5	200.4
WA42-high-Ti pargasite	2.6	5.6	3	450.5	177.4
WA42-hornblende (hydrothermal)	1.9	4.9	3	468	194.9
WA04-high-Ti pargasite	2.5	5.5	3	452.8	179.7
WA04-hornblende (hydrothermal)	2	5	3	465.2	192.1
WA05-high-Ti pargasite	1.7	4.7	3	473.5	200.4
WA33-high-Ti pargasite	2	5	3	465.2	192.1
WA02-whole rock (dark vein)	1.6	4.6	3	476.5	203.4
WA05-whole rock (dark vein)	2.1	5.1	3	462.7	189.6
WA42-whole rock (gabbroic dykelet)	1.9	4.9	3	468	194.9
WA04-whole rock (gabbroic dykelet)	1.1	4.1	3	492.2	219.1
WA33-whole rock (gabbroic dykelet)	4.3	7.3	3	416.5	143.4







## Curriculum Vitae

### Adriana M. Currin Sala

Date and place of birth: 31.05.1989 in Barcelona, Spain  
Spanish citizenship

#### Education

- November 2014 – present **PhD studies at Institut für Mineralogie, Leibniz Universität Hannover (ongoing)**
- September 2012 – August 2014 **MSc Earth Structure and Dynamics**, *Earth materials track, Universiteit Utrecht*  
MSc Thesis: *Structural and metamorphic evolution of the Ericek area (SE Turkey) near the Sürgü fault, N of Berit Mountain, in context of Eurasia-Africa collision*
- September 2007 – June 2012 **BSc Geology** (Spanish Licenciatura), *University of Barcelona*  
*Erasmus year at the University of Southampton, UK (2010/11)*  
BSc Thesis: *Study of the Montnegre metamorphic aureole, Catalan Coastal ranges*
- September 2005 – June 2007 **Bachillerato LOGSE** (Science/Technology A-Levels)  
*Col·legi Claret, Barcelona* (Secondary and High School)

#### Work experience

- July 2011 – August 2012 **Intern at *Journal Geologica Acta***  
Biblioteca de la Facultat de Geologia, c/Martí i Franquès s/n, 08028 Barcelona, Spain
- September - December 2009 **Collaboration in the Consolidated Research Group SGR44 “Mineral Resources: Ore Deposit Models, Applications and Sustainability”**  
Departament de Cristal·lografia, Mineralogia i Dipòsits minerals, Facultat de Geologia, c/Martí i Franquès s/n, 08028 Barcelona, Spain



## **Publications:**

Currin, A., Koepke, J., Almeev, R.R., Beermann, O., 2018. Interaction of highly saline fluid and olivine gabbro: Experimental simulation of deep hydrothermal processes involving amphibole at the base of the oceanic crust. *Lithos*. <https://doi.org/10.1016/j.lithos.2018.09.017> 0024-4937.

Currin, A., Wolff, P.E., Koepke, J., Almeev, R.R., Zhang, C., Zihlmann, B., Ildefonse, B., Teagle, D.A.H., 2018. Chlorine-rich amphibole in deep layered gabbros as evidence for brine/rock interaction in the lower oceanic crust: A case study from the Wadi Wariyah, Samail Ophiolite, Sultanate of Oman. *Lithos*. <https://doi.org/10.1016/j.lithos.2018.09.015> ISSN 0024-4937.

## **Conference abstracts**

Currin, A., Wolff, P.E., Koepke, J., Almeev, R., Ildefonse, B. Amphiboles extremely enriched in chlorine as evidence for interaction between rock and saline fluid. Poster presented at: GeoBerlin 2015, Annual Meeting of DGGV - DMG. 4-7 October 2015; Berlin, Germany.

Currin, A., Koepke, J., Almeev, R., Wolff, P.E. Brine-rock interaction in the oceanic crust as evidenced by formation of Cl-rich amphiboles. Poster presented at: EMPG XV. 4-9 June 2016; Zurich, Switzerland.

Currin, A., Koepke, J., Almeev, R., Ildefonse, B., Wolff, P.E. Chlorine-rich amphibole in deep layered gabbros as evidence for brine/rock interaction in the lower oceanic crust: a microstructural and experimental study. Poster presented at: EGU 2017, Vienna. European Geosciences Union annual meeting. 23-28 April 2017; Vienna, Austria.

Currin, A., Koepke, J., Almeev, R., Wolff, P.E., Teagle, D.A.H., Zihlmann, B. Brine/rock interaction in deep oceanic layered gabbros: petrological evidence from Cl-rich amphibole, high-temperature hydrothermal veins, and experiments. Poster presented at: AGU Fall Meeting 2017. 10-15 December 2017, New Orleans, USA.